JPL PUBLICATION 78-68

A Microwave Pressure Sounder

Dennis A. Flower
Jet Propulsion Laboratory

Gordon E. Peckham
Heriot-Watt University, Edinburgh, Scotland

August 1, 1978

National Aeronautics and
Space Administration

Jet Propulsion Laboratory
California Institute of Technology
Pasadena, California

JPL PUBLICATION 78-68

A Microwave Pressure Sounder

Dennis A. Flower
Jet Propulsion Laboratory

Gordon E. Peckham
Heriot-Watt University, Edinburgh, Scotland

August 1, 1978

National Aeronautics and
Space Administration

Jet Propulsion Laboratory
California Institute of Technology
Pasadena, California

The research described in this publication was carried out by the Jet Propulsion Laboratory, California Institute of Technology, under NASA Contract No. NAS7-100, and by Heriot-Watt University under U.K. Science Research Council Grants.

TABLE OF CONTENTS

Section | Page

LIST OF FIGURES

LIST OF TABLES

ABSTRACT

An instrument to measure atmospheric pressure at the Earth's surface from an orbiting satellite would be a valuable addition to the expanding inventory of remote sensors. The subject of this report is to describe such an instrument - the Microwave Pressure Sounder (MPS) - based on an active millimeter wave technique. It is shown that global-ocean coverage is attainable with sufficient accuracy, resolution and observational frequency for meteorological, oceanographic and climate research applications.

Surface pressure can be deduced from a measurement of the absorption by an atmospheric column at a frequency in the wing of the oxygen band centered on 60 GHz. An active multifrequency instrument is needed to make this measurement with sufficient accuracy. The selection of optimum operating frequencies is based upon accepted models of surface reflection, oxygen, water vapor and cloud absorption. By combining the ratios of transmission of three pairs of frequencies the measurement is made essentially independent of variations in the atmospheric temperature and water vapor profiles, cloud cover and sea state.

Numerical simulations using a range of real atmospheres defined by radiosonde observations have been used to validate the frequency selection procedure. This also shows that the error introduced by unmodellable atmospheric variations is less than 0.4mb. Other sources of error are the instrumental noise and the statistical nature of the ocean surface reflectivity. Analyses are presented of alternative system configurations that define the balance between accuracy and achievable resolution. An MPS system which requires minimum development of new components, when used in an 800 km orbit, can provide measurements of surface pressure with a predicted r.m.s. error of 1.2 mb and a surface resolution of 10 x 100 km.

The global coverage of pressure measurement provided by the MPS has been examined for a variety of implementation schemes. Oceanic coverage which is comparable to the existing density of data points on the continental land masses can be achieved with a network of three instruments in sun synchronous, near-polar orbits.

An ongoing U.K. - U.S. development program is being directed towards an early proof-of-concept flight for the MPS on a Shuttle/Spacelab sortie mission. Subsequent operational deployment of the MPS will provide valuable data for numerical weather forecasting and oceanography while the accumulation over a long time period of consistent measurements of the global pressure field will contribute significantly to the data resources needed for climate studies.

1. Meteorological Background

Global measurements of the Earth's atmospheric pressure are important in synoptic meteorology, numerical weather forecasting, atmospheric dynamics and climate studies. At the present time pressure data are gathered principally from land based weather monitoring stations, and are supplemented over the oceans by reports from ships and aircraft. Stations reporting surface pressure to the National Meteorological Centre at 00Z on February 1, 1976 are shown in Fig. 1 and it is apparent that over the tropical and southern ocean areas in particular there is a deficiency of data. Such non-uniform coverage is inadequate in terms of the requirements for a set of global meteorological data sufficiently accurate to provide the initial conditions for a numerical forecast of the weather.

The World Meteorological Organization has specified (WMO, 1973) a set of observational requirements for the First GARP Global Experiment of the Global Atmospheric Research Programme (GARP). Measurements of pressure in data-sparse regions are required with a horizontal resolution of 500 km and an accuracy of ± 0.3% (equivalent to ± 3 mb at the surface). However, a recent survey of user needs (JPL, 1976) indicates that an accuracy of ± (1 - 2) mb in sea level pressure is desirable and it is probable that a ± 3 mb specification is near the limit of usefulness. Resolution requirements ranged from 250 km down to 10 m but the lower figure is unrealistic and not consistent with the accuracy requirement.

The cost of acquiring this quantity of data by conventional land and ocean monitoring stations would be unreasonable (Mason, 1970) and the variation of instrumentation and calibration between stations would reduce the reliability of the measurements. In contrast, the provision of operational satellite borne instruments for remotely sensing atmospheric temperature has proved inexpensive and has given accurate consistent global coverage for several years. Remote sensing of atmospheric water vapor has been demonstrated with the Nimbus E Microwave Spectrometer (Staelin et al., 1976) and Seasat A, due to be launched in 1978 will carry

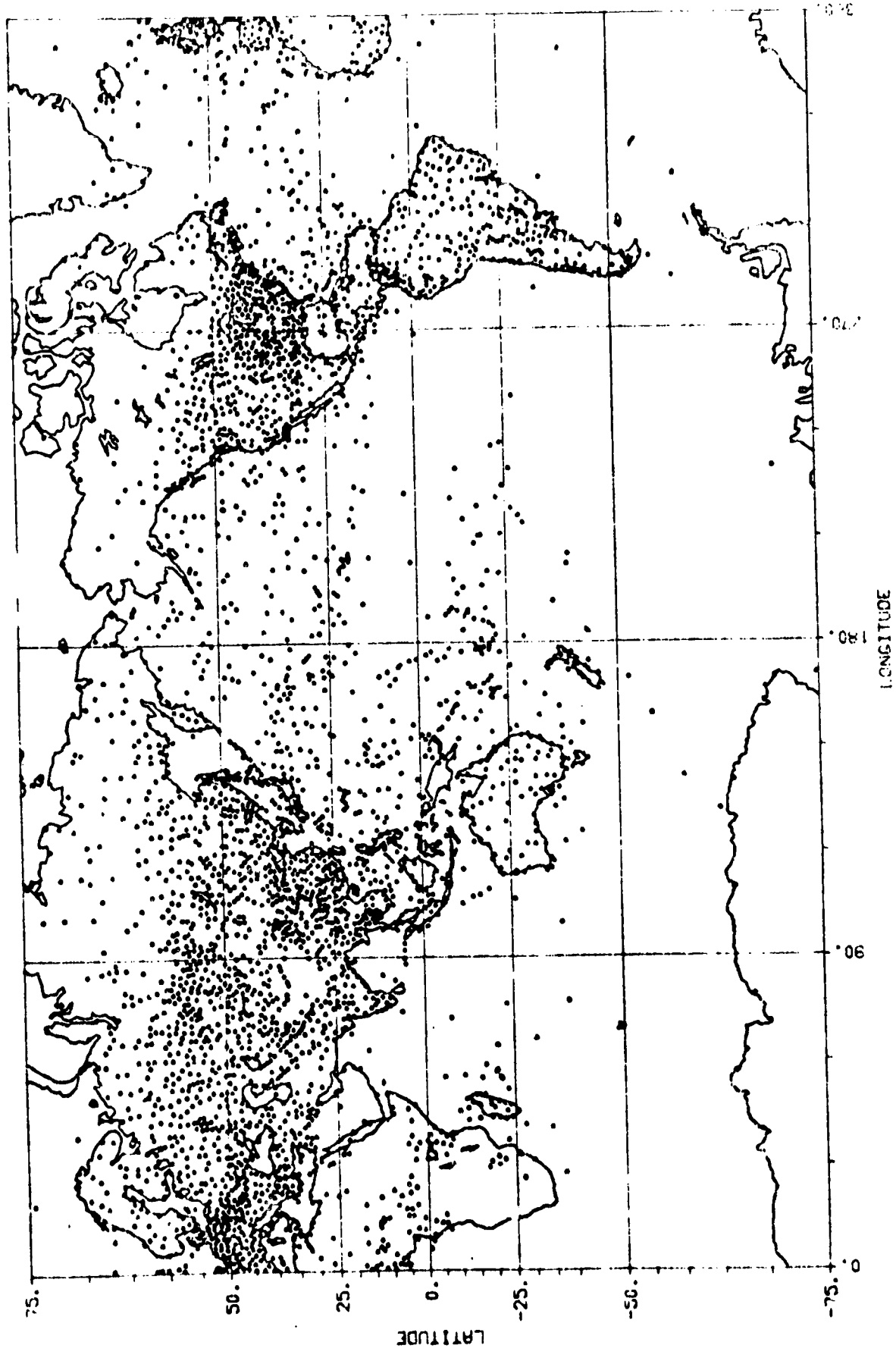

Figure 1. Stations reporting surface pressure February 1st, 1976 00Z

an instrument to obtain surface winds from sea state measurements. The development of an instrument to sense pressure from a satellite platform would be another major advance towards the WMO requirements. It would seem appropriate to aim for an instrument with an accuracy of ±(1-2) mb and capable of a horizontal grid spacing of 100-200 km to correspond with the data at present available from existing land stations.

A network of geostationary satellites at 36,000 km altitude provides near global coverage with a minimum number of satellites. However, satellites in near-polar orbits at 1000 km altitude are required to obtain data for high latitudes and to allow microwave sensing with sufficient resolution. Both types of satellites will be elements in any operational system for comprehensive monitoring of meteorological parameters within the foreseeable future. The active microwave technique for pressure measurement to be discussed here is only feasible from the lower altitudes offered by a polar orbiter.

The accuracy of ±0.3% in pressure measurement corresponds to a height change of only 25 m at sea level so that the height at which the pressure is measured must be known to within this value. This constraint effectively precludes at present the possibility of measuring the three dimensional pressure field. However, a knowledge of the surface pressure together with a measured temperature profile allows the hydrostatic approximation to be used to obtain the variation of pressure with height. An instrument to measure surface pressure is therefore entirely adequate when used in conjunction with a temperature sounder to define the mass field.

The proposed method for measuring surface pressure has been specifically designed for use over the oceans. However, measurements over land may give a valid indication of pressure, but only if a suitable average height can be used and if the surface has appropriate reflection characteristics. This is not a serious disadvantage since oceans cover some 70% of the Earth's surface and while the existing network of weather monitoring stations gives satisfactory coverage of most of the continental land masses, the oceans are almost totally neglected. The satellite surface pressure data for the oceans will complement present land data to approach the GARP requirement.

2. Methods for the Remote Measurement of Pressure

Atmospheric pressure may in principle be determined remotely from measurements of the characteristics of the propagation of electromagnetic radiation through the atmosphere. The accuracy requirement necessitates the use of an active system and several alternative methods have been proposed. The feasibility of their instrumental implementations has been assessed in the literature (Singer 1968, Mason 1970, Smith et al 1972, AMWR 1975) and the following brief summary of some of the limitations of these methods indicates the reasons for adopting the technique to be described in this report.

The three dimensional pressure field can in theory be determined by a range-gated radar or lidar instrument. The pressure dependent contributions to atmospheric backscatter are too weak to be measured but a differential absorption, 0.76 μm lidar relying on aerosol or molecular Rayleigh backscatter appears to be feasible with probable technological advances within the next decade. However, to achieve the coverage and accuracy requirements it would need more primary power than is available in currently planned operational meteorological satellites. Also, because of the inability of infrared radiation to penetrate cloud its operation would be restricted to measurements down to the surface in clear skies and above cloud measurements elsewhere.

Although the impracticality of pressure profile measurements leaves only methods that measure pressure at a reference level this is not a serious limitation. Such data in conjunction with measured temperature profiles allow the full pressure field to be deduced using the assumption of hydrostatic equilibrium. For this purpose, the surface is the most satisfactory reference level. The limitations on coverage in cloudy conditions with infrared instrumentation also apply to visible techniques but to a much lesser extent at microwave frequencies. It is apparent that microwave techniques for measuring surface pressure offer the best possibilities.

Transmissivity measurements through the limb of the atmosphere can provide pressure at a chosen reference level. Above 12 km the pressure

can be obtained by passive microwave measurements but inadequate knowledge of the temperature and water vapor profiles would not allow surface pressure to be deduced from this to sufficient accuracy. To obtain pressure at a lower altitude from a limb measurement would require an active occultation technique with the inconvenience of two satellites whose positions must be continuously monitored to a high accuracy. The horizontal resolution with this method is several hundred kilometers and is thus insufficient to resolve some of the most interesting features of the pressure field.

Similar limitations affect bistatic refractivity measurements recently proposed to determine surface pressure by reflecting a microwave signal from the ocean surface at a low grazing angle. In this case accurate knowledge is required of the water vapor field and the geoid. The 3 mb accuracy and 500 km horizontal separation of measurements can only be approached with a constellation of high-altitude inter-communicating satellites, the orbital characteristics of which are incompatible with other demands on a meteorological satellite network.

An optical path length method measuring the dispersion between two different microwave frequencies requires a time resolution much less than the length of a pulse reflected from the rough ocean surface and is therefore not practicable.

Differential absorption measurements in and near the millimeter wavelength absorption band of oxygen by reflecting signals from the Earth's surface provide the basis of the chosen method. It will be shown that measurements at several frequencies in the wings of the oxygen band centered on 60 GHz combined with measurements closer to the water vapor line at 22 GHz have the potential of achieving the required 1-2 mb accuracy of surface pressure determination without demanding an accurate knowledge of the temperature and water vapor fields. Spatial resolution of the order of 200 km is possible and coverage while not completely global, is better than for the other methods considered. Furthermore the instrument is suitable for flight on operational meteorological satellites and does not demand excessive primary power.

3. An Outline of the Microwave Pressure Sounder Concept

In this section the conceptual basis of the proposed technique is outlined and its plausibility established. An introduction is presented to the various physical aspects of the problem which together will be used as the basis for the instrument design criteria. The necessary details of the analysis will be given in subsequent sections but the symbols to be used are defined here and an indication is given of the order of magnitude of the principal quantities.

3.1 Principle of the Method

With a Microwave Pressure Sounder (MPS) in orbit as depicted in Figure 2 the surface pressure is deduced from measurements of the ratios of atmospheric transmissivity at pairs of frequencies. The primary pair of pressure sensing frequencies lie on the lower wing of the broad 60 GHz oxygen absorption band, one sufficiently far into the band to be significantly affected by changes in the total mass of oxygen in the transmission path with the other frequency on the extreme wing of the band and therefore affected very little by oxygen absorption. The ratio of transmissivities, or differential absorption, is a measure of the total oxygen in the path and hence on the partial pressure of oxygen at the surface. Since oxygen is a uniformly mixed constituent of dry air this is also a measure of the total surface pressure. Differential absorption measurements are necessary at two other pairs of frequencies to make the pressure measurement insensitive to the atmospheric temperature profile, water vapor content, cloud cover and sea state. To make these absorption measurements an active system is required. For each pair of frequencies, signals of equalized power are transmitted and, following reflection from the ocean surface, the ratio of the returned echo powers is measured. When the operating frequencies have been chosen correctly, a combination of the three measured ratios is dependent only on the surface pressure. Thus, the output of the MPS is simply related to the surface pressure and does not rely on subsidiary meteorological measurements for interpretation.

3.2 The Reflected Signal

The radar equation generally used to give the magnitude of the signal received at the antenna from an extended reflector such as the sea surface is (Skolnik 1970).

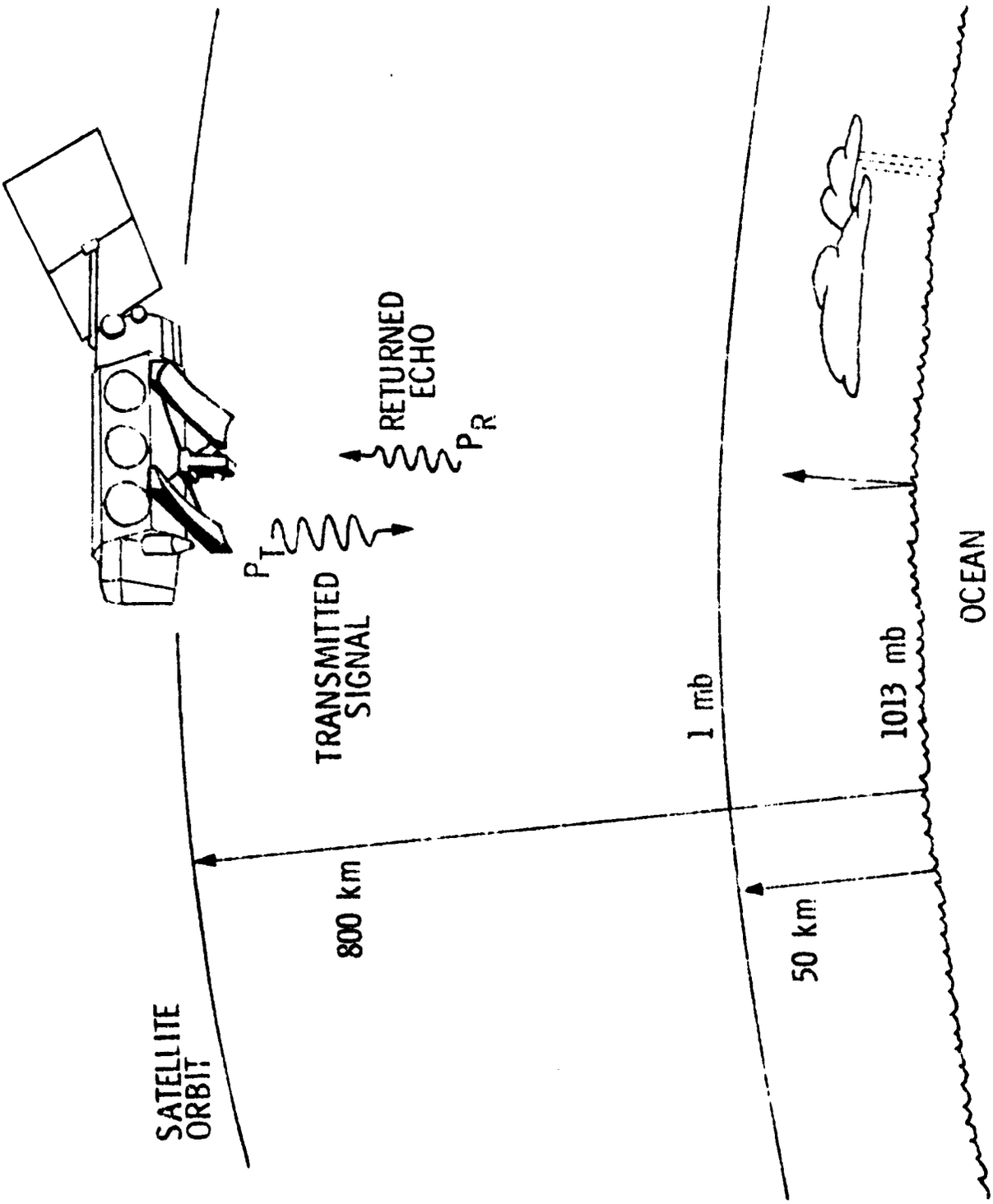

Figure 2. Microwave Pressure Sounder in Orbit

$$P_R = \frac{P_T G^2 \theta_3 \phi_3 \lambda^2 \tau^2(\theta) \sigma(\theta)}{(4\pi)^3 R^2(\theta)} \qquad 3.1$$

where the symbols have the following meanings and are identified on Fig. 3.

P_R	received power at antenna
P_T	transmitted power
G	antenna gain
$\theta_3\phi_3$	antenna 3db angular beam widths
λ	signal wavelength
$\sigma(\theta)$	radar cross-section of reflector
$\tau(\theta)$	total atmospheric transmission coefficient (one-way)
$R(\theta)$	distance between receiver and reflector
θ	angle from nadir

The 3db beam widths are related to the antenna gain thus

$$\theta_3\phi_3 = 4\pi/G \qquad 3.2$$

and the gain is related to the area, A, of the antenna thus

$$G = 4\pi A/\lambda^2 \qquad 3.3$$

It is convenient and less confusing to restrict the equation to the nadir case (θ=0) which is of principal concern. It can be readily extended as necessary for the near nadir situation which will be considered later. Using the relationships 3.2 and 3.3 the radar equation may then be written in the simpler form

$$P_R = P_T \frac{A}{4\pi h^2} \tau^2 \sigma^o \qquad 3.4$$

where h is the satellite altitude.

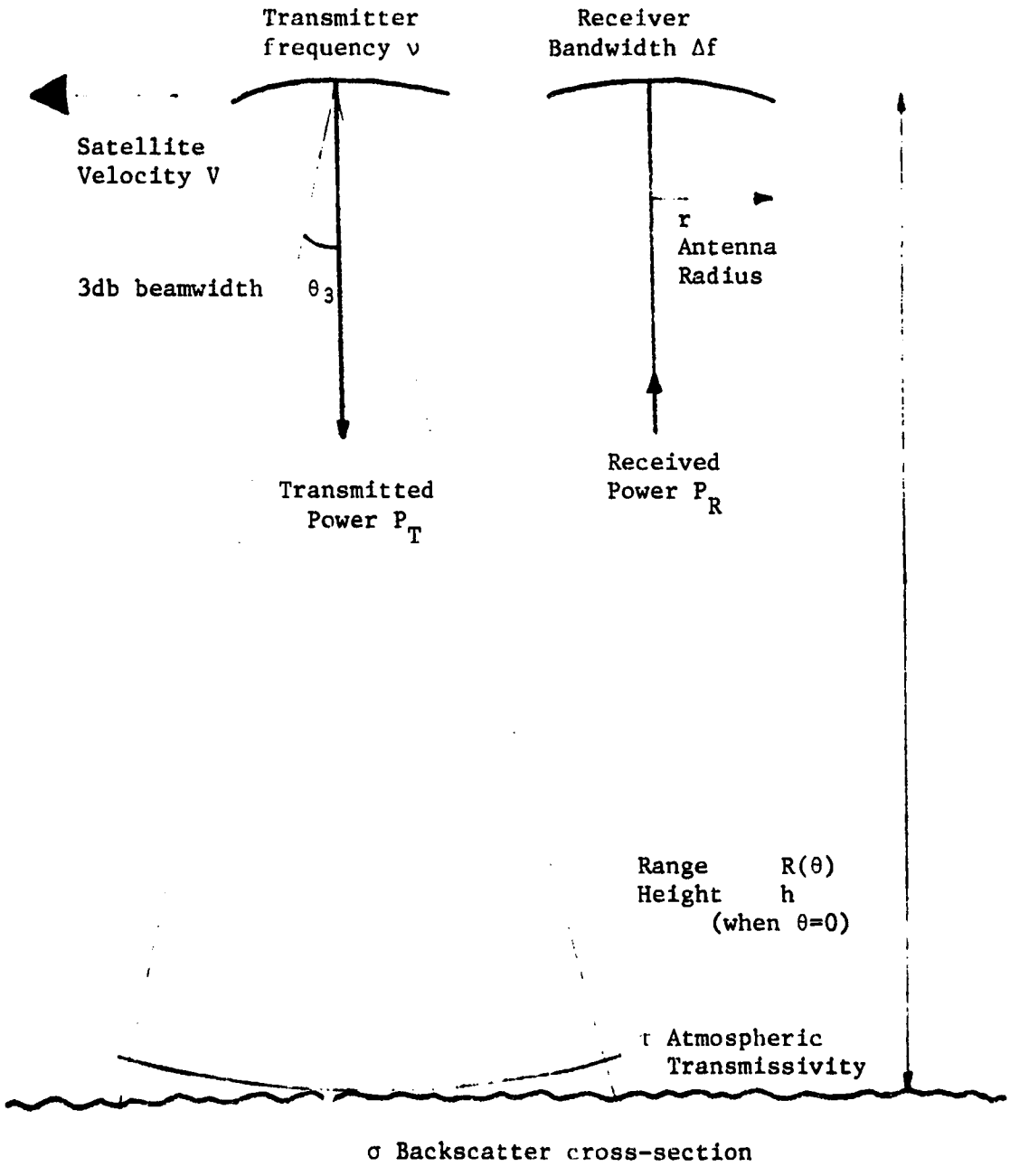

Figure 3. Symbol Definition

The significance of the various factors in equation 3.4 can be readily seen

$P_T\tau$: the power reaching the sea surface is the transmitted power reduced by the atmospheric transmissivity factor

$\frac{A}{4\pi h^2}$: this is a geometrical factor giving the fraction received by an area A at a range H from an isotropic emitter.

σ^o : represents the reflecting ability of the sea surface in relation to an isotropic reflector and includes the directionality of the reflection as well as the reflectivity of the surface.

τ : a further reduction due to the return path through the atmosphere.

For the purpose of instrument design it is better to put the equation in terms of the radius of the antenna, r, using $A = \pi r^2$ and to introduce the efficiencies, η_T, η_R, of the transmit and receive antennae feed systems. In addition the noise, N, must be specifically included since this has a dominating influence on the system design. Introducing the detected power, P_D, which is the sum of the detected return echo, P_R, and the noise we may write

$$P_D = P_R + N = 0.25\, P_T\, \eta_T\, \eta_R \frac{r^2}{h^2} \tau^2\, \sigma^o + N \qquad 3.5$$

The potential of the method for achieving the required accuracy can be demonstrated by estimating the signal to noise ratio using sensible values in this equation. For a 1W source, a .5 m diameter antenna with efficiencies η_T, $\eta_R = 0.5$ at a height of 1000 km above a sea surface of radar cross-section 10 db and an operating frequency such that $\tau = 0.5$ the received signal is $\sim 10^{-14}$ W. The noise equivalent power is

$$N = 4kT\,(\Delta f/t)^{1/2}\, F \qquad 3.6$$

where k is Boltzman's constant and

T	receiver temperature	300 K
Δf	the IF bandwidth	100kHz
t	integration time	10 s
F	receiver noise factor	10 db

These values give a S:N ratio of 600:1 which is compatible with the 0.3% accuracy requirement.

3.3 Design Parameters

The physical factors influencing the magnitude of the received signal can be clearly seen from the various terms in the radar equation (3.5). In addition the parameters availabe for system design can now be identified. The total atmospheric transmissivity should first be separated into terms covering oxygen, τ_o, water vapor, τ_w, and other atmospheric constituents, τ_A. So

$$P_D = 0.25\, P_T \eta_T \eta_R \frac{r^2}{h^2} \tau_o^2 \tau_w^2 \tau_A^2 \sigma^o + N \qquad 3.7$$

P_T and P_D are the source and detected powers. Source power of the order of 1W is required and solid state Impatt oscillators are probably the most suitable for space applications because of their low voltage requirements and high efficiency. The power available from single devices has an upper limit of about 1W but by 1978 sources delivering several watts should be available when techniques for combining several diodes together are extended to frequencies up to 70 GHz.

The antenna feed efficiency, η, has a value dependent on antenna design and system losses, but a working figure of 0.5 can be used. The antenna radius, can be chosen to optimize system performance by balancing signal-to-noise error, which demands a larger antenna, against a statistical error due to sea surface effects, which demands a smaller antenna. The optimum value for r is of the order of 25 cm so that antenna subsystem design problems due to excessive size are not encountered. The field of view at the surface is determined by r and it has a diameter of $\sim$30 km for r = 0.25 m with the satellite at a height of 1000 km.

The orbit height h should preferably remain reasonably constant to avoid the need for a receiver with a large dynamic range. A high orbit provides more favorable geometry for meaningful measurements away from the sub satellite path but as h is decreased the signal-to-noise ratio and consequently the accuracy of the measurement are improved. Too low an orbit however will limit the operational lifetime of the satellite and a value for h between 250 km and 1000 km is desirable.

τ_o^2 the transmissivity of the atmosphere due to oxygen over a double path can be written as $10^{-0.2\Gamma_o}$ where Γ_o is the integrated absorption coefficient in db for a single path. Γ_o can be calculated from theoretical models of the oxygen absorption band (Waters 1976, Rosenkranz, 1975) in terms of the variables surface pressure, p_g, and temperature profile, $T(z)$, for any value of the disposable parameter, ν, frequency. The zenith attenuation due to atmospheric oxygen as a function of frequency is shown for a U.S. standard atmosphere in Fig. 4. The principal operating frequency of the instrument should be chosen around 52-53 GHz. Further into the band the signal and S:N ratio are reduced while at lower frequencies the effect of surface pressure on the signal is reduced.

The presence of water vapor in the atmosphere has both indirect and direct effects. It affects τ_o because it modifies the pressure broadening of the lines within the oxygen band. It contributes to absorption in the spectral band of interest through τ_w^2 which can be written as $10^{-0.2\Gamma_w}$ and Γ_w, the integrated absorption coefficient for water vapor, is calculable from existing models in terms of the pressure profile of water vapor $p_w(z)$ and $T(z)$ for given values of ν. Finally, water vapor can make a significant contribution to the total surface atmospheric pressure. The water vapor spectrum is also shown in Fig. 4 for a surface density of 12.3 gm m^{-3}, decaying exponentially with a scale height of 2.2 km.

With the exception of ozone, other atmospheric gases do not significantly absorb in this region of the spectrum, but clouds and rain both absorb and scatter. Numerous weak ozone lines exist throughout the microwave spectrum but only close to the line centers is the absorption strong enough to affect this experiment. These frequencies can be easily avoided.

The frequency dependence of atmospheric constituents other than oxygen and water vapor can be modelled by an absorption coefficient, Γ_A which is a second order function of frequency, viz

$$\Gamma_A = a + b\nu + c\nu^2 \qquad 3.8$$

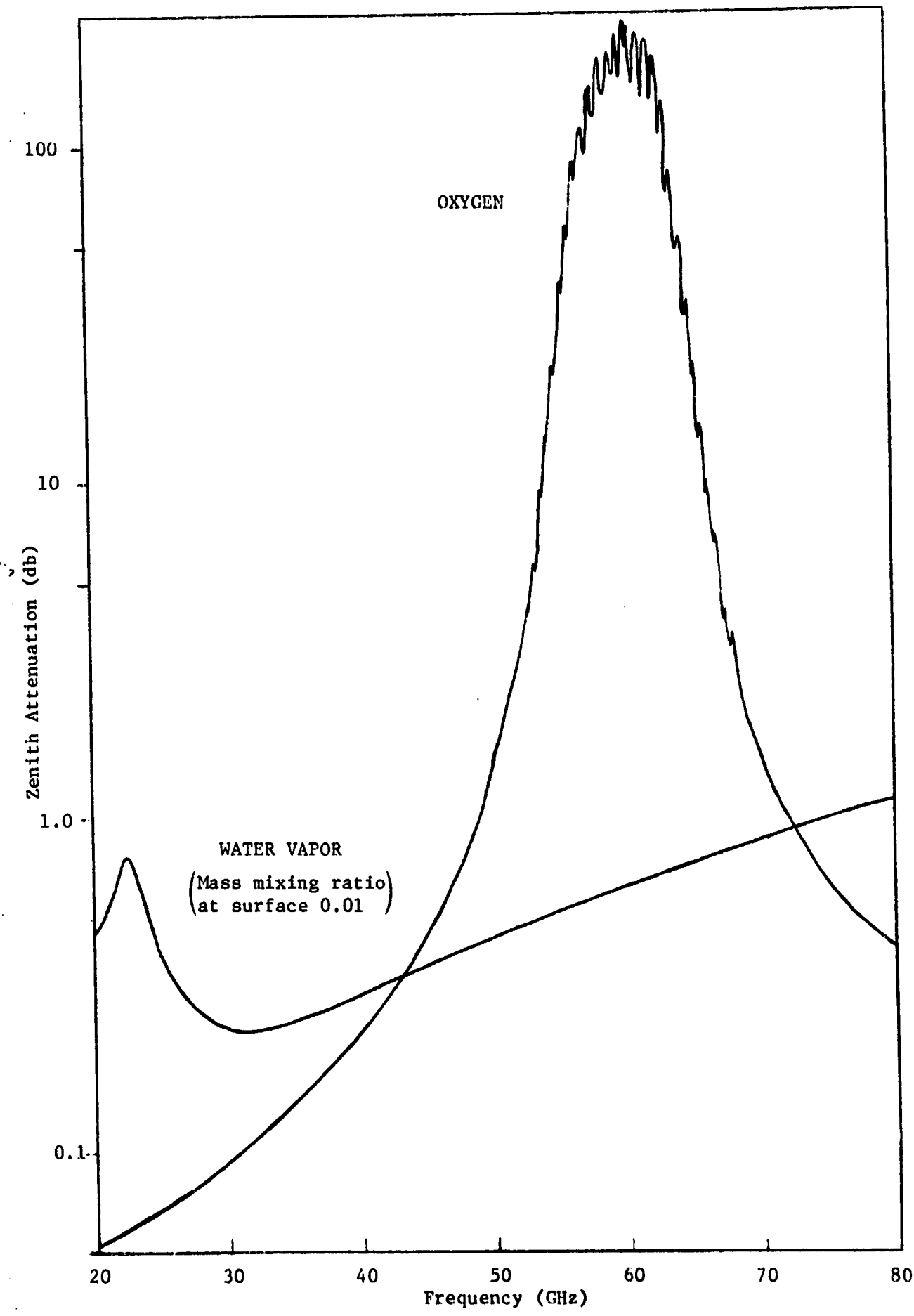

Figure 4. Zenith Attenuation of U.S. Standard Atmosphere.

The coefficients a, b and c are highly variable both in space and time because equation 3.8 represents the effects of cloud and rain. The experiment must be designed so that the transmissivity measurements allow these coefficients to be either evaluated or eliminated when deducing surface pressure.

The radar cross-section of the sea surface, $\sigma(\theta)$, depends upon the sea state, the angle of incidence and the frequency. The smooth variation with frequency is adequately modelled by a second order function so that equation 3.8 also includes sea surface frequency dependence. $\sigma(\theta)$ has a maximum value, σ^o, for normal incidence. It reduces more rapidly for calm seas than for rough seas as the angle of incidence decreases. For most sea states it should be possible to make measurements with the proposed instrument at angles of up to about 15^o from the vertical. Such measurements away from the subsatellite path will allow the surface pressure gradient to be determined and this is of much greater value than pressure only along the orbit path. For a 1000 km orbit altitude the 15^o limitation means that the swath width at the surface is about 500 km across which significant pressure differences frequently occur. Variations in the sea state due to surface winds can change the average value of σ^o by a factor of 10 or more so the dynamic range of the instrument must accommodate this as well as atmospheric absorption variability.

Perhaps the most important effect of the sea surface is that because of its constantly changing nature, both spatially and in time, the coherence of the reflected signal is destroyed. The intensity of the return echo varies statistically with a Rayleigh distribution, the standard deviation of which is equal to the mean. The average of a large number of independent samples is required to achieve the necessary accuracy. The relationship between the sample collection rate and the antenna radius is discussed in detail in Section 11 together with the consequences this has for system design.

The noise N includes contributions from background emission, atmospheric reflection and instrumental noise. It depends most importantly on the bandwidth, Δf, of the detection system and on the integration time, t.

Choice of t will, for a given satellite speed, determine the ground resolution of the instrument along the orbital path. A typical satellite speed is $\sim 7\ \mathrm{kms}^{-1}$ so that the 500 km resolution required for GARP can be achieved with t up to 1 min. However, shorter integration times and consequently better spatial resolution are anticipated because although 500 km is adequate resolution for the input data set of numerical global circulation models many meteorologically significant features in the pressure field have dimensions less than this.

Backscatter from atmospheric constituents is small except perhaps from heavy rain, but under these conditions the increased absorption will probably make the instrument unusable. To reduce noise to a minimum the bandwidth should be limited to that necessary to include all the return signal. A direct measurement of noise must be made to enable the best estimate of signal level to be determined.

3.4 Summary

This overview of the proposed technique for determining atmospheric pressure at the surface of the Earth from transmissivity measurements has identified the following parameters, the values of which are at our disposal for designing a system with optimized performance:

P_T	transmitter power
h	orbit height
r	antenna radius
ν	operating frequencies
t	integration time
Δf	receiver bandwidth

Measurements must be made at several frequencies to enable signal level changes due to pressure variation to be distinguished from the effects of all of the other factors mentioned here. It is necessary next to discuss in detail the theory of these physical factors so as to establish a basis for system design and choice of operating frequencies

using the disposable parameters that have been identified. It will be shown that an instrument can be designed for which

- the sensitivity of the measurement of pressure to the temperature profile T(z) and to the presence of water vapor in the atmosphere is reduced to an insignificant level;

- multifrequency measurements are used to eliminate the effects of the other unknown quantities which are described by the variable coefficients a, b and c;

- averaging over a large number of independent samples provides the accuracy demanded;

- useful near global-ocean coverage can be obtained;

- available technology is used for all components except the transmitter source and these are currently being developed.

4. Absorption of Millimeter Waves by Oxygen

To be able to determine pressure from multifrequency measurements of zenith attenuations detailed knowledge must be available of the oxygen absorption coefficient as a function of frequency, pressure and temperature. This section summarizes the relevant characteristics of the most recent theoretical spectroscopic model of oxygen (Rosenkranz 1975). The theory produces results in close agreement with experimental data (Liebe et al. 1977).

4.1 Absorption Coefficient

The transmission of radiation at a frequency ν through an absorbing medium is generally described by the equation

$$I_\nu(x) = I_\nu(0) \exp(-\gamma(\nu)x) \qquad 4.1$$

where the intensity $I_\nu(x)$ after the radiation has travelled a distance x is given in terms of the initial intensity $I_\nu(0)$ and the absorption coefficient $\gamma(\nu)$.

For a path through an inhomogeneous medium the absorption can be obtained by integrating $\gamma(\nu)$. In particular for a vertical path through the atmosphere the absorption of millimeter waves due to oxygen is expressed in terms of the integrated absorption coefficient Γ_o given by

$$\Gamma_o \int_0^\infty \gamma(\nu)dz \qquad 4.2$$

where z is the vertical coordinate.

4.2 The Microwave Spectrum of Oxygen

The absorption by molecular oxygen of electro-magnetic waves in the millimeter spectral region was first described quantitatively by Van Vleck (1947). The quantum number N, of which only odd values are allowed, describes the rotational angular momentum of the molecule. This couples with electronic spin to form a triplet of states with total angular momentum J = N-1, N or N+1. Selection rules permit magnetic dipole transitions with $\Delta J = \pm 1, 0$. The transitions $\Delta J = \pm 1$ give rise to a broad band of lines between 50 and 70 GHz and an isolated line at 118 GHz. The resonant frequencies are denoted

ν_N^+ or ν_N^- for transitions (J = N) → (J = N+1) and (J = N) → (J = N-1) respectively. $\Delta J = 0$ transitions correspond to "non-resonant" absorption at zero frequency. The total absorption at any frequency is calculated by summing over those lines with significant absorption and it is found to be sufficient to include only those lines with $N \leq 39$.

In the pressure range from 1 to 1000 mb the dominant line broadening mechanism is intermolecular collisions. Rosenkranz gives the absorption in db km^{-1} as

$$\gamma(\nu) = 1.434\ p \left(\frac{\nu}{T}\right)^2 F(\nu) \qquad 4.3$$

where the pressure p is in mb, the frequency ν is the GHz and the temperature T is in K. The function $F(\nu)$ is a line shape factor which together with ν^2 describes the spectral intensity distribution and is given by

$$F(\nu) = p \left\{ \sum_N \Phi_N \left[f_N^+(\nu) + f_N^+(-\nu) + f_N^-(\nu) + f_N^-(-\nu) \right] + \frac{0.70 w_b}{\nu^2 + (p w_b)^2} \right\} \qquad 4.4$$

where

$$f_N^{\pm}(\nu) = \frac{w_N (d_N^{\pm})^2 + (\nu - \nu_N^{\pm})\, y_N^{\pm}}{(\nu - \nu_N^{\pm})^2 + (p w_N)^2} \qquad 4.5$$

It can be seen that the summation is over a set of lines at both positive and negative frequencies with line shapes (eqn. 4.5) of Lorentzian form modified by the interference coefficients $y_N^{\pm}$. The final term of equation 4.4 is the contribution from the zero frequency lines where w_b is the non-resonant linewidth.

The population factor Φ_N is given by

$$\Phi_N = \frac{2N + 1}{0.725T} \exp\left(-2.0685\, N(N+1)\, T\right) \qquad 4.6$$

and the line amplitudes $d_N^{\pm}$ are

$$d_N^+ = \left[\frac{N(2N+3)}{(N+1)(2N+1)}\right]^{1/2} \qquad 4.7$$

$$d_N^- = \left[\frac{(N+1)(2N-1)}{N(2N+1)}\right]^{1/2} \qquad 4.8$$

Following Rosenkranz the interference coefficients are approximated by

$$y_N^{\pm} = d_N^{\pm} \left\{ \frac{2d_{N+2}^{\pm}\ w_N^{\uparrow}}{\nu_N^{\pm} - \nu_{N+2}^{\pm}} + \frac{2d_{N-2}^{\pm}\ w_N^{\downarrow}}{\nu_N^{\pm} - \nu_{N-2}^{\pm}} - \frac{w_b}{\nu_N^{\pm}} - \frac{w_b}{\nu_N^{\pm} + 60} \right\} \qquad 4.9$$

where $w_N^{\uparrow}$ and $w_N^{\downarrow}$ are near-diagonal elements of the [w] matrix when $2\pi p[w]$ is the transition rate matrix. The approximation restricts the coupling of each positive frequency line to the two adjacent lines in the same branch, to the line at zero frequency and to the lines at negative frequencies. Two conditions can be applied to the elements $w_N^{\uparrow}$ and $w_N^{\downarrow}$ which then allow them to be evaluated by an iterative procedure from the relationships

$$w_N^{\downarrow} = w_b - w_N - w_N^{\uparrow} \qquad 4.10$$

and

$$w_{N-2}^{\uparrow} = w_N^{\downarrow}\ \Phi_N/\Phi_{N-2} \quad . \qquad 4.11$$

The procedure is initiated by arbitrarily setting $w_{39}^{\uparrow} = 0$. This produces a relatively large error in the interference coefficient for large N but it is not significant since these are weak lines and the error is progressively damped by application of the conditions 4.10 and 4.11.

The experimentally measured values of frequencies, $\nu_N^{\pm}$, and linewidths, $w_N^{\pm}$, given in Table 1 were used to compute the microwave spectrum of oxygen. The non-resonant linewidth is the least accurately known parameter and it has a significant impact on the integrated absorption calculations away from the individual line centers and in the wings of the broad band. Rosenkranz uses the value

$$w_b = 0.48 \left(\frac{300}{T}\right)^{.89} \text{ MHz mb}^{-1} \qquad 4.12$$

which is the average of measurements made by Kaufman (1967) and Maryott and Birnbaum (1960). This value is preferred to a later measurement by Liebe et al (1977) which is 0.54 MHz mb^{-1} at 300°K because it gives a better fit to Reber's (1972) opacity measurements from 66 to 71 GHz (Fig. 5) and Liebe's technique is not particularly sensitive to variations in w_b.

N	Frequencies, GHz		Linewidths, MHz mb^{-1}	
	ν_N^+	ν_N^-	$W_N^+(300)$	$W_N^-(300)$
1	56.2643	118.7503	1.66	1.61
3	58.4466	62.4863	1.47	1.49
5	59.5910	60.3060	1.39	1.42
7	60.4348	59.1642	1.34	1.36
9	61.1506	58.3239	1.30	1.32
11	61.8002	57.6125	1.27	1.29
13	62.4112	56.9682	1.24	1.25
15	62.9980	56.3634	1.22	1.23
17	63.5685	55.7838	1.20	1.20
19	64.1278	55.2214	1.18	1.18
21	64.6789	54.6712	1.16	1.16
23	65.2243	54.1300	1.13	1.13
25	65.7647	53.5957	1.12	1.12
27	66.3021	53.0668	1.10	1.10
29	66.8368	52.5422	1.08	1.08
31	67.3695	52.0212	1.06	1.06
33	67.9007	51.5030	1.04	1.04
35	68.4308	50.9873	1.02	1.02
37	68.9601	50.4736	1.00	1.00
39	69.4887	49.9618	0.98	0.98

Table 1: Frequencies and Linewidths of the Oxygen Microwave Spectrum (From Liebe et al, 1977)

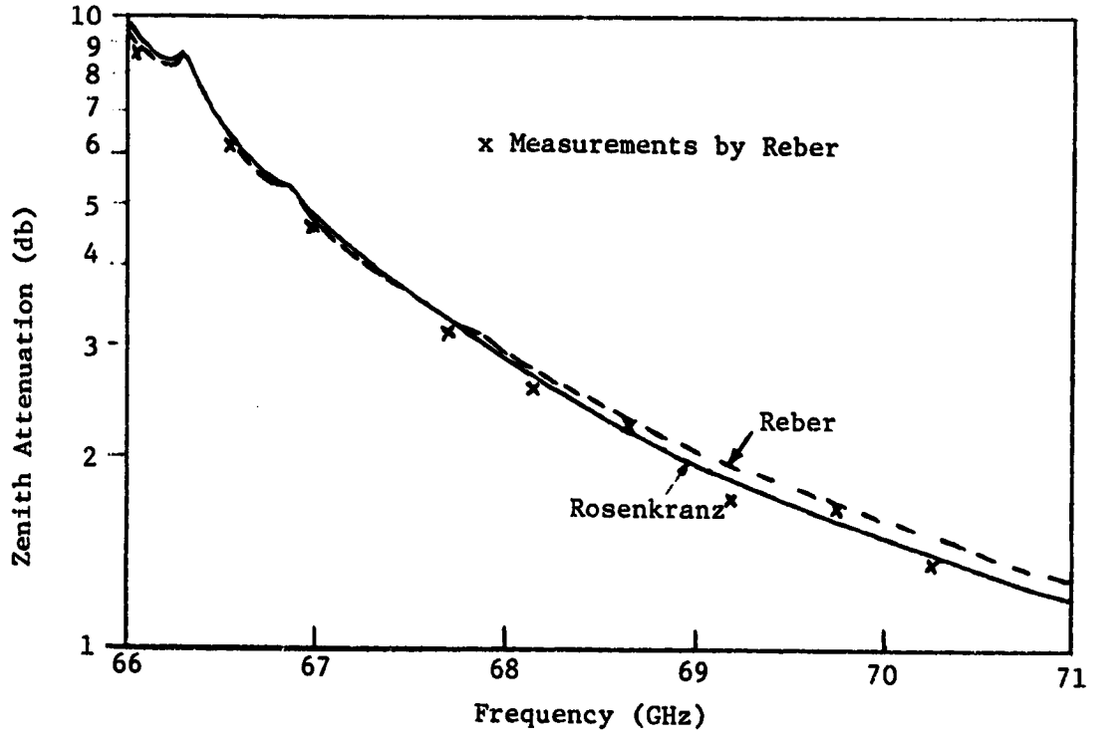

Figure 5. Rosenkranz theory of oxygen absorption fitted to Reber's measurements of Zenith attenuation.

This formulation of the oxygen spectroscopy is the best model at present available. It allows the absorption coefficient to be calculated with a reasonable amount of computer time and the fit to measurements at frequencies above 55 GHz is better than for other models and at least equal to them below 55 GHz. The pressure dependence is given explicitly in equations 4.3, 4.4 and 4.5 while temperature effects are included in Φ_N, y_N, w_b and w_N.

4.3 Absorption by Atmospheric Oxygen

When the pressure p is the total atmospheric pressure then the absorption for pure oxygen must be reduced by the fractional content, f, of oxygen in a dry atmosphere. In equation 4.3, the value of f used is .2085, which is for $^{16}O_2$, the predominant isotopic molecule. Absorption by the ($^{16}O^{18}O$) molecule must also be considered but is only of significance near its line centers (Section 9.2).

Broadening of the lines by O_2-N_2 collisions is found to be smaller than broadening by O_2-O_2 collisions. Liebe gives a modified linewidth expression which may be written in the form

$$w_N = w_N(300) \left[m\left(\frac{300}{T}\right)^{0.9} + m_w \beta \left(\frac{300}{T}\right) \right] \text{ MHz mb}^{-1} \qquad 4.13$$

where $w_N(300)$ is the measured linewidth at 300K and the foreign gas broadening coefficient, m, has a value 0.929 for dry air. The second term in this equation accounts for the variable effects of water vapor on the oxygen linewidth through the mass mixing ratio β and the coefficient m_w which has a value of 0.52.

5. Microwave Absorption by Water Vapor

As well as modifying the linewidths of the oxygen spectrum (Section 4.3) atmospheric water vapor affects the measurements to be made with the pressure sounder by absorbing millimeter waves and by contributing to the total surface pressure.

The microwave spectrum of water vapor is caused by electric dipole transitions between rotational states of the molecules. The lines of particular interest here are centered at 22.235 and 183.310 GHz and the best agreement between theory and experiment is obtained by using a kinetic lineshape (Waters, 1976). However, in the window region calculated absorption is significantly less than that measured. Waters shows that for frequencies up to 100 GHz the discrepancy can be satisfactorily accounted for by grouping together the contributions from all lines other than that at 22 GHz and by including an empirical correction term. The absorption coefficient in db km^{-1}, $\gamma_w(\nu)$, is then

$$\gamma_w(\nu) = \frac{\rho \nu^2 \Delta\nu}{T^{3/2}} \left\{ \frac{3.12 \times 10^6}{T} \frac{\exp(-644/T)}{(22.235^2 - \nu^2)^2 + 4\nu^2 \Delta\nu^2} + .012 \right\} \qquad 5.1$$

where the linewidth in GHz is

$$\Delta\nu = 2.96 \left(\frac{p}{1013}\right) \left(\frac{300}{T}\right)^{0.626} \left(1 + 0.018 \frac{\rho T}{p}\right) \qquad 5.2$$

The water vapor density ρ is in gm m^{-3} and all other symbols are as previously defined. Equations 5.1 and 5.2 enable the absorption due to atmospheric water vapor to be determined for given values of p, T, ρ, and ν. These computations agree with measured absorption within the 5 to 10% accuracy of measurement generally achieved with this difficult test gas (e.g. Liebe and Welch, 1973). The anomalously high absorption away from the line centers has no satisfactory theoretical basis. At higher frequencies there are strong indications that water vapor dimer effects contribute significantly to the absorption (Harries and Ade 1972). However, below 100 GHz there is no evidence of a dimer associated spectral structure which could affect the choice of pressure sounder operating frequencies.

To account most conveniently for the contribution from water vapor to the total surface pressure, the effect of absorption due to any partial pressure of water vapor on the instrumental pressure index obtained from multifrequency measurements should be equivalent to the effect of an equal pressure of dry air.

6. Zenith Attenuation

6.1 The Vertical Path

The equations of Sections 4 and 5 permit the evaluation of the absorption of microwaves with frequencies up to 100 GHz by a homogeneous atmosphere of specified pressure, temperature and water vapor content. By integration, absorption through a vertical and thus non-homogeneous path can also be obtained. This has been computed for the U.S. Standard Atmosphere with added water vapor shown in Fig. 6. The water vapor content was specified in terms of its mass mixing ratio, β, such that at any pressure, p, β is given in terms of the surface mixing ratio β_g and pressure p_g by

$$\beta = \beta_g \left(\frac{p}{p_g}\right)^3 \qquad 6.1$$

Thus the water vapor falls exponentially with height with a scale height of about 2 km compared to the 8 km scale height for pressure.

To carry out the numerical integration the atmosphere must be divided into a reasonable number of layers. The absorption of each layer was approximated by the value for an equally thick homogeneous layer using average values of temperature, pressure, and water vapor mixing ratio. Several different methods have been used to evaluate these average values and various numbers of layers tried. It was found that as the number of layers was increased beyond 24, divided equally between the troposphere and stratosphere, the resulting changes in calculated absorption were not significant for the purpose of system design. However, for consistency with the numerical simulations of Section 8 it is convenient to use the heights and temperatures of the standard atmosphere at the 36 standard pressure levels between 1013 and 2 mb used for reporting radiosonde observations.

The zenith attenuation thus calculated is shown in Figure 4 for a water vapor mass mixing ratio at the surface $\beta_g = 0.01$ which corresponds to a density of 12.9 gm m^{-3}.

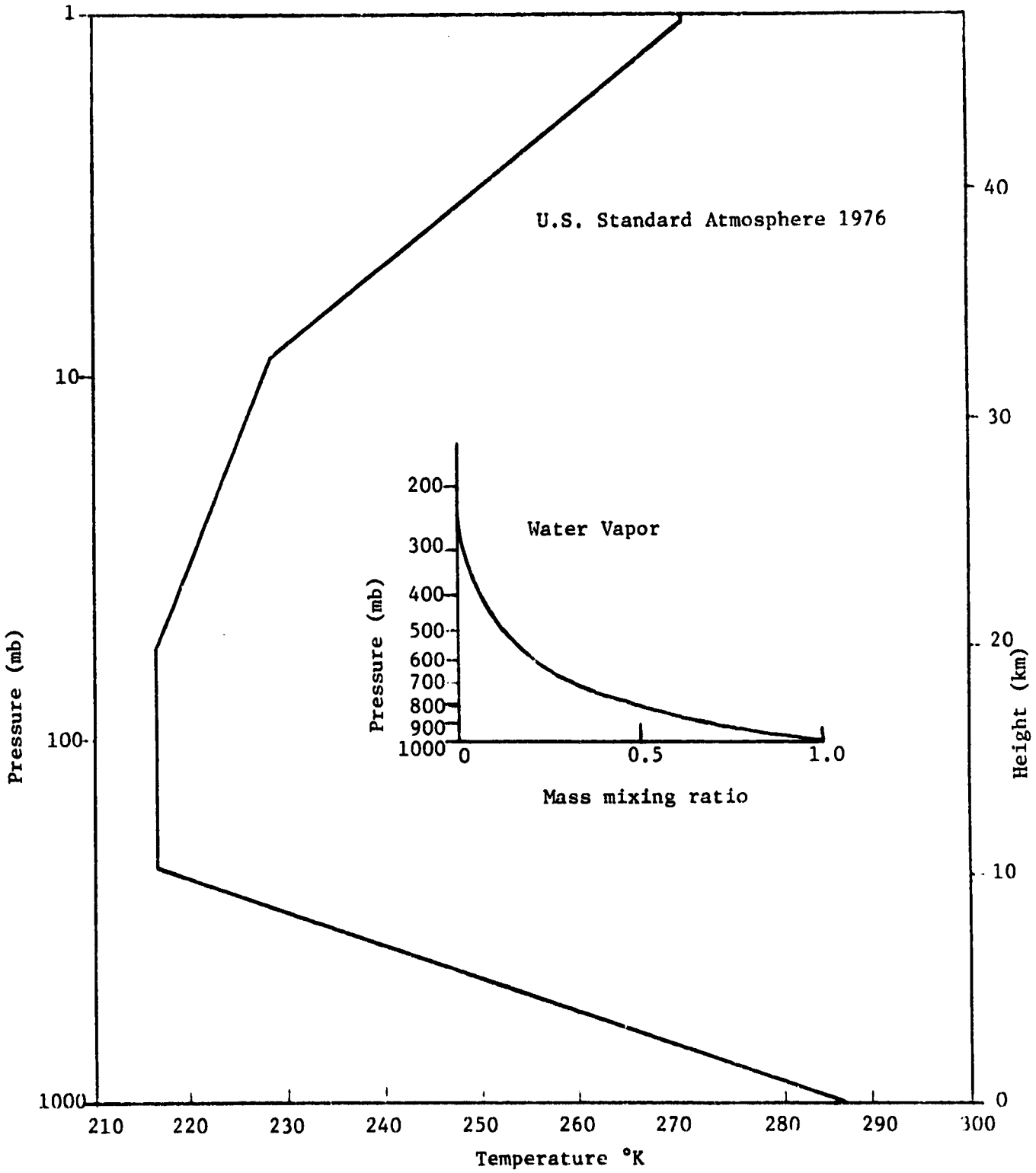

Figure 6. U.S. Standard Atmosphere 1976
Inset: Water Vapor Profile

6.2 Derivatives w.r.t.T, p and Water Vapor

To enable the operating frequencies of the pressure sounder to be chosen so that the measurement is insensitive to temperature profile and water vapor content of the atmosphere the change in integrated absorption coefficient due to changes in T(z) and water vapor content must be determined. The sensitivity of the sounder to pressure can be obtained from the derivative with respect to pressure. The method by which the derivatives are calculated is given here but the reasons for defining them in the following way are given in Section 7.

For convenience we introduce a total integrated absorption coefficient, Γ_T, which is the sum of the coefficients, Γ_o, for oxygen and Γ_w, for water vapor. At a particular frequency Γ_T can be expressed as

$$\Gamma_T = \Gamma_o + \Gamma_w = \Gamma_{To} \left(\frac{p_g}{p_o}\right)^x \left(\frac{T_g}{T_o}\right)^{(y+1)} \qquad 6.2$$

where the surface pressure, p_g, and temperature, T_g, are normalized to some standard values p_o and T_o for which the coefficient has the value Γ_{To}. The indices x and (y+1) are functions of frequency. Thus the derivatives w.r.t. fractional changes in the surface pressure and temperature are, respectively

$$\frac{\partial \Gamma_T}{\left(\partial p_g / p_g\right)} = x\, \Gamma_T \qquad 6.3$$

and

$$\frac{\partial \Gamma_T}{\left(\partial T_g / T_g\right)} = (y+1)\, \Gamma_T \qquad 6.4$$

The index x was determined by repeating the calculation of Section 6.1 for an atmosphere with 2% increase in surface pressure and appropriate increases at other levels to maintain hydrostatic equilibrium. The values of zenith attenuation, Γ_T and Γ_T^1, thus give x

$$x = \frac{\log \Gamma_T / \Gamma_T^1}{\log (1.02)}$$

The index (y+1) can be similarly obtained from a calculation of zenith attenuation for a 2% increase in temperature throughout the atmosphere so

that a change in T_g is taken to be representative of a change in the profile T(z). These are then used with equations 6.3 and 6.4 to give the derivatives which are shown in Fig. 7 as functions of frequency. In Figures 8 and 9 the data for the important wing regions is presented with an expanded frequency scale to show the fine structure associated with individual oxygen lines within the broad band.

The effect of a change in the water vapor content was also determined by recalculating the zenith attentuation when the surface mixing ratio β_g is increased by 2%. However it is plotted in Figure 7, 8 and 9 as the change, $(\Delta\Gamma_T)_{wv}$, in Γ_T directly in db for effectively a 100% change in water vapor content calculated by multiplying the difference in Γ_T for the 2% change in β_g by 50.

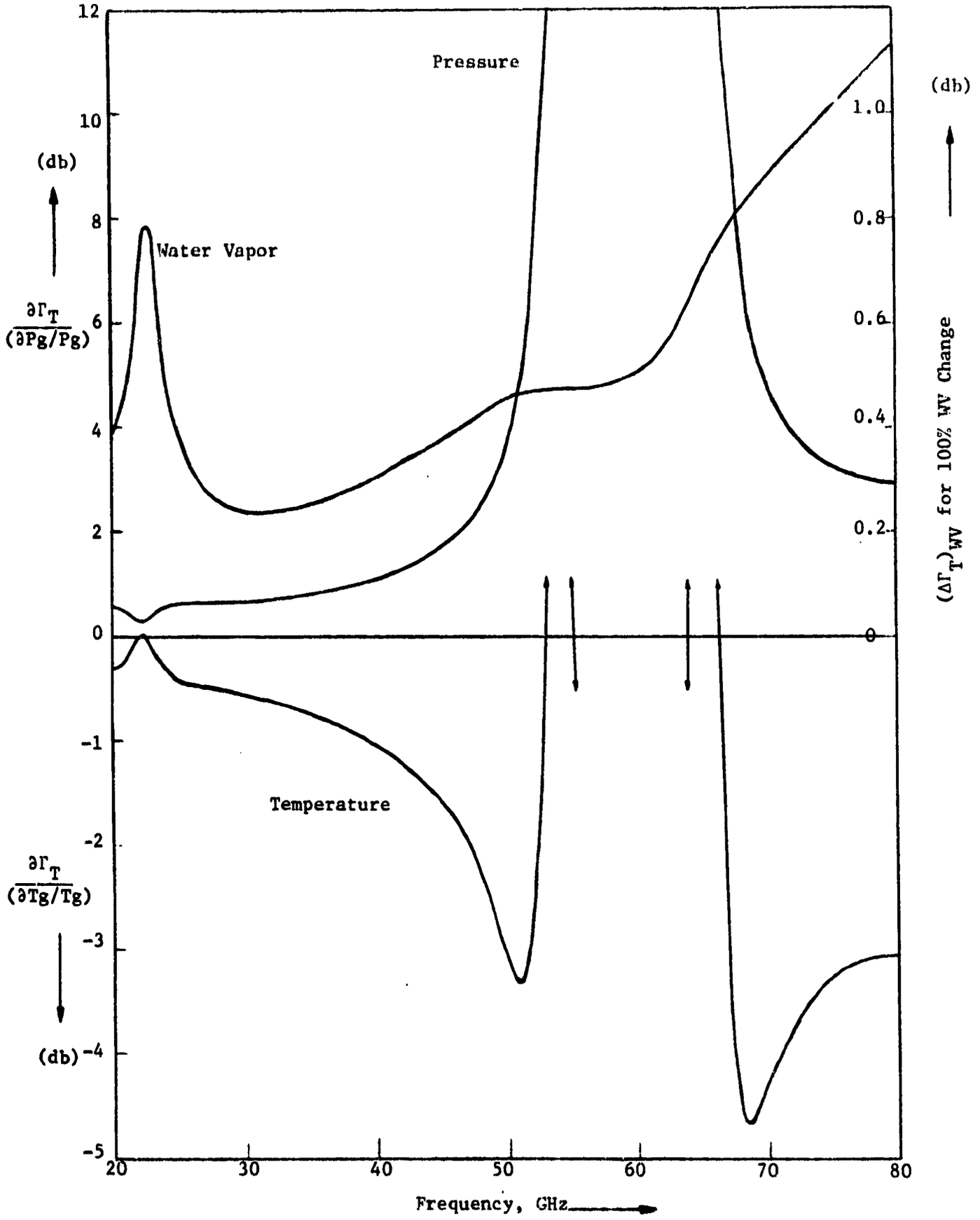

Figure 7. Derivatives of the integrated absorption coefficient w.r.t. pressure, temperature and water vapor.

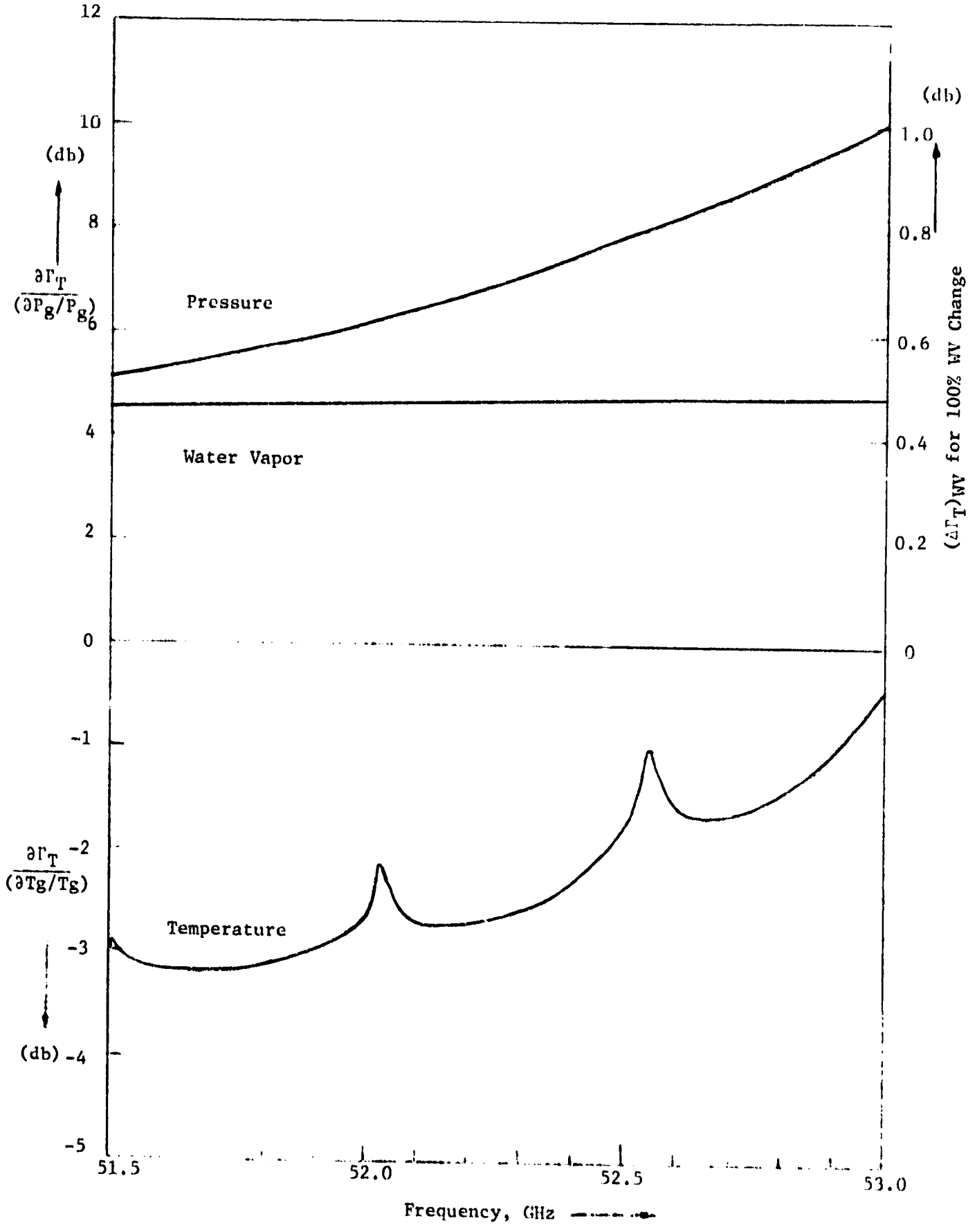

Figure 8. Derivatives of the integrated absorption coefficient.

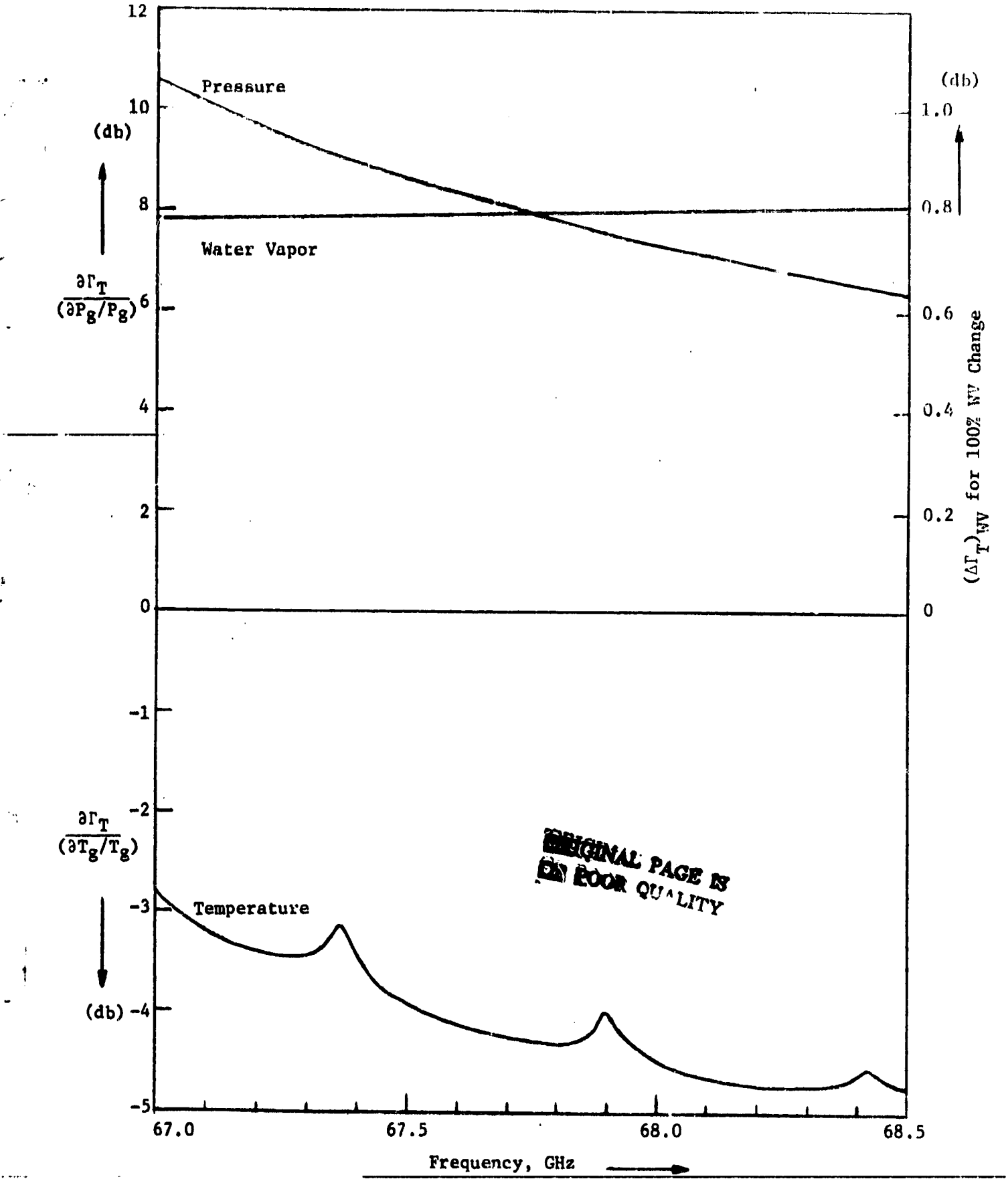

Figure 9. Derivatives of the Integrated Absorption Coefficient.

7. Choice of Operating Frequencies

7.1 The Index of Surface Pressure

The basic measurements from which surface pressure can be deduced are of the return echo signal strengths, P_R, at several frequencies. We define an index of pressure, S, which is obtained by combining the measurements together as a product thus

$$S = \prod_i \left[\left| P_R(\nu_i) \right|^{r_i} \right] \qquad 7.1$$

and the indices r_i are introduced to give greater flexibility in the choice of operating frequency. From equation 3.7 we can write the return signal at a frequency ν_i as

$$P_R(\nu_i) = \frac{0.25}{h^2} \left(P_T \eta_T \eta_R r^2 \right)_{\nu_i} \left(\tau_o^2 \tau_w^2 \right)_{\nu_i} \left(\tau_A^2 \sigma^0 \right)_{\nu_i} \qquad 7.2$$

so that S can be expressed as the product of instrumental, atmospheric and background factors:

$$S = S_I S_A S_B \, . \qquad 7.3$$

The instrumental factor

$$S_I = \prod_i \left| \frac{0.25}{h^2} \left(P_T \eta_T \eta_R r^2 \right)_{\nu_i} \right|^{r_i} \qquad 7.4$$

should be a constant and this requirement affects the system design but not the choice of frequencies. Measurements will be made of the ratio of return signals at a pair of frequencies since experimentally this is easier than measuring absolute intensity. With this technique

$$r_i = -r_{i+1} \quad \text{(for odd values of i)} \qquad 7.5$$

and it can be seen that neither the antenna radius, if it is the same for all frequencies, nor the orbit height will affect S_I. If the transmitted powers at each pair of frequencies are controlled to have a constant ratio and if the system efficiencies do not change then S_I will have a constant value which can be determined.

The atmospheric factor

$$S_A = \prod_i \left\{ \left(\tau_o^2 \, \tau_w^2 \right)_{\nu_i} \right\}^{r_i} \qquad 7.6$$

includes contributions from oxygen and water vapor transmissivities only. The operating frequencies must be chosen so that this is dependent on pressure but independent of the temperature profile and the water vapor profile. Details of the selection procedure to satisfy these conditions are given in Section 7.3.

The background factor

$$S_B = \prod_i \left\{ \left(\tau_A^2 \, \sigma^o \right)_{\nu_i} \right\}^{r_i} \qquad 7.7$$

characterizes the effects of absorption by other atmospheric constituents and sea surface reflectivity. Although these by nature vary widely it will be shown in Section 7.2 following that with reasonable assumptions the product S_B can be made constant when the frequencies are simply related.

When the conditions established here are met by the appropriate choice of operating frequencies and system design then the index, S, will be the desired measure of pressure. Measurements of other atmospheric parameters are not needed.

7.2 Sensitivity to Background

The assertion in Section 3.3 that the frequency dependence of the reflected signal strength, due to ocean reflectivity and atmospheric absorption other than by oxygen and water vapor, can be expressed as $10^{(a+b\nu+c\nu^2)}$ will be justified later. However it will be shown here that undesirable background sensitivity of this form can be eliminated from the ultimate determination of pressure by combining the measured reflected intensities at appropriately chosen frequencies. This removes the necessity for simultaneous subsidiary measurements to determine the unknown and variable coefficients a, b and c.

Using

$$\left(\tau_A^2\,\sigma^0\right)_{\nu_i} = 10^{(a+b\nu+c\nu^2)} \qquad 7.8$$

it is readily shown by substitution that S_B is independent of the coefficients a, b and c which describe the background variation of the following conditions on r_i and ν_i are satisfied

$$\sum_i r_i = 0$$

$$\sum_i r_i \nu_i = 0 \qquad 7.9$$

$$\sum_i r_i \nu_i^2 = 0 \ .$$

Adopting the ratio measuring technique, where the indices are related by equation 7.5, immediately satisfies the first condition in equation 7.9. To satisfy the other conditions a minimum of three pairs of frequencies are required in which case the conditions simplify to

$$(\nu_2-\nu_1) + \alpha(\nu_4-\nu_3) + \beta(\nu_6-\nu_5) = 0$$

and $\qquad 7.10$

$$(\nu_2^2-\nu_1^2) + \alpha(\nu_4^2-\nu_3^2) + \beta(\nu_6^2-\nu_5^2) = 0$$

where $-r_3 = r_4 = \alpha$ and $-r_5 = r_6 = \beta$, while making $-r_1 = r_2 = 1$ is not an effective limitation on either system design or performance.

The relationships 7.10 between α, β and the frequencies ν_i are purely mathematical with an infinite number of solutions. It should be noted that the conditions can still be fulfilled if $\nu_2 = \nu_3$ and/or $\nu_4 = \nu_5$, so that the instrument can have 4, 5 or 6 operating frequencies.

7.3 Temperature and Water Vapor Sensitivity

The contribution to the strength of the return signal, P_R, due to oxygen and water vapor absorption has been written in terms of the total integrated

absorption coefficient Γ_T as $10^{-0.2\Gamma_T}$. Then the contribution of these constituents to the atmospheric factor, S_A, of the pressure index, S, expressed as a product in equation 7.6 can now be put in terms of the sum of the coefficients $\Gamma_T(\nu_i)$ as

$$S_A = 10^{-0.2 \sum_i |r_i \Gamma_T(\nu_i)|} \qquad 7.11$$

The sensitivities of S then to changes in surface pressure, temperature and water vapor content (characterizing profile changes) are thus simply related to the corresponding sensitivities of the summation term.

For S to be independent of the temperature profile we require that

$$\frac{\partial}{(\partial T_g/T_g)} \left[\sum_i r_i \Gamma_T(\nu_i)\right] = 0 \qquad 7.12$$

which becomes, using equation 6.4

$$\sum_i r_i \, (y_i+1) \, \Gamma_T \, (\nu_i) = 0 \qquad 7.13$$

Similarly for S to be independent of water vapor content we obtain the condition that

$$\sum_i r_i \left[\Delta\Gamma_T(\nu_i)\right]_{wv} = 0 \qquad 7.14$$

Equations 7.13 and 7.14 represent further constraints on the choice of operating frequencies which, in contrast to conditions 7.10, are dependent on atmospheric absorption characteristics. The derivative data of Fig.7 are necessary to enable a set of frequencies related by equations 7.10 simultaneously to satisfy these conditions.

7.4 Pressure Sensitivity and Signal to Noise Ratio

Since pressure is the parameter to be determined it is important that the sensitivity of the index S to pressure changes should be maximized. The fractional change in S for a fractional change δ in the surface pressure can be obtained from equations 7.11 and 6.3 thus

$$\frac{\delta S}{S} = -0.2 \ln(10) \, \delta\left(\sum_i r_i x_i \Gamma_T(\nu_i)\right) \qquad 7.15$$

It is apparent from an examination of Fig.7 that this is greatest when the main pressure sensing channels are well into the oxygen absorption band. However the very heavy atmospheric absorption reduces the strength of the return signal and a consideration of the signal to noise characteristics becomes essential. Obviously a compromise between increasing pressure dependence and decreasing signal to noise must be achieved. This affects the choice of operating frequencies in a way which will depend on the optimization criterion adopted.

The potential instrument performance can be analysed with sufficient accuracy for the present purpose by considering the noise generated within the receiver and omitting the much lower noise contributed by atmospheric emission and reflection. It is assumed that the bandwidth of the signal, Δf, can be adjusted to optimize the system performance and that the detector and signal bandwidths are equal. When the received signal is measured with a square law detector followed by an integration of time constant t, the noise-to-signal ratio at a frequency ν_i is

$$\frac{N_i}{P_R(\nu_i)} = \frac{1}{(t\Delta f)^{\frac{1}{2}}} \left\{1 + \frac{4kT\Delta fF}{P_R(\nu_i)}\right\} \qquad 7.16$$

and the overall noise-to-signal ratio of a multifrequency instrument is obtained by adding the squares of the individual ratios thus:

$$\left(\frac{N_s}{S}\right)^2 = \frac{1}{(t\Delta f)} \sum_i r_i^2 \left\{1 + \frac{4kT\Delta fF}{P_R(\nu_i)}\right\} \qquad 7.17$$

If the bandwidth is chosen to minimize this then the minimum occurs when

$$(4kT\Delta fF)^2 = \frac{\sum_i r_i^2}{\sum_i \left\{r_i^2 / P_R^2(\nu_i)\right\}}$$

which by substituting for Δf in equation 7.17 gives

$$\left(\frac{N_s}{S}\right)^2 = \frac{8kTF}{t}\left[\left\{\sum_i r_i^2 \sum_i r_i^2/P_R(\nu_i)^2\right\}^{\frac{1}{2}} + \sum_i r_i^2 / P_R(\nu_i)\right] \qquad 7.18$$

Assuming that in the absence of atmospheric attenuation the received power is the same, P_o, in all channels then

$$P_R(\nu_i) = P_o\, 10^{-0.2\Gamma_T(\nu_i)} \qquad 7.19$$

and equation 7.18 may be written in terms of $\Gamma_T(\nu_i)$.

The overall accuracy of the instrument can be conveniently described by an index of performance, I, obtained by dividing equation 7.15 squared by equation 7.18 to give

$$I^2 = \frac{(.21\ln(10))^2\, \delta^2\, t\, P_o}{8kTF} \cdot M \qquad 7.20$$

where

$$M = \frac{\left\{\sum r_i x_i\, \Gamma_T(\nu_i)\right\}^2}{\left\{\left[\sum r_i^2 \sum r_i^2\, 10^{0.4\Gamma_T(\nu_i)}\right]^{\frac{1}{2}} + \sum r_i^2\, 10^{0.2\Gamma_T(\nu_i)}\right\}} \qquad 7.21$$

The index I is the ratio of (the change in pressure index for a fractional change in pressure, δ) to (noise). The minimum value of I = 1 determines the limiting sensitivity of the instrument. M is a merit function which depends only on the choice of operating frequencies and the properties of the atmosphere. The numerator is a measure of sensitivity to pressure and the denominator is a measure of atmospheric absorption. The system performance is optimized by choosing frequencies which maximize M.

Another useful indicator of the suitability of a chosen frequency set can be obtained from the change in index S for a fractional change in the surface pressure. This is the fractional accuracy which the signal processing of the instrument must be designed to provide. The total fractional accuracy will be divided among the channels and when equally distributed between n channels this may be written as

$$F_A = 0.2\ \ln(10)\ \frac{\delta}{|r_i| n^{\frac{1}{2}}}\ \left|\ \sum_i r_i x_i \Gamma_T(\nu_i)\ \right| \qquad 7.22$$

The value of F_A is determined by the choice of frequencies and has important consequencies for system design which will be considered in Section 11 when the errors associated with sea surface statistics are analysed. Meanwhile, it is important to recognize that a relatively large value of F_A will pose less technical problems than a small value.

7.5 Operating Frequencies

The conditions established in the preceding sections and the derivative data of Fig.7 enable a systematic search to be made for suitable sets of operating frequencies. Such a search has been made both numerically and by hand with different restrictions on the number and range of operating frequencies. The results are presented in Table 2 to enable easy comparison of the alternatives available.

Numerical optimization for the selection of up to six frequencies plus the two indices, α and β, has been performed with the frequency range restricted to between 40 and 60 GHz. Over this relatively narrow range the smooth frequency dependence of water vapor absorption is adequately represented by the background expression and it is not necessary to impose separately the water vapor independence constraint, equation 7.14. The results of these calculations, Table 2, line 1, show that the best performance is obtained using five frequencies. The maximum of 51.2 GHz is effectively limited by the requirement for temperature independence. This keeps M low and leads to the need for very precise measurement as indicated by the fractional accuracy, F_A = 0.05%. When the requirement for temperature independence is relaxed only four frequencies are needed, Table 2, line 2. The maximum frequency at 53.2 is further into the band and consequently the merit function is larger. In this case, the required fractional accuracy of 0.31% can more easily be met but a subsidiary measurement of the atmospheric temperature to an accuracy of 1.2^{o} is required to allow the pressure to be accurately determined.

An indication of the typical behavior of the merit function as the frequencies are changed is shown in the example of Fig. 10. This contour plot of log M for continuous changes in the lowest frequencies and the spread of frequencies shows that M falls rapidly as the highest frequency increases above about 53 GHz. The maximum value of M lies on something of a plateau so that a

Line	System Restrictions	Operating Frequencies ν_i, GHz	Indices α, β	Temperature Sensitivity	Water Vapor Sensitivity	Merit Function M	Fractional Accuracy Required Per Channel
				Change in surface value ≡ 3mb pressure change			
1	40-60 GHz range	40.0 43.0 (43.0) 48.1 48.2 51.2	-1.14 0.97	1200°C	(not computed)	0.075	0.05%
2	As 1, but with temperature requirement relaxed	40.0 43.9 (43.9) 50.2 (50.2) 53.2	-1.29 1.42	1.2°C	(not computed)	0.605	0.31%
3	4 Frequencies 22-60 GHz range	32.0 36.8 (36.8) 45.8 (45.8) 52.2	-1.5 1.5	20°C	0.5 gm cm^{-2}	0.24	0.15%
4	4 Frequencies below and 2 above 60 GHz	27.94 35.30 44.76 52.76 67.44 73.28	-1.65 1.0	500°C	25 gm cm^{-2} (from derivatives)	3	0.76%
5	4 Frequencies below and 2 above 60 GHz	29.25 36.55 44.80 52.80 67.51 73.01	-1.6 1.0	2500°C	26 gm cm^{-2} (from numerical simulation)	3	0.74%

Table 2: Characteristics of Various Sets of Operating Frequencies

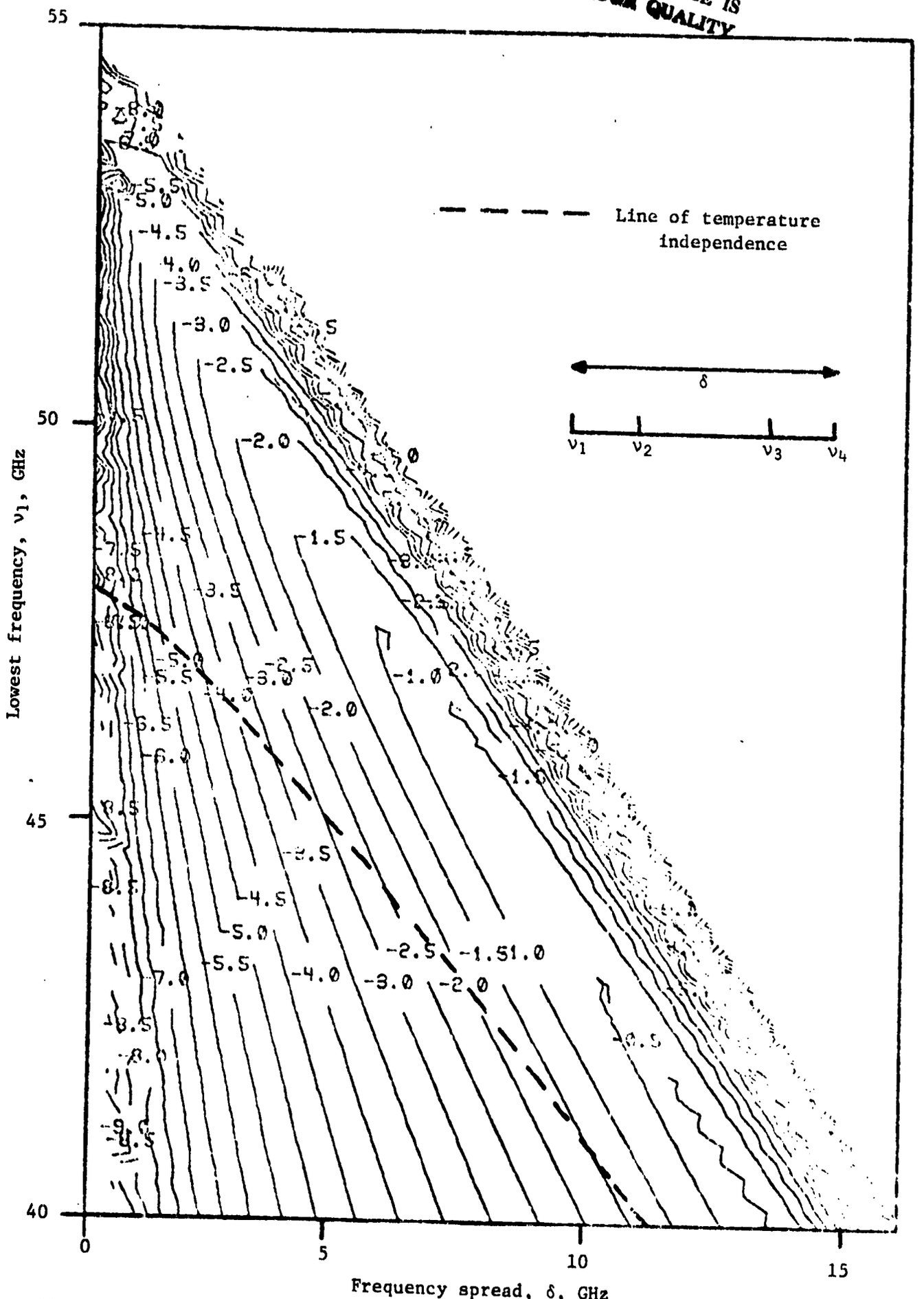

Figure 10. Contour plot of the log of the Merit function, M, for a four frequency system.

reasonably wide range of sets of operating frequencies are available without excessive reduction in M. Superimposed on the contour plot is a line of temperature independence and it is seen that within the range of frequencies on the plot maximum M and temperature insensitivity cannot simultaneously be obtained and a compromise choice must be made. This plot was obtained using smooth derivative data so that detailed structure associated with the individual lines of the oxygen band is not included. The smoothing was done to ensure that the optimization routine did not select a local maximum of M but naturally any final choice of operating frequencies would allow for this structure. The plot shown here is representative of several which were computed for different numbers of and arrangements of frequencies and is a useful indicator of where to look for appropriate sets of frequencies. It is apparent that for maximizing M the spread for frequencies should be as wide as possible and the main pressure sensing channel should not be further into the band than about 53 GHz. There would also seem to be advantage to be gained by extending the lower frequency limit below 40 GHz.

With the lower boundary set to 22 GHz it is necessary to introduce specifically the water vapor independence constraint equation 7.14, because of the effect of the spectroscopic line at 22 GHz. Operating frequencies were sought by hand and near optimum sets could be obtained in which the fine structure of the derivative data was also used. In this case the requirements for temperature and water vapor insensitivities were found to be competing constraints. Consequently compromise solutions were sought in which temperature and water vapor sensitivities were reduced to reasonable levels. The results of this analysis are shown on line 3 of Table 2 and the required knowledge of temperature (better than $\pm$ 20^{o}C) and total water vapor content (better than 0.5 gm cm^{-2}) are well within the capabilities of current instrumentation. However, so long as the operating frequencies are restricted to the lower side of the oxygen absorption band little improvement in Pressure Sounder performance can be expected.

When the possibility of using one pair of frequencies in the 60 to 100 GHz range was explored systems with significantly better potential performance were obtained. In the six frequency schemes shown in lines 4 and 5 of Table 2 sensitivity to the temperature profile has been reduced to an insignificant level.

The water vapor content change of 25 gm cm^{-2} which gives a change in the pressure index equivalent to a 3mb pressure change is approximately three times larger than the 7 gm cm^{-2} maximum value of this parameter and if necessary a correction could be applied using climatological models. The sensitivity to pressure as indicated by the merit function and fractional accuracy is better than when only the lower wing is used. This is the result of using two channels with high sensitivity to pressure. The consequently less exacting demands on signal processing accuracy allow more flexibility in system design as will be discussed in Section 11.

7.6 Summary

The procedure which has been used for the selection of sets of operating frequencies is summarized in the block diagram of Figure 11. The examples of Section 7.5 show that sets can be chosen which reduce or effectively eliminate dependence of the signal on background effects, temperature profile and water vapor content. The following section is devoted to the validation of the selection procedure which is indicated at the bottom of Figure 11.

The selection of an optimum set of operating frequencies is the subject of continuing investigation. The numerical optimization routine is being extended to include a reformulation of the background effects. No great improvement in the sensitivity to pressure is to be expected since this is limited by how close the main pressure sensing channels are to the band center. So long as maximum global coverage is required with transmitter powers of a few watts, the limit has probably been reached in the final examples of Table 2. However gains may be possible in the treatment of temperature, water vapor and background effects by using slightly different frequencies or perhaps by using an arrangement of frequencies not yet examined although it is not anticipated that more than six frequencies will be used.

The ultimate decision on which of the possible sets should be implemented will depend on other factors which are considered in later sections of this report. The advantages apparent in Table 2 which are gained by using a wide frequency range must be carefully weighed against the disadvantages of a degree of uncertainty in the applicability of the background model over the full range and more difficult instrument design, particularly with regard to absolute calibration.

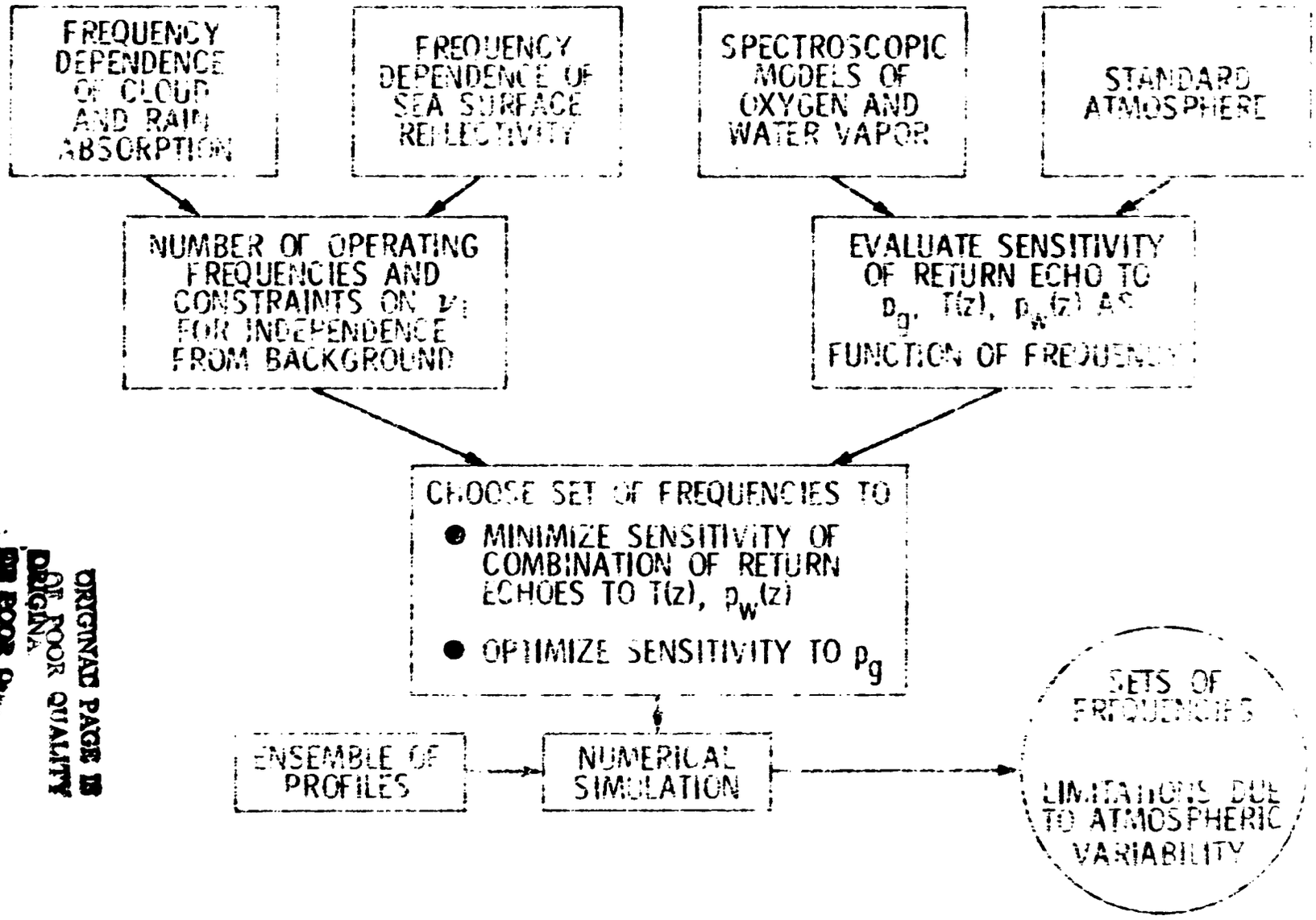

Figure 11. Summary of procedure for selecting operating frequencies.

8. Numerical Simulations

8.1 The Use of Radiosonde Data

The method was detailed in Section 7.3 by which the operating frequencies of the pressure sounder could be chosen such that the measurement of pressure was independent of variations in atmospheric temperature and water vapor profiles. The very simple form of the standard atmosphere and the simplest of profile variations were used as a basis for the necessary calculations, but in practice the atmosphere varies greatly from this stylized profile, particularly so for the water vapor content. It is necessary therefore to assess the validity of the design procedure by examining whether the desired independences are achieved with a much wider range of profiles.

Radiosonde measurements provide a data set ideally suited to this purpose. The standard radiosonde observations made and recorded on punched cards are pressure, temperature, relative humidity and wind velocity for the surface and height, temperature, relative humidity and wind velocity at 35 standard pressure levels from 1000mb to 2mb. Surface pressure is recorded to the nearest mb, temperature to an accuracy of $0.1^{\circ}C$, relative humditiy to 1% and height to the nearest 10 m. The wind velocity data is not needed for the numerical simulations. The standard pressure levels are at intervals of 50 mb from 1000 to 200 mb, at 25 mb intervals to 100 mb, at 80 mb, at 10 mb intervals to 30 mb and then for the pressures 25, 20, 15, 10, 7, 5, 4, 3 and 2 mb.

A test set of radiosonde data from two weather stations was used. The data were from a) Cold Bay, Alaska where the surface temperature varied from $4^{\circ}C$ to $18^{\circ}C$ and the total water vapor content varied between 0.89 and 4.02 gm cm^{-2} and b) Balboa, Panama with corresponding variations of $23^{\circ}C$ to $31^{\circ}C$ and 4.13 to 5.61 gm cm^{-2}. In Figure 12 some of these profiles are plotted to indicate the typical variations. The U.S. Standard Atmosphere is included for comparison.

8.2 Calculations

Numerical simulation of the experiment was carried out by the following method. At each of the frequencies of a set chosen by the procedures of Section 7 the transmissivity was calculated for a vertical path through the

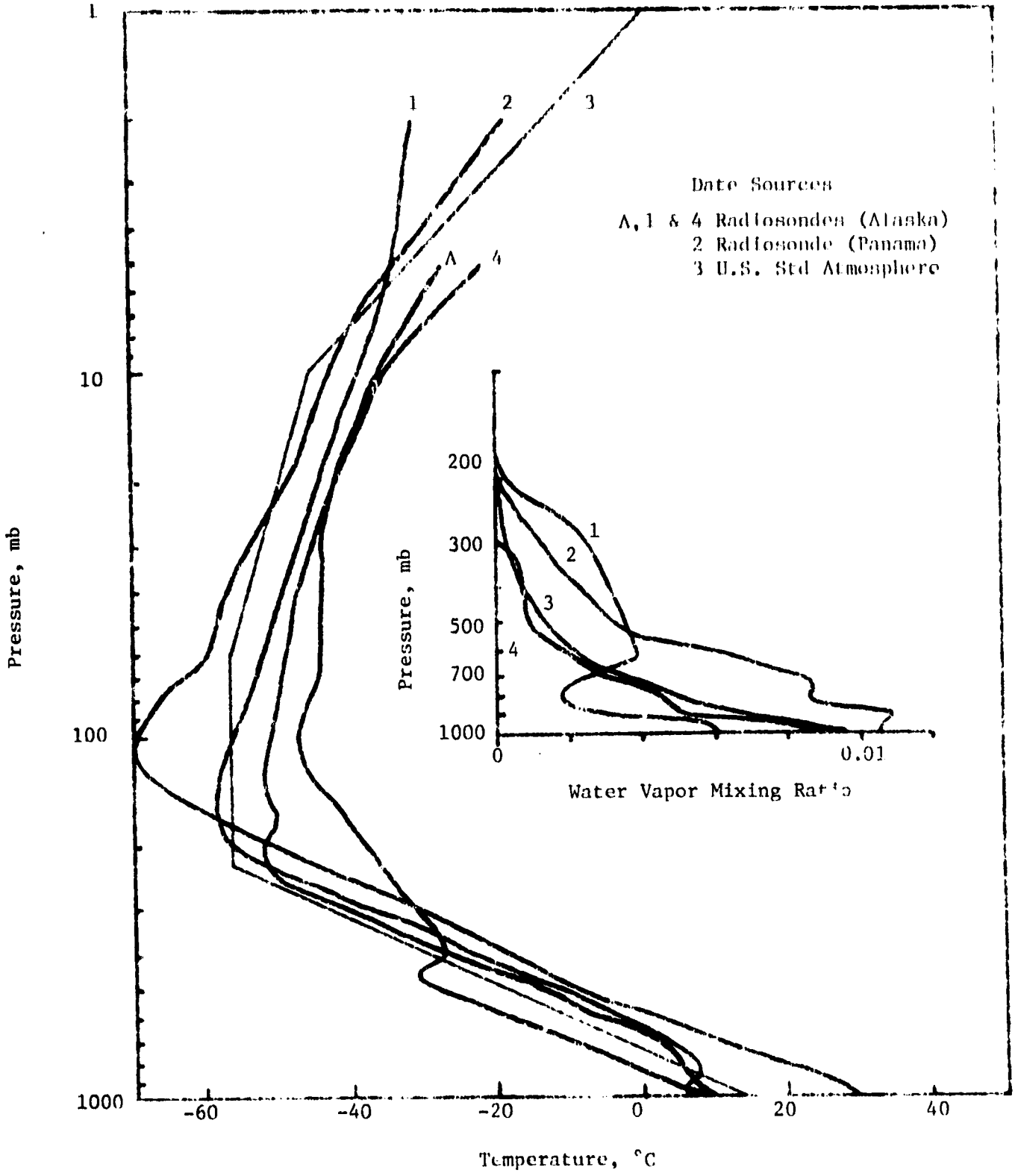

Figure 12. Some typical temperature and water vapor profiles.

atmosphere defined by a radiosonde observation data set. The absorption due to oxygen and water vapor for each layer between the standard pressure levels was determined from the spectroscopic models of Sections 4 and 5. The thicknesses of the layers were obtained directly from the height data and corresponding average values of temperature, pressure and water vapor mass mixing ratio were found from the radiosonde measurements. The average values used were simply the linear means of the parameter values at the standard pressure levels bounding each layer. This linear averaging procedure is sufficiently accurate since a large number of layers are involved and it was the method used when the derivatives for Section 6 were computed.

An estimate was also included of the absorption by the atmosphere remaining above the highest pressure level for which data was recorded. The chosen frequencies are away from the line centers so that this contribution is small. It was approximated by the absorption of a layer of thickness equal to twice the scale height at 2mb with a pressure of half the minimum recorded level.

The integrated transmissivities thus computed were combined according to equation 7.11:

$$S_A = 10^{-0.2 \sum_i \left| r_i \Gamma_T (\nu_i) \right|} \qquad 8.1$$

The frequency set is one for which the background factor, S_B, is 1 and if a design is assumed such that the instrumental factor is unity then S_A is also the index of pressure, S.

This procedure was repeated for the large number of radiosonde observations of the test set so that a scatter diagram could be plotted of the measured surface pressure against the simulated pressure index, S.

However, the radiosonde measurement of surface pressure is not the best value for an atmosphere characterized by the parameter averages which were used to compute the transmissivities. Furthermore, it is only recorded to an accuracy of ±0.5 mb and this was found to be comparable to the standard

deviation in the scatter of points. Consequently, the surface pressure was computed by integrating through the vertical column sampled by the radiosonde. The total pressure is the sum of contributions Δp from each of the layers where

$$\Delta p = \frac{g}{R} \frac{\Delta h}{T^*_{ave}} p_{ave} \qquad 8.2$$

Here g is the acceleration of gravity, R is the gas constant for dry air, Δh the thickness of the layer, p_{ave} is the average pressure and T^*_{ave}, the average virtual temperature is given in terms of the average water vapor mass mixing ratio β_{ave} and the average temperature, T_{ave} as

$$T^*_{ave} = \frac{1 + 1.609\ \beta_{ave}}{1 + \beta_{ave}} \quad T_{ave} \qquad 8.3$$

The factor of 1.609 derives from the ratio of the mean molecular weight of dry air and the molecular weight of water vapor.

In Figure 13 the measured surface pressure is plotted against the computed value. The systematic difference of about 1.2mb is attributable to the inadequacies of the parameter averaging procedure. The distribution of points about the best fit line has a standard deviation of about 0.4mb and most of this is probably rounding error associated with the integral representation of the measured surface pressure.

8.3 Results

The six frequency system defined in line 4 of Table 2 was evaluated in this way and the resulting scatter diagram of measured surface pressure against simulated pressure index, S is plotted in Figure 14. This diagram shows that the relationship between the index and surface pressure is satisfactorily represented by a straight line over the range of pressure from 950 to 1020 mb. All of the points lie within ±1.5mb about this straight line so that the pressures as deduced from the simulated signals are within ±1 mb of the actual surface pressures. From the Gaussian distribution curve fitted to the histogram of errors, inset in the figure, the standard deviation of the deduced pressure can be estimated to be about 0.65 mb. In Figure 15 the error in pressure (deduced minus actual to the nearest mb) is plotted as a function of

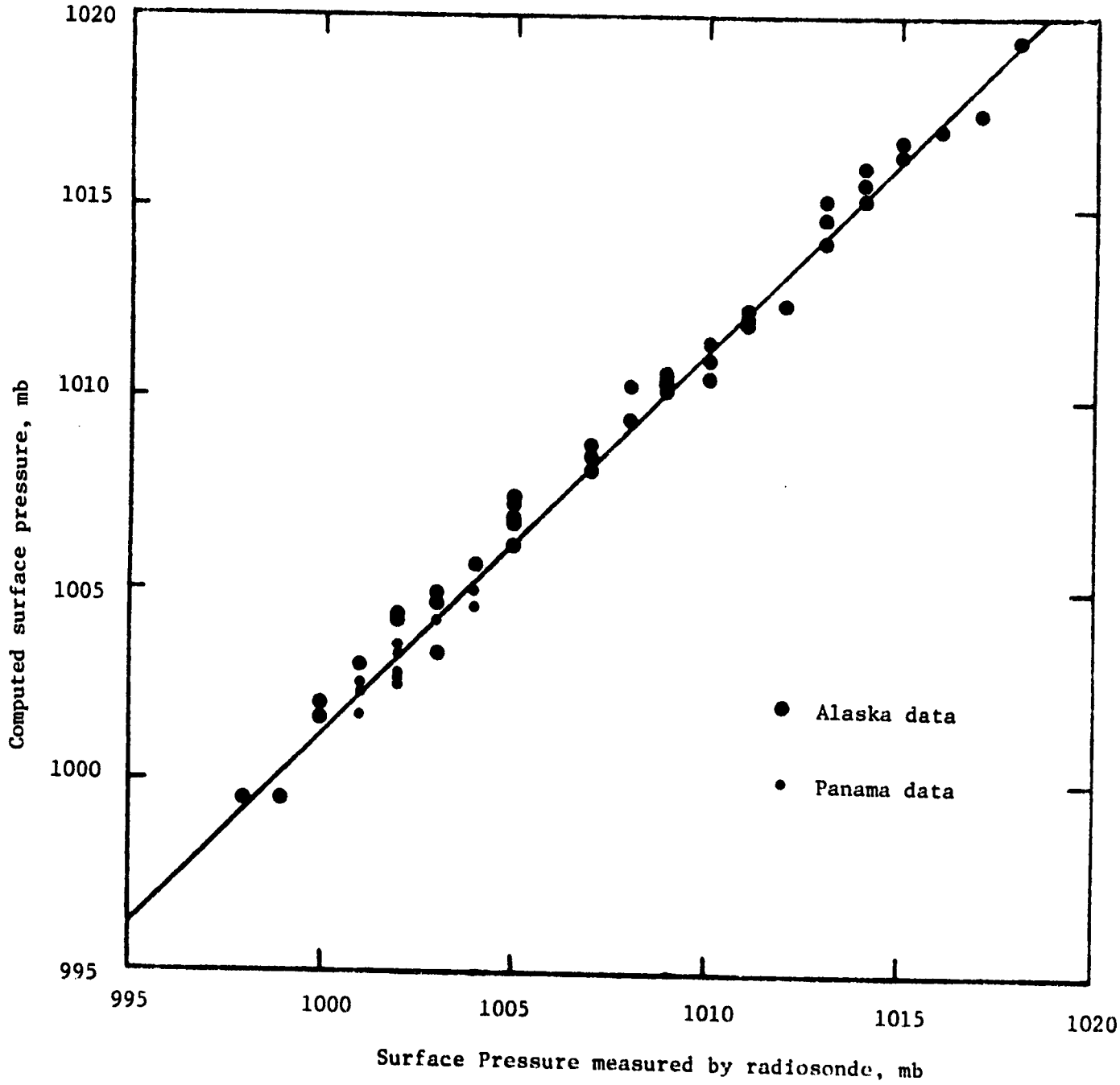

Figure 13. Computed surface pressure vs. reported surface pressure.

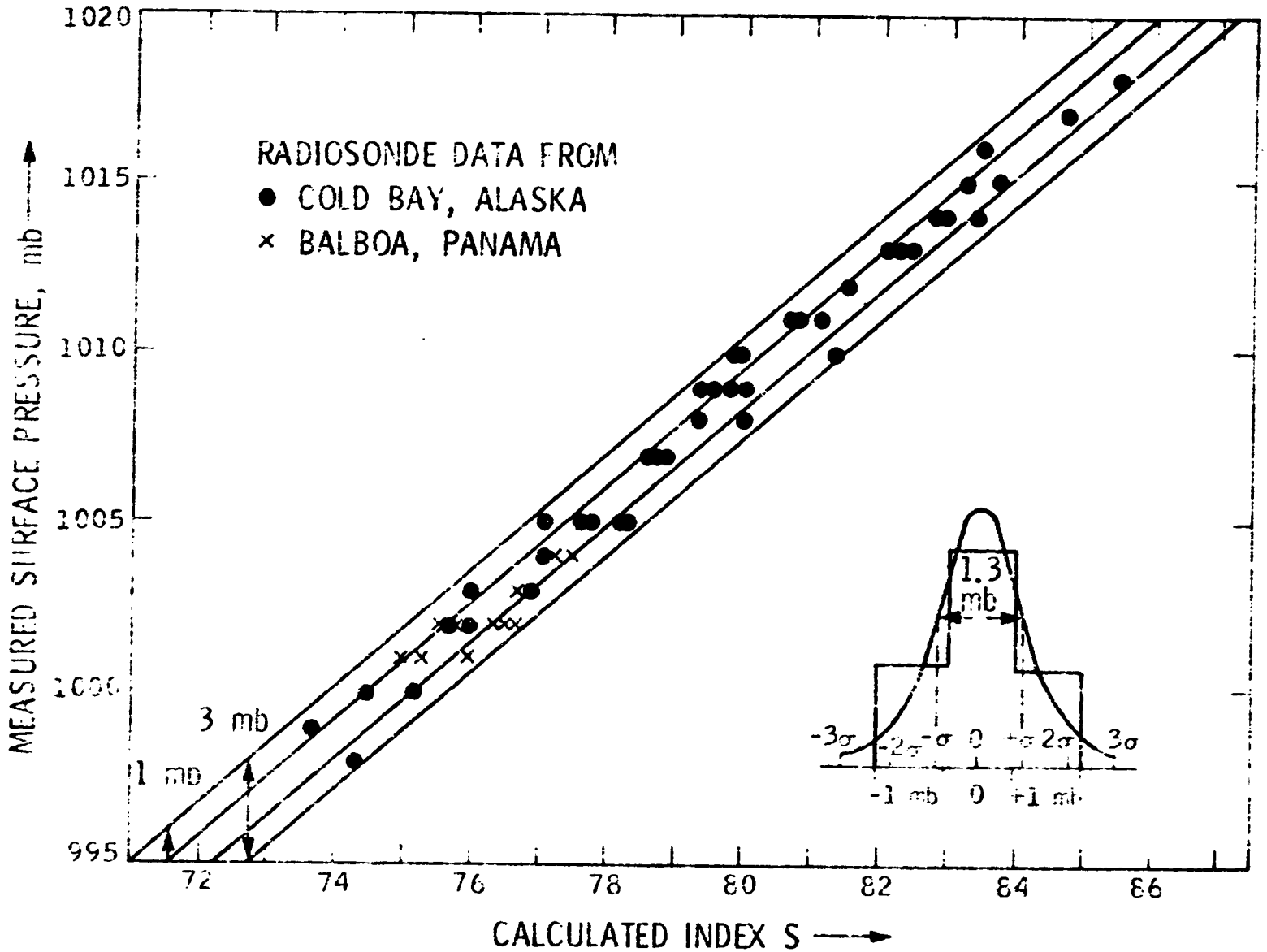

Figure 14. Scatter Diagram. Numerical Simulation of Index From a 6 Frequency 3 Ratio Pressure Sounder

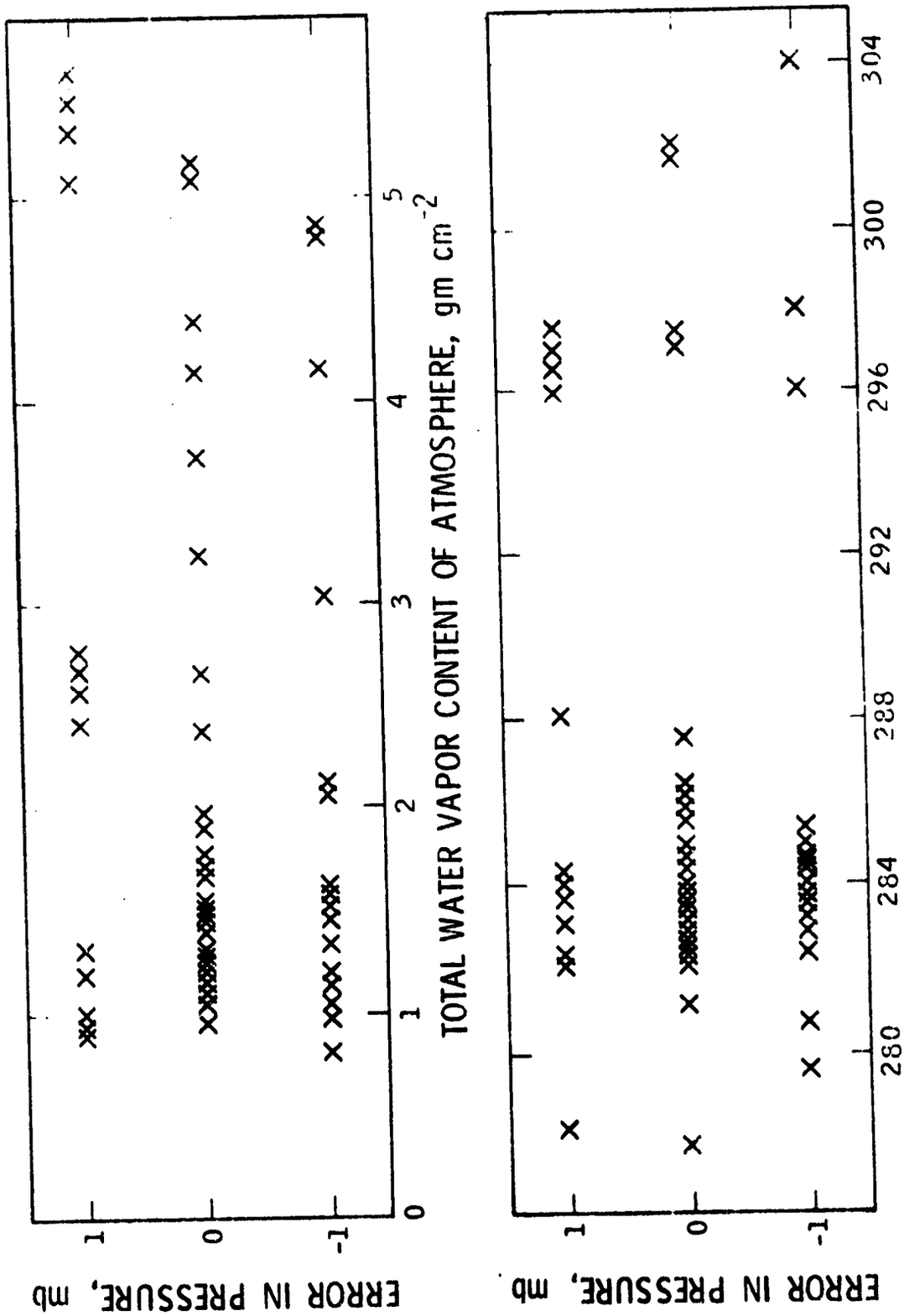

Figure 15. Error in pressure vs. atmospheric water vapor and surface temperature.

both surface temperature (Fig. 15a) and total water vapor content (Fig. 15b). It can be seen that no correlation exists and that the designed independence of the measurement from temperature and water vapor appears to have been achieved.

When the computed rather than the measured surface pressure is plotted on a scatter diagram against the simulated index, Figure 16, the scatter of points is noticeably reduced. This reduction in scatter reveals an offset of the Panama data points which is indicative of a small residual temperature and/or water vapor sensitivity. If due solely to temperature effects then the sensitivity is such that a 30° change in surface temperature will change the pressure index by an amount equivalent to a 3mb pressure change while if solely a water vapor effect then a 7 gm cm^{-2} change is equivalent to a 3 mb change. For these levels of dependence a correction with climatological models is satifactory.

However, with a slight modification to the operating frequencies the required insensitivities can be restored. Using the six frequencies of line 5, Table 2, the pressure index was computed for the test set of radiosonde data. The resulting scatter diagram, Figure 17, exhibits no temperature or water vapor sensitivity and the standard deviation in the deduced pressure is about 0.4mb. While some of this scatter is probably a computational effect due to summation over a finite number of layers there is evidence that variability in the atmospheric structure is also a contributory factor. For example, the point most seriously in error, marked A on Figure 17, corresponds to the profile A in Fig. 12 which has a temperature inversion at 7 km.

These numerical simulations employing a wide range of atmospheric structures have demonstrated that frequency sets may be chosen so that a pressure index can be determined which is sufficiently insensitive to the temperature and water vapor profiles that subsidiary measurements of other meteorological parameters are unnecessary. It has also been demonstrated that a measurement error of not more than 0.4mb, attributable to variability of the atmospheric structure which cannot be modelled, can be achieved with an appropriate choice of operating frequencies. Refinement of the selection procedure may enable this error to be decreased further while sophistication

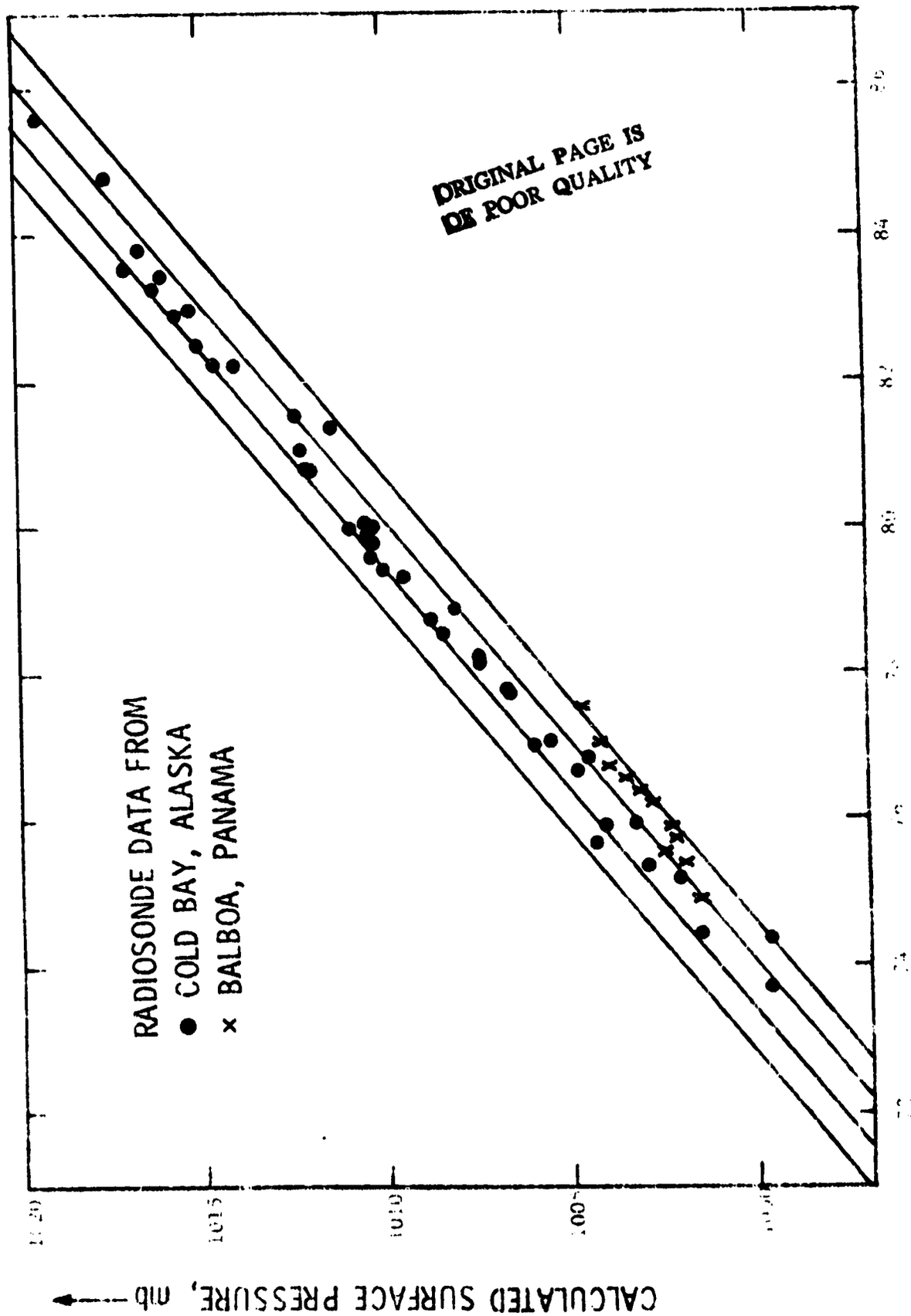

Figure 16. Scatter diagram. As for Figure 14 but using the calculated surface pressure.

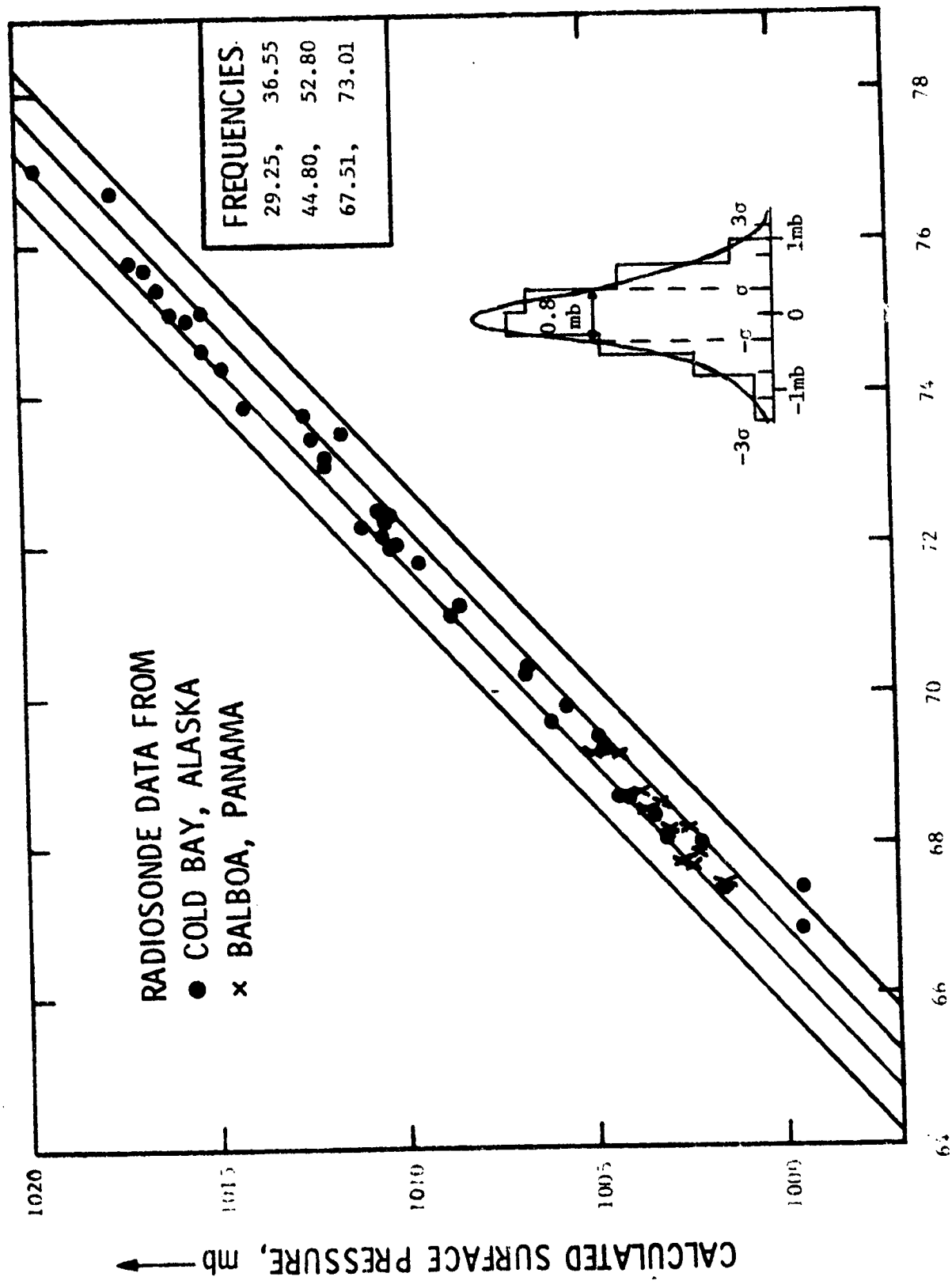

Figure 17. Scatter diagram. Numerical simulation with the same radiosonde data as in Figure 14 but with a different set of frequencies.

of the computational analysis may reduce its upper limit. This atmospheric variability error is one contribution to the total error in surface pressure as measured by the microwave sounder. Other sources of error will be considered in later sections of this report.

9. The Effects of Other Atmospheric Constituents

The presence in the atmosphere of absorbing gases, other than those already considered, has a slight effect on the choice of operating frequencies. In contrast, atmospheric aerosols have considerable influence on the optimum frequencies as well as on other aspects of the system design.

Several minor constituents have spectral lines in the 25 to 75 GHz band of interest (Waters, 1976) but only ozone has absorption through a zenith path of sufficient strength that it may possibly affect the measurement. In addition some attention must be given to the spectrum of the $O^{16}O^{18}$ isotopic form of molecular oxygen so that the line centers may be avoided.

Cloud and rain are the principal aerosols and of these non-precipitating cloud is of greater concern because of its more frequent occurrence. The particular advantage that a microwave sounder has over an optical instrument is its ability to penetrate clouds. Nevertheless, clouds do absorb millimeter waves and both the degree of absorption and its variation with frequency affect the system design. The assumption made in Section 3.3 concerning the form of the frequency variation will be justified and the absolute value of absorption, which is needed to determine the signal-to-noise errors associated with a variety of cloud cover conditions. will be obtained from an analysis of scattering by aerosols.

9.1 Ozone

The mixing ratio of ozone in the atmosphere varies with altitude and exhibits a maximum at between 20 and 30 km. Although the total zenith path attenuation is small, frequencies near the line centers should be avoided because the ozone content and hence the absorption varies by up to 50% daily, seasonally and spatially. The strongest ozone lines between 20 and 75 GHz are listed in Table 3 (Depannemaecker et al, 1977) with their peak absorption coefficients. The strongest line is at 67.356 GHz and at this frequency the integrated ozone zenith opacity is typically .04db based on an integrated depth of 20 cm. By comparison oxygen zenith opacity is nearly 5db at the same frequency. This is the only line of any real concern.

Frequency, GHz	Absorption, nepers km^{-1} at 220°K
23.860	2.3
28.960	2.1
30.052	4.6
30.181	2.6
36.022	3.4
37.832	7.2
42.832	3.9
43.653	6.8
44.871	2.1
50.034	2.6
51.976	6.3
53.688	14.3
55.356	6.0
58.094	5.1
61.347	4.5
61.927	16.4
63.072	2.7
65.236	16.9
66.059	5.9
67.250	4.0
67.356	48.4
68.421	3.1

Table 3. The strongest ozone lines in 20 to 75 GHz range with approximate peak absorptions at pressure of one atmosphere. [From Depannemaecker et al., 1977 and Kakar, R.K., private communication.]

A Lorentz line shape is generally used and the linewidth parameter has a value of about 2.3 MHz mb^{-1} (Waters, 1976). Calculations of the zenith attenuation are shown in Figure 18 for various ozone profiles. At frequencies greater than 100 MHz from the line center the absorption is reduced to less than 1/4 of the peak value. For the operating frequencies in Table 2 the closest are 80 MHz and 150 MHz from the line center. Ozone absorption for these is respectively about 0.010db and 0.005db while a 3mb pressure change causes a change in attenuation of about 0.03db. A correction to the pressure measurement based on the known global distribution of ozone would probably reduce ozone associated errors by a half. In the first case this is still significant at 0.5mb but in the latter case, the final frequency set of Table 2, the error is reduced to an acceptable level of about 0.2mb.

9.2 $^{16}O^{18}O$

The isotopic species of oxygen, ^{16}O, ^{17}O and ^{18}O, are present in the atmosphere in the following fixed relative abundancies:

^{16}O	99.76 %
^{17}O	.037%
^{18}O	.204%.

Thus the relative abundancies of the principal molecular forms of oxygen are

$^{16}O_2$	99.52%
$^{16}O^{18}O$	.41%
$^{16}O^{17}O$	.07%

Each of these has a distinct spectrum but in Section 5 and 6 the spectrum of only the dominant $^{16}O_2$ molecule was used as the basis for the frequency selection calculations. Since absorption accuracies at the level of fractions of 1% are needed to satifactorily measure pressure the proportion of $^{16}O^{18}O$ present in the atmosphere is possibly sufficient to affect the calculations.

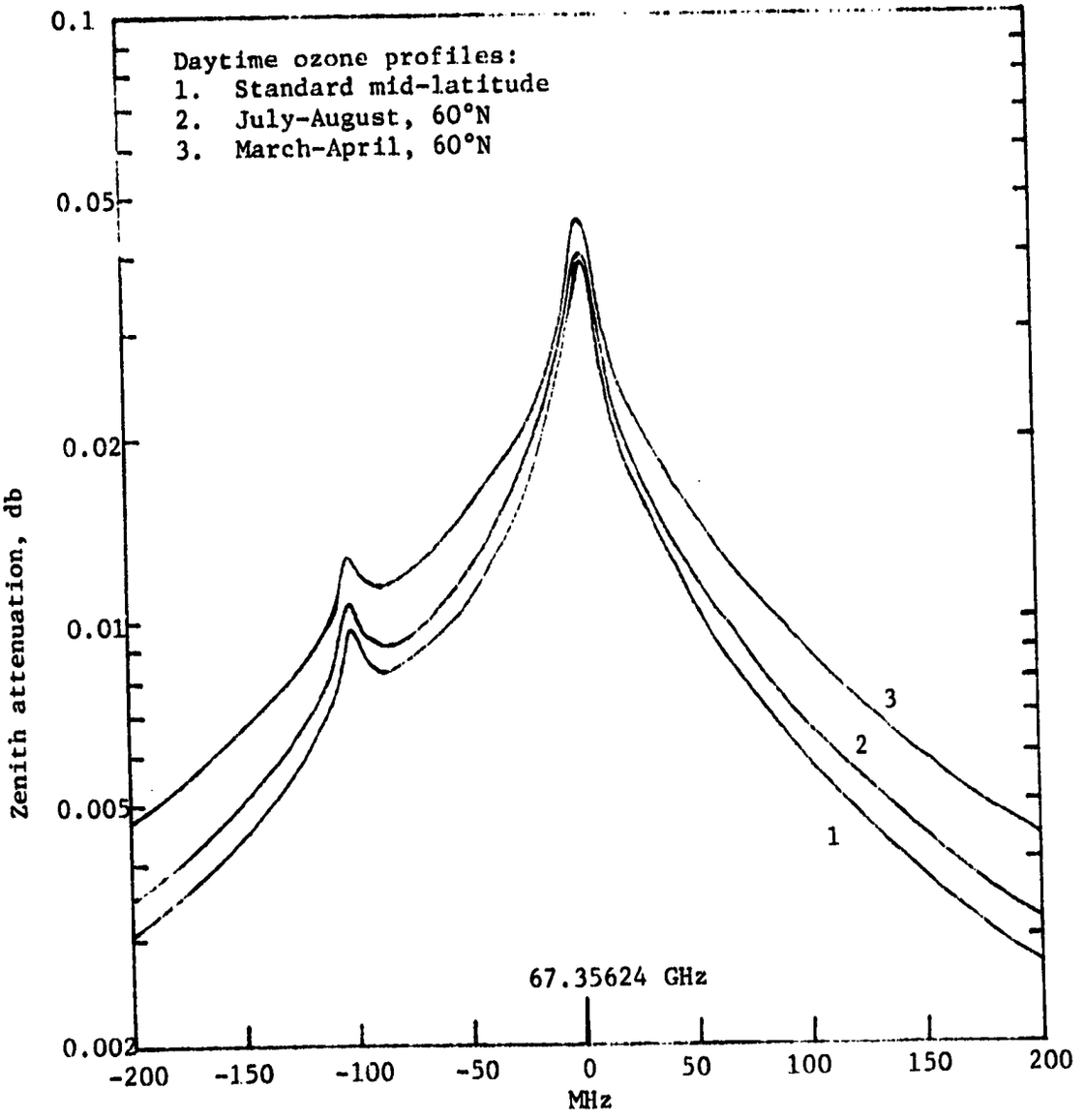

Figure 18. Zenith attenuation due to ozone near the 67.356 GHz line for various profiles.

The spectrum of $^{16}O^{18}O$ differs from that for $^{16}O_2$ in having twice the number of lines. This is because the lack of symmetry allows for even as well as odd values for the rotational quantum number N. As a consequence the line intensities for $^{16}O^{18}O$ are approximately half as strong as those of the corresponding transitions for $^{16}O_2$. Accurate values for the resonance frequencies of $^{16}O^{18}O$ have been published for only a few lines near the band center (Steinbach and Gordy, 1975). Typically the lines for $^{16}O^{18}O$ are displaced from the corresponding $^{16}O_2$ lines by a few hundred MHz. Since there are also lines for even N resonance peaks will be scattered throughout the $^{16}O_2$ valleys. However, in the band wings, where the operating frequencies of the pressure sounder have been chosen, even the $^{16}O_2$ peaks are not very prominent. It can therefore be expected that little if any effect of the isotope substitution will be noticeable except perhaps within a few MHz of the $^{16}O^{18}O$ line centers. Calculations are being undertaken using the molecular constants of $^{16}O^{18}O$ to determine the positions of other line centers so that these may be avoided if absorption effects are found to be significant.

9.3 Absorption by Clouds

9.3.1 Water Clouds

The presence of cloud in the vertical path through the atmosphere will affect the return signal through absorption and scattering of the incident radiation. Much theoretical work has been published using electromagnetic scattering theory to compute attenuation coefficients, γ, and backscattering cross sections, σ (Ryde and Ryde, 1945, Goldstein, 1951, Gunn and East, 1954). Rigorous experimental verification of the following theoretical calculations for cloud absorption (as well as other aerosol effects) is generally unsatisfactory because it is not possible with a reasonable number of measurements to fully specify the spatial and temporal fluctuations in aerosol density and drop size distribution. However, the measure of agreement which is obtained, is commonly accepted as evidence that the theory provides an adequate basis for the description of electromagnetic wave interaction with aerosols.

For a theoretical analysis of the absorption by clouds at the frequencies of interest here, the Rayleigh scattering approximation is valid

since the wavelengths are much larger than the diameter of the water droplets in cloud (<0.05 mm). Frequency dependences in γ and σ arise from this and also from the dielectric properties of the scattering water droplets. To complete the quantitative description of absorption by clouds, assumptions must be made about the distribution of drop sizes. Laws and Parsons (1943) made extensive measurements and their results are most commonly used.

With an analysis using these fundamentals Gunn and East showed the attenuation coefficient, γ, due to water cloud to be given, in db km^{-1}, by the expression

$$\gamma = 0.434 \frac{6\pi}{\lambda} \frac{M}{\rho} \mathrm{Im}(-K) \qquad 9.1$$

where the wavelength, λ, is in cm, the density of water, ρ, is in gm cm^{-3} and the density of water in the cloud M is in gm m^{-3}. There is a frequency dependence within Im(-K) which is given in terms of the real and imaginary parts, ε' and ε'', of the complex dielectric constant, $[\varepsilon]$, as

$$\mathrm{Im}(-K) = \frac{3\varepsilon''}{(\varepsilon' + 2)^2 + \varepsilon''^2} \qquad 9.2$$

and details are given in Section 10 of the Debye model from which ε' and ε'' can be obtained.

Benoit (1968) fitted straight lines through Gunn and East's discrete data shown in Figure 19 and arrived at the following empirical expression for the absorption coefficient:

$$\gamma = M \nu^{b_1} e^{a_1} \text{ db km}^{-1} \qquad 9.3$$

The frequency, ν, is in GHz, the frequency index, b_1, for water cloud has a value of 1.95 and the temperature coefficient, $a_1 = -6.866\ (1 + 0.0045T)$ when T is in ^{o}C. More recent calculations by Crane (1971) extend the data available to 100 GHz, Figure 20.

In Section 3.3 it was assumed that integrated cloud absorption could be modelled by a second order polynomial variation with frequency, viz

$$\Gamma_A = a + b\nu + c\nu^2, \qquad 9.4$$

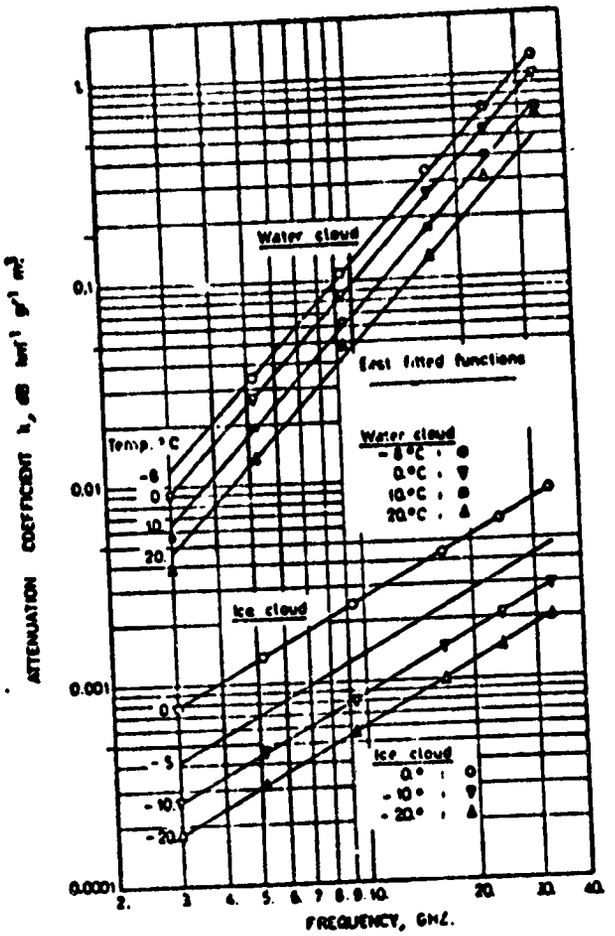

Figure 19. Attenuation coefficient for clouds (From Gunn and East, 1954)

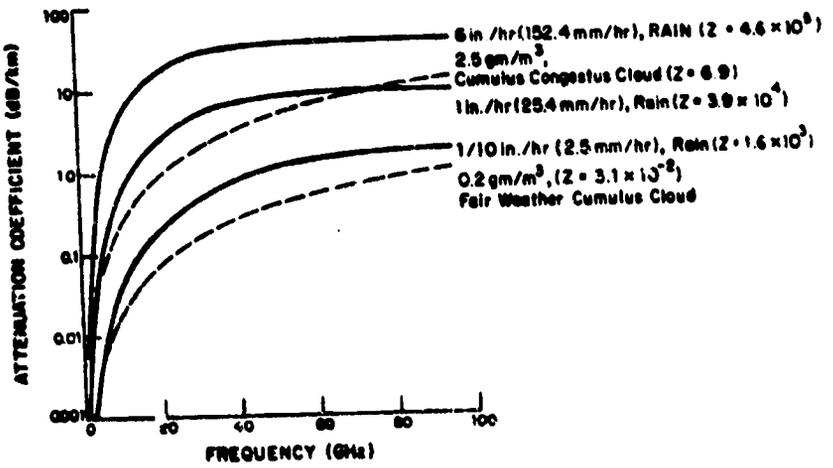

Figure 20. Attenuation coefficient as a function of frequency for liquid scatterers (From Crane, 1971)

and it can readily be shown now that the above data fits such an expression. In Table 4 values for the absorption coefficient, calculated assuming the empirical relationship, 9.3 above, are compared with values from a best fit polynomial. The values agree to better than 0.2%. Cranes smooth curves in Figure 20 can also be fitted, within the 25 to 75 GHz range by other second order polynomials and the computed lines are indistinguishable from the original lines. Of course, the actual values of a, b and c are not important since selecting frequencies which satisfy the conditions 7.9 makes the pressure index, S, independent of these coefficients.

The magnitudes of the absorption coefficients for various cloud types are important since these will determine the strengths of the received signals. Thus heavier clouds will produce a reduction in signal-to-noise ratio which ultimately limits the accuracy of the pressure measurement. Several models of water clouds are commonly used, in which the cloud is characterized by the density, M, and its thickness. The product of these two factors gives the integrated liquid water content, W_L, usually expressed in gm cm^{-2} and in accordance with equation 9.3 attentuation is directly proportional to W_L at any fixed frequency. Cloud temperature is also significant, being generally in the range -10^oC to $+20^oC$ and varying with cloud altitude, latitude and season. Table 5 shows attenuation for a representative set of cloud types at 0^oC for the frequencies 25, 50 and 75 GHz. The values will be slightly less for higher temperatures.

For more than half the time, atmospheric liquid water is essentially zero (Staelin et al, 1976) while the overwhelmingly dominant cloud types have $W_L < 0.05$ gm cm^{-2}. Occasionally liquid water exceeds 0.6 gm cm^{-2}, the highest example in the table but these are generally small scale phenomena. The presently envisaged pressure sounder designs should allow meaningful pressure measurements to be made with attenuations of up to 5db in the highest frequency channel. Since this corresponds to $W_L \sim .1$ gm cm^{-2} almost all cloud conditions will be accommodated. Further discussion of potential coverage is reserved for Section 12 following a complete description of the instrument and an analysis of signal-to-noise errors in Section 11.

Frequency GHz	Cloud Absorption, db	
	From $\gamma = (\text{constant}) \times \nu^{1.95}$	From $\gamma = -4.412 \times 10^{-2} + 4.175 \times 10^{-3}\nu + 8.412 \times 10^{-4}\nu^2$
25	0.5869	0.5860
35	1.1312	1.1325
45	1.8466	1.8472
55	2.7309	2.7302
65	3.7825	3.7814
75	5.0000	5.0008

Table 4. Approximation of cloud absorption by a second order polynomial.

Density gm m^{-3}	Depth km	Integrated Liquid Water gm cm^{-2}	Absorption, db		
			25 GHz	50 GHz	75 GHz
Stratus Clouds					
0.1	1.0	0.01	0.05	0.21	0.48
0.25	1.0	0.025	0.13	0.54	1.21
Fair Weather Cumulus					
0.5	1.0	0.05	0.27	1.07	2.41
1.0	1.0	0.1	0.54	2.14	4.82
Tall Cumulus					
1.0	2.0	0.2	1.07	4.29	9.64
2.0	3.0	0.6	3.22	12.9	28.9
Cirrus					
0.05	0.5	0.0025	.00006	.00012	.00018
0.10	1.0	0.01	.00023	.00046	.00070

Table 5. Integrated absorption for some typical clouds.

9.3.2 Ice Clouds

High altitude cirrus clouds frequently occur and will often extend for 1000 km or more. These clouds consist of small ice crystals, are of low density, $M < 0.1$ gm m^{-3}, and are generally thin layers, $\lesssim 1$ km. The dielectric constant for ice is very much different from that for water and this results in a much lower absorption coefficient. Gunn and East's data for ice cloud attenuation are also shown in Figure 19 and Benoit fitted these with an empirical expression of the same form as equation 9.3. The indices for ice clouds have the values $b_1 = 1.006$ and

$$a_1 = 8.261(1 - 1.767\times10^{-2}\,T - 4.374\times10^{-4}\,T^2) \qquad 9.5$$

This is very close to a linear variation with frequency and is consequently readily accounted for by a second order polynomial. However, the values in Table 5 for attenuation by typical ice clouds, at 3 or 4 orders of magnitude less than for water clouds, indicate that the presence of cirrus will have an insignificant effect on pressure measurement.

9.4 Absorption by Precipitation

The distribution of drop sizes in rain typically exhibits a maximum number of drops with radii near 0.5 mm (Marshall and Palmer, 1948) and, depending on the rain rate, some drops may have radii up to 4 mm. The wavelengths most suitable for pressure sounding are $\sim$ 4 mm and longer. Because of the similarity of these dimensions it is necessary to use Mie scattering theory to determine the absorption coefficients for rain. The results of such calculations by Crane are included in Figure 20 and the smooth curves can be adequately fitted with a second order polynomial in frequency. Absorption by rain can therefore be accounted for provided the total attentuation is not excessive. Typical rain cloud states must next be examined to establish the conditions under which this requirement may be satisfied.

Figure 21, taken from Valley (1965) shows how the liquid water content of clouds varies with altitude for surface rain-rates between 2 and 20 mm hr^{-1}. The total atmospheric liquid water in these cases can be estimated to vary from 0.04 to 0.15 gm cm^{-2}, partly in the form of small cloud aerosols and the

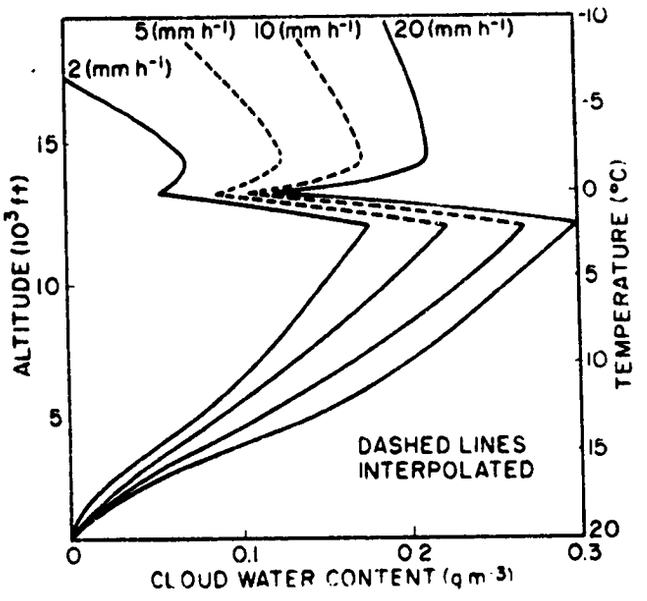

Figure 21. Liquid water content of cloud for various precipitation rates. (From Valley, 1965)

remainder as larger rain drops. Without more detailed information on the vertical extent of the rain it is impossible to evaluate with any accuracy the total attenuation but assuming, for the 2 mm rain rate, a 3 km rain depth the total rain and cloud attenuation can be estimated using Figure 20 to be less than 5db at 75 GHz. Other precipitation conditions occur with rather thinner cloud of perhaps higher density which could result in similar total absorption. It is possible then that the pressure sounder may give meaningful measurements with rain rates of a few millimeters per hour. Its use in heavier rain appears to be limited by attenuation rather than inaccuracies in the frequency variation model.

More detailed and accurate analysis of absorption by rain is not necessary at this time since an instrument whose use was limited to non-precipitating clouds would nevertheless be worthwhile. Similarly, although models exist for absorption by other forms of precipitation which would allow a superficial assessment, a detailed consideration of the possibilities for measurements in hail, sleet and snow is of no great value because of their comparatively infrequent occurrence.

9.5 Backscatter from Aerosols

If it is sufficiently strong, backscatter from aerosols could affect the measurement of surface pressure by this proposed microwave transmissometer technique since the return signals would not have been attenuated by the important lower levels of the atmosphere. However, the following analysis shows that cloud reflectivity is not significant for those conditions when attenuation is small enough to allow the pressure measurement to be made. The reflectivity of rain has been used extensively in weather radars to monitor the position and extent of precipitation. At millimeter wavelengths the backscatter cross-section is large enough to affect the pressure sounder and will probably be a more severe limitation on measurement capability than attenuation by rain.

The electromagnetic scattering problem was solved using the Rayleigh approximation by Gunn and East (1954) to give the magnitude of the radar signal reflected by cloud as

$$P_R = P_T \frac{\pi^4 A L}{8 h^2 \lambda^4} |K|^2 \sum D^6 . \qquad 9.6$$

Most of the symbols have been defined in Section 3. L is the depth of the cloud, D is the particle diameter and the summation is over the distribution of drops in unit volume. There is an implicit frequency dependence in $|K|^2$ which is given in terms of the complex refractive index $[\varepsilon]$ by

$$K = \frac{[\varepsilon] - 1}{[\varepsilon] + 2} \quad . \tag{9.7}$$

It is convenient for our purposes to define a normalized cloud backscatter cross-section, σ_c, which may be directly compared with the sea surface cross-section, σ^o, as used in equation 3.4. At the same time we follow convention by introducing the radar reflectivity factor

$$Z = \sum D^6. \tag{9.8}$$

Then

$$\sigma_c = \frac{\pi^5 |K|^2 L Z}{\lambda^4} \times 10^{-7} \tag{9.9}$$

and is a dimensionless ratio when a confusing array of units is used: L in km, Z by convention in $mm^6\ m^{-3}$ and λ in cm. Using the Laws and Parsons drop-size distribution for cloud Z can be computed and this results in the following empirical relationship with M, the cloud liquid water density in $gm\ cm^{-3}$ (Valley, 1965)

$$Z = 0.048\ M^2 \quad . \tag{9.10}$$

Now we are in a position to evaluate σ_c. Sufficient indication of the possible effects of cloud backscatter can be obtained with an estimate of σ_c for cloud conditions some five times worse than can be penetrated by the pressure sounder. At the highest operating frequency $\lambda = 0.4$ cm and $|K|^2 \sim 0.5$, depending on temperature. For a deep, heavy, essentially opaque cloud with $M = 1\ gm\ m^{-3}$ and $L = 5$ km, equivalent to a total water content $W_L = 0.5\ gm\ cm^{-2}$, then equation 9.9 gives

$$\sigma_c = 1.43 \times 10^{-4} \text{ or } -38\text{db}. \tag{9.11}$$

This is insignificant when compared to the sea surface cross-section, $\sigma^o \sim +8$db so that backscatter from water clouds will not affect the measurements.

Little data is available on the reflectivity of cirrus (ice) clouds but Valley gives an order of magnitude estimate of Z, viz

$$Z \sim 570\ M^{1.6} \qquad 9.12$$

Particularly bad cirrus clouds might have M = 0.1 gm m^{-3} and L = 1 km so that at λ = 0.4 cm for which $|K|^2 \sim 0.2$ equation 9.9 gives

$$\sigma_c = -25\text{db}. \qquad 9.13$$

This is more than three orders of magnitude less than σ^o and will therefore not influence measurements at nadir. Off nadir measurements may occasionally be affected by cirrus cloud reflections if equation 9.12 is accurate.

For rain, the backscatter cross-section σ_r is also given by equation 9.9 except that Z must be replaced by Z_e, an equivalent radar reflectivity factor. This is necessary because the Rayleigh approximation becomes invalid and Z must be computed using the exact Mie equations with the Marshall-Palmer rain drop-size distribution. Valley has surveyed the data relating Z_e to the rainfall rate R (mm hr^{-1}) and at millimeter wavelengths a good approximation is

$$Z_e = 300\ R^{1.5}\ (mm^6 m^{-3}) \qquad 9.14$$

Thus, when R = 5 mm hr^{-1} and L = 1 km the normalized backscatter cross section at a wavelength of 0.4 cm is

$$\sigma_r = 3\text{db}. \qquad 9.15$$

This is consistent with the results from Godard (1970). Being of the same order of magnitude at σ^o it can only be overcome with a pulsed radar and precision range-gating. The marginal improvement in coverage which would be provided by this technique does not by itself warrent the increased complexity and expense.

Sleet, snow and hail also reflect at millimeter wavelengths. For these the equivalent radar reflectivity has a similar value to Z_e for rain and measuring capability will be similarly limited.

9.6 Broken Cloud and Other Non-Uniformities

All of the design considerations to this point have implicitly assumed that the properties of the field of view, smeared for the integration time for a single pressure measurement , are constant and hence that the signal levels are constant, except for statistical fluctuations due to the sea surface. Any non-uniformity along the orbit track such as pressure changes, temperature or water vapor profile differences, the presence of broken cloud and sea state changes will cause the strength of the return signal to vary. Of these the most important is broken cloud since it can produce sudden large changes in the echo signal from nearly adjacent points while the other factors will cause smooth changes. When the cloud sizes are comparable with the instantaneous field of view then the received signal will fluctuate along the track. However, if the cloud sizes are much smaller but extend over a large area then the changes will be smooth. In either case the effect is to modify the frequency dependence of the background as modelled by equation 7.8. An analysis of this problem indicates how all non-uniformities may be accounted for since they can all be incorporated into the background effect.

It has been shown that the appropriate choice of frequencies will make the background factor, S_B, unity when the cloud absorption coefficient is represented by the second order polynomial, equation 7.8. When uniformly thick cloud covers a fraction p of the field of view smeared along the orbit track then the cloud transmissivity, τ_A, can be written

$$\tau_A^2 (\nu_i) = (1 - p) + p\ 10^{-0.2(a + b\nu_i + c\nu_i^2)}. \qquad 9.16$$

The background factor is obtained from the combination

$$S_B = \prod_i \left\{\tau_A^2 (\nu_i)\right\}^{r_i}. \qquad 9.17$$

This will be unity only when p = 0, 1 and can be expected to have the largest error when p = 0.5.

It was indicated in Section 9.3 that the worst cloud through which measurements would be possible will attenuate the signal by 5db at 75 GHz over a one-way path. Using the values of the coefficients a, b and c

given in Table 4 for this cloud state and the frequencies of Table 2, line 5 the calculated value of S_B when p = 0.5 is

$$S_B = .9763.$$

This represents an error in the measured index S of 2.4% which is equivalent to a 3mb pressure error. This is a significant error but it is for the worst case and generally errors will be much less or zero. For example, when the cloud attenuation is 1db at 75 GHz and p is again 0.5 the error is < 0.5 mb.

The effects of broken cloud can be mitigated in several ways. The most easily implemented method is to divide the integration time into several shorter periods, calculate the index S for each subdivision and finally to average S over the total integration time. Processing the measurements in this way means that errors only occur when the subdivisions are partially filled with cloud. Alternatively, or indeed additionally, fluctuations in the return signal strength due to broken cloud might be utilized to apply a correction to S.

Other possibilities involve modifications to the procedure for selecting the operating frequencies. A different function of frequency to describe the background effects may be advantageous. Water cloud is the most important background effect and it has a nearly quadratic frequency dependence (equation 9.3). Thus a three parameter model for background with the form

$$\Gamma_A = a + b\nu^2 + c\nu^4 \qquad 9.18$$

would adequately account for uniform cloud and at the same time significantly reduce the effect of broken cloud. The alternative to this is to extend the numerical optimization routine, as indicated in Section 7.6, so that it includes a cloud effect term. This can be used with a set of cloud states to select operating frequencies which minimize sensitivity to uniform and partial cloud cover conditions.

All of these methods for reducing the broken cloud errors are the subject of continuing studies as are the effects of smooth variations in the other factors. A quantitative assessment of the relative frequency of various atmospheric states is necessary to enable a decision to be made on which of the alternative techniques is most appropriate.

10. Sea Surface Reflectivity

10.1 Normalized Backscatter Cross-Section

Reflection of electromagnetic waves by the sea surface is characterized by the normalized backscatter cross-section, $\sigma(\theta)$, which is defined as the ratio of (the radar backscatter cross-section) to (the horizontal surface area intercepted by the antenna beam) (Tomiyasu, 1974). Being a ratio, $\sigma(\theta)$ is dimensionless and physically represents how good a reflector the sea surface is in comparison to a perfectly reflecting sphere. The average value of $\sigma(\theta)$ is a function of surface roughness, complex dielectric constant, temperature, frequency, polarization and angle of incidence. Of equal importance to the average value of $\sigma(\theta)$ is the statistical variation in the reflected signal due to the nature of the sea surface and this is considered in Section 10.8. Many papers have been published in recent years on both the theory of sea surface reflectivity and its experimental measurement (see Barton,1975, Skolnik, 1970 for bibliographies).

Measurements of the angular dependence of $\sigma(\theta)$ confirm the theoretical results of Barrick (1968) shown here in Figure 22. With transmitter powers limited to a few watts it will only be possible to make measurements at or near to the vertical. The nadir value, σ^{o}, is greatest for low values of the mean sea slope, s. For these calm sea states $\sigma(\theta)$ falls off rapidly as the angle from nadir increases. As the sea becomes increasingly rough the maximum value is reduced but $\sigma(\theta)$ falls less rapidly away from the normal. Consequently rough sea states are better for making measurements away from the subsatellite track. The rapid fall-off of $\sigma(\theta)$ at angles greater than $\sim 15^{o}$ for commonly occurring sea states limits the use of the Microwave Pressure Sounder to nadir and near nadir operation.

10.2 Theory

In the composite model commonly used the slope of the sea surface is characterized by two roughness scales corresponding to gravity and capillary waves. Significant waveheights, H, associated with the first range typically up to 10m while for the latter the characteristic length is of the order of centimeters. The sea surface is considered to be rough

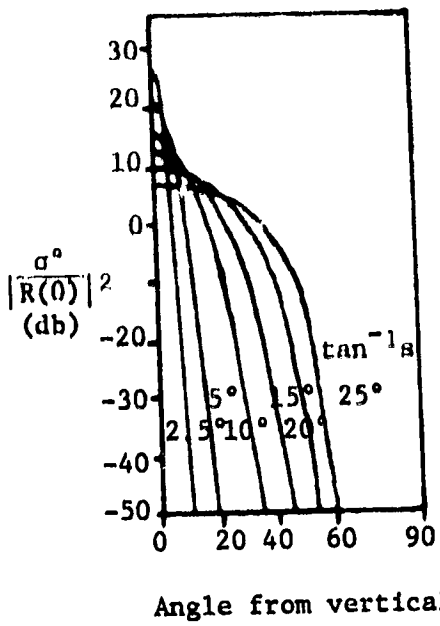

Figure 22. Average backscatter cross-section per unit area, σ°, vs incident angle. s is r.m.s. roughness slope, Gaussian slope probability. (From Barrick, 1968)

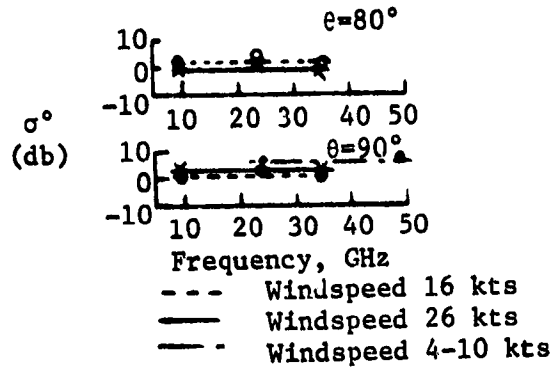

Figure 23. Variation of σ° with frequency for different values of θ (vertical polarization). (From Wiltse et al, 1957)

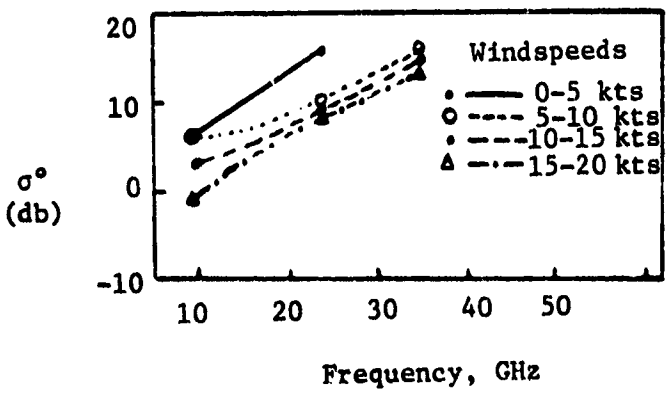

Figure 24. σ° as a function of frequency (From Grant and Yaplee, 1957)

if $H > \lambda/2\pi$, where λ is the wavelength of the incident radiation, while a slightly rough surface has $H \sim \lambda/2\pi$. Both scales are present at the same time in the sea surface and the superposition of microstructure on the large scale roughness obviously affects the distribution and size of the specularly reflecting facets. However, scattering by each scale may be analyzed separately and to a first approximation the total backscatter cross-section is the sum of the two individual contributions (Barrick and Peaks, 1968). At normal incidence the influence of the larger scale dominates since backscatter due to the gravity waves is 3 or 4 orders of magnitude greater than that due to the capillary waves. The operating frequencies of the microwave pressure sounder are between 25 and 75 GHz (wavelengths between 12 and 4 mm) so that even on the calmest days the sea surface will be "rough."

For rough surfaces the recognized technique for the derivation of σ^o is the specular point theory (Barrick, 1968). Various formulations (e.g. Kodis,1966; Stogryn, 1967) of the problem arrive at the same result for the backscatter cross-section which, with the assumption of a Gaussian probability distribution of the sea slopes (or heights), Barricks gives as:

$$\sigma^o = \frac{|R(0)|^2}{s^2} \qquad 10.1$$

for normal incidence, where s is the mean sea slope and R(0) is the Fresnel reflection coefficient at normal incidence. $\sigma^o/|R(0)|^2$ is independent of frequency and Barrick's values of this lie between 5 and 27 db for various sea states while $|R(0)|^2$ is between -2.5 and -4.5 db. At normal incidence, σ^o does not depend on polarization and the reflected signal suffers no depolarization. Cox and Munk (1954) showed that the distribution of wave heights is approximately Gaussian and this has most recently been verified by Weissman and Johnson (1977). However, Barrick and Snider (1977) show that the Gaussian assumption is not necessary while Barrick (1968) shows that other statistical distributions lead to similar values and properties of σ^o.

Although the contribution to the total backscatter cross-section from the surface microstructure is small a brief consideration of it is

desirable. In the circumstances where the surface is slightly rough, i.e. $H \leq \lambda/2\pi$, σ^o is determined by the boundary perturbation method of Rice (1951). This leads to a Bragg scattering criterion which make $\sigma(\theta)$ dependent on frequency, angle and polarization. However, at normal incidence $\sigma^o/|R(0)|^2$ is again independent of frequency and polarization as the measurements of Guinard et al. (1971) show.

10.3 Temperature and Frequency Dependence of σ^o

The temperature and frequency dependence that there is in σ^o at normal incidence arises because of the inclusion of R(0) in equation 10.1. The Fresnel reflection coefficient may be expressed in terms of the complex dielectric constant, $[\varepsilon]$.

$$|R(0)|^2 = \left| \frac{1 - [\varepsilon]^{\frac{1}{2}}}{1 + [\varepsilon]^{\frac{1}{2}}} \right|^2 \qquad 10.2$$

and ε at microwave frequencies is given by the Debye expression, which, in its most general form is:

$$\varepsilon = \varepsilon_\infty + \frac{\varepsilon_s - \varepsilon_\infty}{1 + (j\omega\tau)^{1-\alpha}} - \frac{\sigma}{\omega\varepsilon_o} \qquad 10.3$$

$\omega = 2\pi\nu$	is the radian frequency with ν in Hertz
ε_∞	is the dielectric constant at infinite frequency (=4.9 ± 20%)
ε_s	is the static dielectric constant
τ	is the relaxation time in seconds
σ	is the ionic conductivity in S m^{-1}
α	is an empirical constant (best value = 0.02 ± 0.007)
ε_o	= 8.85×10^{-12} Fm^{-1} is the permeability of free space

Klein and Swift (1977) have reviewed the recent work done to establish accurate microwave values for the real and imaginary parts of ε demanded by advances in precision microwave radiometry. Uncertainties exist in the absolute values at millimeter wavelengths because of the high error associated with ε_∞ but of principal concern in the design of the pressure sounder

is the variation with frequency expressed explicitly by equation 10.3.

The quantities ϵ_s, τ and σ are temperature and salinity dependent. Klein and Swift (1977) give polynomial expressions from which they may be obtained. For the purpose of identifying the frequency dependence of $|R(0)|^2$ from equations 10.2 and 10.3 the following values at 15°C and 35‰ salinity were used: $\epsilon_s = 74.10$, $\tau = 10.50 \times 10^{-12}$s and $\sigma = 4.290$ Sm^{-1}. In addition α was approximated by zero. The values of $|R(0)|^2$ thus determined for $\nu = 20$ through 80 GHz are given in Table 6. The frequency variation can be adequately represented by the second order expression

$$10^{(a + b\nu + c\nu^2)}$$

where $a = -.1696$, $b = -.00294S$ and $c = 4.163 \times 10^{-6}$, as illustrated by the values based on this approximation given for comparison in the third column.

Temperature dependence is such that at 50 GHz $|R(0)|^2 = .452$ and .523 at 5°C and 25°C respectively. Such variation is not significant in the context of the proposed instrument where the values of the coefficients a, b and c are eliminated by the combination of transmissivity ratios.

10.4 Measurement of σ^o

Of the many measurements that have been made of sea surface backscatter cross-section few have been in the frequency range of interest here. The first such measurements reported are those of Wiltse et al. (1957) taken with a 17° beamwidth radar, mounted on the bow of a ship, at frequencies of 9.6, 24, 35 and 48.7 GHz for a range of angles and sea states. The angular dependence has the form given by theory and the measurements at and near normal are summarized in Figure 23. Wiltse et al. conclude that σ^o does not vary with frequency - at least to within the limits set by their 2.5db accuracy. The normal incidence values of σ^o at 48.7 GHz is 7 db for a wind speed of 4-10 knots.

Making measurements at 9.4, 24 and 35 GHz from a bridge with beamwidths of about 3°, Grant and Yaplee (1957) obtained a normal incidence significantly higher values of σ^o and (Figure 24) a variation with frequency which has not since been corroborated.

Frequency GHz	$\|R(0)\|^2$ from Equation 10.2	$\|R(0)\|^2$ Approx.	$\|R(0)\|^2$ db
20	0.5928	0.5932	-2.27
30	0.5574	0.5569	-2.54
40	0.5241	0.5239	-2.81
50	0.4937	0.4938	-3.07
60	0.4661	0.4663	-3.32
70	0.4411	0.4412	-3.56
80	0.4184	0.4182	-3.78

Table 6. Variation of the Fresnel Reflection Coefficient with Frequency

Surface Wind Speed (knots)	12.5	25	29.5	36	45	48.5
σ^o (db)	10	13	3	8	9	4

Table 7. Normalized Backscatter Cross-Section at 13.3 GHz, 5^o Angle of Incidence (From Krishen, 1971).

Later work has concentrated on confirming the theoretical angular dependence of the backscatter with the intention of relating this to sea state parameters and wind speed. Guinard et al. (1971) made multifrequency (0.4 to 9.0 GHz) measurements but absolute values of σ^o were not determined. Measurements by Krishen (1971) with a fan beam at 13.3 GHz are given in Table 7. These are for an angle of 5^o from nadir but should not be very different from normal incidence values. At the high wind speeds for which the measurements were made the sea is likely to have significant foam coverage but no indication of this is reported. Barrick (1974) reports measurements made by Genest at 9.0 GHz to an accuracy of ±.9 db (Figure 25). It can be seen that as the wind speed increases σ^o reduces to a minimum value of about 9 db in agreement with the values based on Barrick's theory represented by the line. The most accurate measurements (±.7 db) are those made by Jones et al. (1977), at 13.9 GHz, with an antenna of beamwidth 1.5^o. Their results at normal incidence are summarized in Table 8 and in Figure 26. These again fit Barrick's theory well except at the highest wind speed where again probable foam coverage was not reported.

Measurements have also been made of radar backscatter cross-sections at .63μ to 10.6μ from rough metallic surfaces. Cheo and Renau (1969) show that the specular point theory can be applied at these very short wavelengths and that σ^o is independent of frequency for rough surfaces satisfying the condition $h/\lambda \geq 1/4$. For a surface with rms height from the mean $h \sim 7\mu$ and the mean scale size along the surface $1 \sim 50\mu$, σ^o is 15 db and when $h \sim 1\mu$ and $1 \sim 10\mu$ then σ^o is 17 db. These correspond to the results of Barrick's theory (Figure 22) when the surface slopes are $s = \tan 10^o$ and $s = \tan 8^o$ respectively.

10.5 Sea State and Foam

The roughness of the sea is driven by the wind but the relationship of sea state to wind is rather imprecise. This is because gravity waves take on the order of hours to build up and decay while the capillary waves are much more immediately responsive to wind variations. The smooth curve of Figure 27 from Barrick (1974) relating sea surface slope to wind speed disguises the very wide range of values that have been measured particularly at lower speeds. However, s^2 approaches a limiting value of less than .09, corresponding to $\tan^{-1} s = 16^o$, for winds in excess of 40 knots. From Figure 22 it can be seen

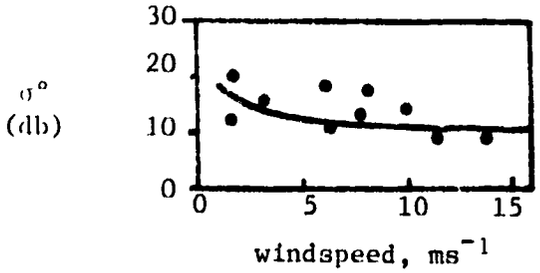

Figure 25. Dependence of σ° on windspeed at 9.0 GHz.

- • Measured values
- — Theory
  (From Barrick, 1974)

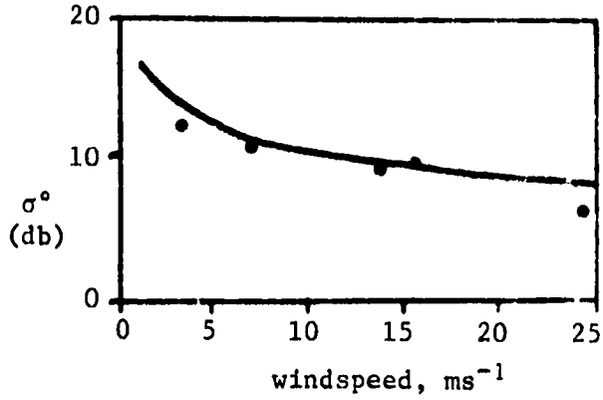

Figure 26. Dependence of σ° on windspeed at 13.9 GHz.

- • Measured values
- — Theory
  (Measurements from Jones et al, 1977)

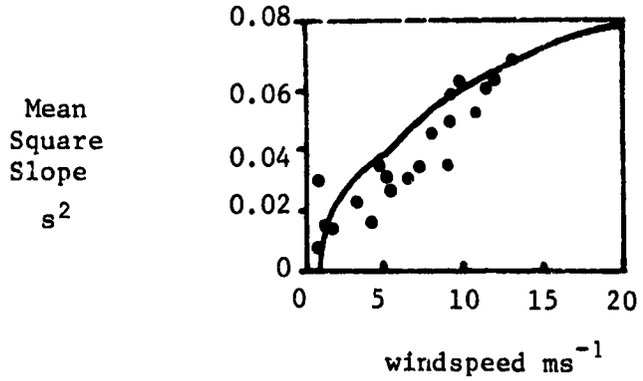

Figure 27. Dependence of sea surface slope on windspeed. (From Barrick, 1974)

	θ (°)	σ^o (db)	Error in σ^o (±db)	θ (°)	σ^o (db)	Error in σ^o (±db)
$3ms^{-1}$	Horizontal Polarization			Vertical Polarization		
UPWIND	1.26	11.87	0.72	1.25	11.51	0.72
DOWNWIND	0.82	12.49	0.76	0.77	12.16	0.76
CROSSWIND	0.69	13.44	0.72	0.94	12.86	0.72
$6.5ms^{-1}$	Horizontal Polarization			Vertical Polarization		
UPWIND	1.10	11.19	0.67	0.89	11.17	0.67
DOWNWIND	1.06	9.67	0.70	1.05	9.39	0.69
CROSSWIND	1.34	11.14	0.67	1.37	10.77	0.64
$13.47ms^{-1}$	Horizontal Polarization			Vertical Polarization		
UPWIND	0.12	9.12	0.59	0.12	9.04	0.59
DOWNWIND	0.12	9.51	0.59	0.11	9.41	0.59
CROSSWIND	1.04	9.26	0.55	1.06	9.34	0.55
$15ms^{-1}$	Horizontal Polarization			Vertical Polarization		
UPWIND	1.33	10.41	0.75	1.28	9.96	0.74
CROSSWIND	1.42	9.69	0.77	1.76	9.55	0.74
$24ms^{-1}$	Horizontal Polarization			Vertical Polarization		
UPWIND	0.41	6.93	0.54	0.35	6.67	0.53
DOWNWIND	1.03	6.58	0.54	1.05	6.54	0.54
CROSSWIND	0.30	6.38	0.53	0.27	6.38	0.53

θ is the mean angle of incidence in degrees.

Table 8. Normalized Backscatter Cross-Section at 13.9 GHz (From Jones et al., 1977).

that $\sigma^o/|R(0)|^2$ should vary from a minimum value of about 11 db up to perhaps 25 db. The measurements of σ^o by Genest in Figure 25 and Jones et al. in Figure 26 demonstrate that such a minimum of σ^o is indeed approached with a value close to that given by Barrick's theory.

Meteorological data indicates that surface wind speeds in the range 3 to 12 ms^{-1} overwhelmingly predominate so that, in the absence of foam, σ^o at any frequency will generally vary by only a few db although occasionally it will substantially increase in exceptionally calm conditions.

No measurements have been made to determine directly the effect of foam on sea surface backscatter cross-scatter cross section. However, radiometric observations of the microwave emissivity, e, of sea surface show that at 9.4 GHz (Williams, 1971) and at 19.3, 22.2 and 31.2 GHz (Nordberg et al., 1971) e increases from .4 to nearly 1 as the density of foam coverage increases. The distribution of bubble sizes as determined by Monahan and Zietlow (1969), Figure 28, reaches a maximum of .5 mm radius and falls off rapidly so that few have radii in excess of 2 mm. Resonance effects can therefore be ruled out for the frequency range of interest here and e can be expected to be similar for all the pressure sounder channels. Since, $e = 1 - |R(0)|^2$ the presence of foam will reduce σ^o, at worst, in proportion to the fractional foam coverage. Ross and Cardone (1974) have related wind speed to foam coverage but the curve of Figure 29 smooths out the large fluctuations expected since the state of development of the sea also affects foam coverage. For wind speeds up to 15 ms^{-1} there is usually less than 5% coverage but as much as 30% coverage has been observed with winds of 25 ms^{-1}. Under these extreme conditions back-scatter cross section can thus be reduced by about 1.5 db and this could account for the deviation from theory of Jones 24 ms^{-1} measurement of σ^o in Figure 26.

The experimental and theoretical evidence reviewed in 10.2 through 10.5 substantiates the earlier assumption of an average value of σ^o at normal incidence in excess of 5 db with a frequency dependence expressible by a second order polynomial.

10.6 The Effect on Pressure Measurement of Higher Order Frequency Dependence in σ^o

An instrument with operating frequencies satisfying conditions 7.9 gives

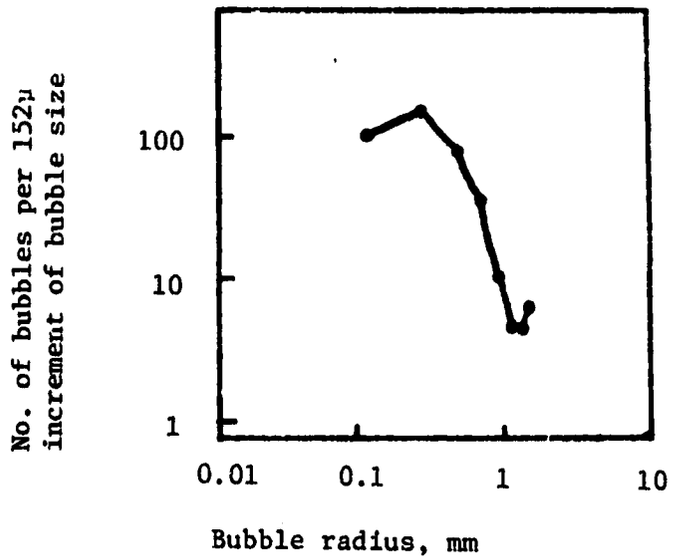

Figure 28. Bubble size spectra from seawater pouring experiments (From Monahan and Zietlow, 1969)

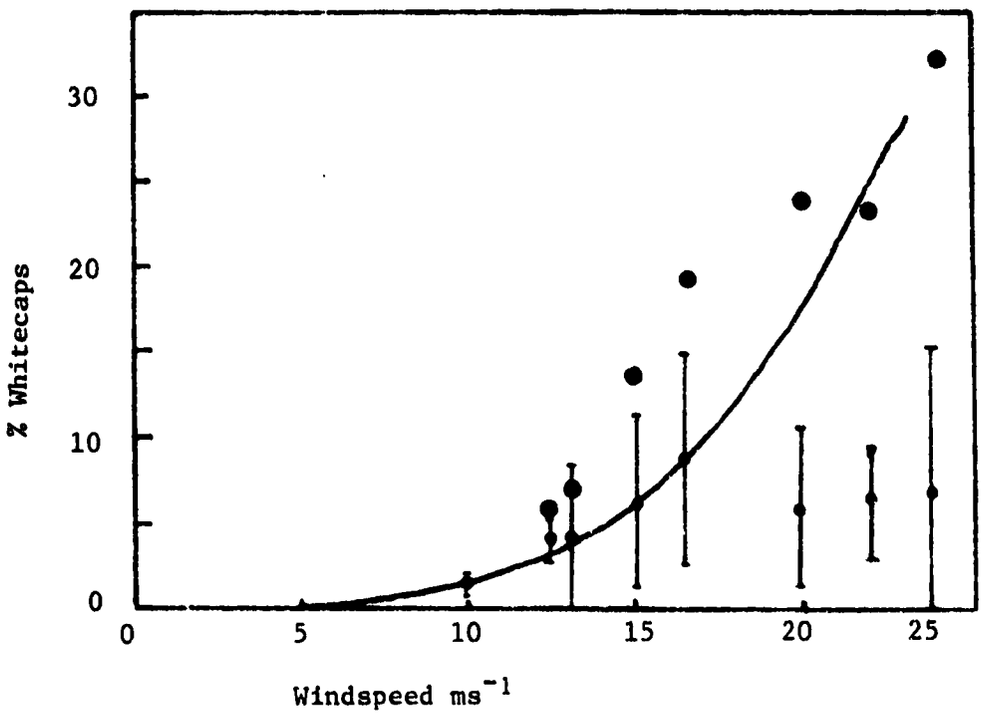

Figure 29. Observations of

Whitecap density and
Whitecaps + streaks compared with the predictions of Cardone (From Ross and Cardone, 1974)

a measurement of pressure which is not affected by the second order frequency dependence of σ^o given in Section 10.3. Since conclusive measurements of σ^o have not been made over a wide frequency range there remains the possibility of 3rd and 4th order dependencies of σ^o on frequency. In this case σ^o would have the form

$$\sigma^o = \exp (a + b\nu + c\nu^2 + d\nu^3 + e\nu^4) \qquad 10.4$$

For a particular set of operating frequencies it is possible to quantify the change in σ^o which would give a change in the index S, equivalent to a change in the surface pressure of the nominal design accuracy, 3 mb.

This calculation has been carried out for the six frequency system of Table 2, line 4 and the measurement technique is found to be relatively insensitive to high order frequency dependence. To give an error in S equivalent to a 3 mb change in pressure, σ^o must change by 1.5 db between 25 and 75 GHz due to 3rd order dependence alone or by 0.75 db for the same frequency range due to 4th order dependence alone.

10.7 $\sigma(\theta)$ Away from Normal Incidence

While an ability to remotely measure pressure along a subsatellite path is of great significance, it would be of even greater value if the two-dimensional pressure field could be mapped by making off-nadir measurements. The limiting factor is the reduction of $\sigma(\theta)$ at angles away from nadir and this is most severe for calm sea conditions. Figures 22 and 27 allow a quantitative assessment of these limits to be made.

Surface wind speeds of a few ms^{-1} and their associated sea states frequently occur but only rarely does the wind speed fall below 1 ms^{-1} and the corresponding sea state occurs less often since the calm wind must prevail for many hours before the sea surface becomes calm. We can therefore expect $s^2 = 0.04$ frequently and $s^2 = 0.01$ rarely. For these $\tan^{-1} s$ is 10^o and 5^o respectively and in Figure 22 the corresponding values of σ^o are plotted as a function of angle of incidence.

Off nadir measure will be limited by the reduction in σ^o and the consequent reduction in signal to noise which can be tolerated. Presently envisaged

designs allow for a combined loss due to σ^o and attenuation by cloud and rain of about 10 db. Since calm seas are usually accompanied by little cloud, a minimum value of $\sigma^o = -5$ db should still enable useful measurements to be made. From Figure 22 it is apparent that measurement could be made at angles of up to 15^o from the vertical except on occasions of a calm sea.

For these low angles of incidence the value of σ^o is still dominated by the gravity wave structure so that frequency variation due to Bragg resonance does not occur (Guinard et al. 1971) but frequency dependence through the Fresnel reflection coefficient applies as before.

10.8 The Statistics of Sea Surface Reflectivity

It is common practice when considering the statistical variation of a microwave signal reflected by the ocean in a particular direction to assume that the surface is composed of many randomly-distributed, specularly reflecting facets with appropriate orientations. The experimental results of Weissman and Johnson (1977) confirm that the distribution of wave heights is approximately Gaussian. Then, provided that the radar footprint is larger than any coherence length in the sea-surface wave field, the return signal of a beamwidth-limited monochromatic radar is the (voltage) sum of a very large number of echoes, the in phase, x, and quadrature, y, components of which have independent Gaussian distributions.

The total power received is

$$I(t) = X^2(t) + Y^2(t) \qquad 10.5$$

where $X = \Sigma x$ and $Y = \Sigma y$ and the summations are over all the reflecting elements. The distribution of power then has the form

$$P(I) = \frac{1}{I_o} \exp\left(-\frac{I}{I_o}\right) \qquad 10.6$$

which is the Rayleigh probability distribution for which the mean is I_o and the r.m.s. deviation

$$\left[\overline{(I - \bar{I})^2}\right]^{\frac{1}{2}}$$

is also I_o. The very large fluctuations in signal amplitude that this implies is known to observers as Rayleigh fading.

It is proposed to measure the ratio of the return signals at a pair of frequencies and if the instantaneous reflectivities at the two frequencies are related a single measurement is sufficient. However, Weissman's dual-frequency radar experiment shows that coherence of the signals extends over a frequency separation of less than 40 MHz. Although the frequency coherence width is greater for a space platform it does not approach the several GHz separation which is required for the pressure sounder. Consequently it is necessary to effectively measure the average value of the normalized sea-surface backscatter cross section.

To obtain an accurate value for the average reflected power (or equivalently, the average σ^o) which has the probability distribution of equation 10.6 a large number of independence samples N must be averaged. The standard deviation of the average is $I_o/\sqrt{N}$ and the fractional accuracy is $1/\sqrt{N}$. In Section 7.4 a fractional accuracy in the signal processing was identified which was related to the design accuracy of the instrument, δ = 3 mb/1000mb. Sufficient independent samples must therefore be obtained to ensure that the contribution to the error in pressure measurement from the reflectivity statistics is below this value. For a fractional accuracy of between .01 and .001 then N must be between 10^4 and 10^6. The methods by which this number of independent samples can be collected are discussed in the following Section.

11. System Design and Measurement Errors

The parameters available for the design of a Microwave Pressure Sounder were identified in Section 3. The most important are the operating frequencies and in Section 7 a detailed analysis was presented for the selection of the optimum frequencies. In this section we establish criteria for deciding values of the other parameters. The analysis is dominated by the accuracy requirement. The r.m.s. pressure error of ±3mb has been transformed using the pressure sensitivities of the chosen operating frequencies to a measurement accuracy specification, equation 7.22. The two major sources of error which interrelate all of the parameters are the sea-surface reflection statistics and the signal-to-noise ratio. It is necessary to determine a set of system design parameter values so that the total error is within the specification.

The size of the antenna will be determined largely by the need to collect many independent samples and this fixes the receiver bandwidth. The integration time and orbit height are also related to the antenna radius through the sea-surface error but are further limited by coverage and resolution requirements. The final parameter, transmitter power, has no optimum value but should have as high a value as possible to reduce the signal-to-noise error.

The sea-surface statistical problem and its consequences for system design are considered first.

11.1 Collection of Independent Samples and Signal Bandwidth

The antenna size to be used can be determined from a consideration of the methods for collection of the independent samples required for an accurate measurement of σ^0 as discussed in Section 10.8. Statistically independent samples are produced in the following ways:

1. By a change in the reflecting surface due to its own motion.
2. By illuminating a different reflecting surface due to motion of the satellite.
3. By a (small) change in the radar frequency.
4. By illuminating a different reflecting surface by swinging the antenna beam direction.

5. By using multiple antennae.

Methods 1 and 2 occur naturally and we must examine whether they provide an adequate number of independent samples within a reasonable integration time. The other methods require some appropriate action and may be used to increase the number obtained naturally or to provide some advantage in system design which outweighs the disadvantage that these imply for system complexity. The details of each alternative are given in the following subsections.

It is convenient to illustrate the various system options as they are discussed in this section with numerical examples and to base these on a single set of parameter values. We shall use the following set and refer to it later as System A:

Speed of satellite	$V = 7.2$ km s^{-1}
Antenna radius	$r = 25$ cm
Orbit height	$h = 500$ km
Integration time	$t = 10$ sec
Duty cycle	$D = .167$

The analysis is primarily intended to determine the antenna radius and the above value will only be used as a reference figure when this is not the object of the calculation. The orbit height and integration time given here are reasonable intermediate values and further discussion of coverage and resolution for a range of values will be given in Section 14. The duty cycle represents the fraction of the total time that each transmitter is switched on. We also chose, for illustration, an accuracy of 0.5% in each channel which, for the six frequency schemes of Table 2, represents a 1.5% accuracy overall or ±2mb rms error in pressure.

11.1.1 Surface motion

To change the reflecting surface sufficiently for statistical independence of the echo signals the linear changes in the positions of the specularly reflecting facets must be of the order of half the wavelength. The worst case conditions which limit reliance on this method for the provision of an adequate rate of collection are for a calm sea where it is not unreasonable to expect speeds as low as 0.5 ms^{-1}. In these circumstances

C.2

the coherence time of the sea surface for $\lambda/2$ = 6 mm (the longest wavelength presently envisaged) is about 12 ms. Thus it would take ~ 480 s to obtain the number of samples (N) needed for 0.5% measurement accuracy ($1/\sqrt{N}$) in a single channel and the integration time for the six frequency instrument is totally unsatisfactory.

11.1.2 Satellite Motion

11.1.2.1 Spatial Coherence Length

Satellite motion means that the reflecting surface is constantly being changed . The displacement of the satellite for statistical independence of two successively reflected signals may be obtained by application of the Van Cittert-Zernike theorem (Born and Wolf, 1975). This gives an expression for the complex degree of coherence between signals at two points, P_1, P_2, in a plane illuminated by an extended quasi-monochromatic source. For a uniform circular source of radius R there is complete incoherence of the signals when the separation of P_1 and P_2 is

$$d = 0.61\ h\lambda/R \qquad 11.1$$

where h is the distance between the source and the plane of P_1P_2. Applying [illegible]ent situation, the illuminated area of sea surface is the [illegible]ich approximates well to a continuous distribution since [illegible] large number of reflecting facets. The radius of this circular sourc[illegible] related to the angular beam width ω of the radar antenna by

$$\omega = R/h \qquad 11.2$$

The angular beam-width may be approximated by the angle to the first minimum of a diffraction limited aperture (the antenna of radius r)

$$\omega = .61\ \lambda/r \qquad 11.3$$

Combining these three equations gives d = r. However we can expect the phase changes between P_1 and P_2 to be double that implied here since the phases in the extended source are affected by the motion of the radiating antenna. So that the separation of points for complete incoherence is

$$d = r/2 \qquad 11.4$$

Independent samples are thus obtained by displacement of the antenna by this spatial coherence length of half the antenna radius.

The limitations which make this an approximation to within a small numerical factor are: firstly that the extended source is not uniform but has a Bessel function distribution and the radius used in equation 11.2 is that of its first minimum; secondly the signal is detected not at a point but is the sum over the antenna area. A more rigorous analysis of the problem by Peckham (1975) takes these factors into account and gives the spatial coherence length as 0.89 r for a circular antenna.

With this value of the spatial coherence length, 1.5% accuracy is obtained in a time $0.89\,r\,/[VD(0.5 \times 10^{-2})^2]$ seconds, which for System A is 7.7 s. Thus the rate of collection of samples by the natural satellite displacement overwhelms that due to changes in the sea surface with time. When other methods for increasing the collection rate are not used, the antenna radius is fully determined by the required fractional accuracy, F_A, and is given by the relationship

$$r = \frac{t\,V\,D\,F_A^2}{0.89} \qquad 11.5$$

It is apparent from the above numerical example that for the six frequency sets of Table 2, F_A is large enough for adequate collection rates to be achieved by this natural process with a reasonable antenna size.

Of course, it is not essential to use a circular antenna. The most favorable arrangement would be to have a small antenna dimension along the direction of satellite motion, which ensures a high sample collection rate, and a large transverse dimension to maintain a large receiver aperture and hence small signal-to-noise errors. However, the antenna dimensions determine the surface spot size so that ground resolution considerations will also influence the ultimate choice of aperture shape and size.

For a non-circular antenna the spatial coherence length must be re-examined. Peckham (1975) shows that a rectangular aperture of side 2a in the direction of motion has a coherence length of 1.08 a and it can be expected that for an elliptical antenna the coherence length is between this

and the circular value is about equal to the semi-minor axis.

11.1.2.2 Bandwidth

A Microwave Pressure Sounder relying on satellite motion to provide independent samples would be operated in an intermittent c.w. mode. The return signal is $\gtrsim$ 130 db below the transmitted power and the necessary isolation is not possible to allow simultaneous transmit and receive operation. Consequently a fixed frequency signal would be transmitted for the few milliseconds required for the signal to return after reflection at the ocean surface. The return echo has a larger bandwidth than the transmitted signal because of Doppler frequency shifts produced by components of the satellite velocity over the angular spread of the beam. The velocity component along the 3db beam direction is $\pm 0.25\ V\lambda/r$ so that the Doppler shift is $\pm 0.5\ V/r$ and a total 3db receiver bandwidth

$$\Delta f = V/r \qquad 11.6$$

is needed to match the natural bandwidth of the return signal. For System A this has a value close to 30 kHz.

Satellite pitch instabilities will cause deviations of the antenna boresight from the nadir direction and will consequently offset the band of received frequencies from its symmetrical arrangement about the transmitted frequency. The specified inertial pointing accuracy of Spacelab is $\pm 0.5^{o}$ and since this is of similar magnitude to the beamwidth the frequency offset would be comparable to the bandwidth. Methods are available for improving the pointing accuracy of the platform and hence reducing the offset if this is desirable. However, this is not a restricting problem so long as the overall pressure sounder system is designed to accommodate such bandwidth offset effects.

11.1.3 Frequency Sweeping

A combined consideration of the sea surface statistical error, the signal-to-noise error and surface resolution suggests that significant improvement in accuracy is possible if the natural rate of collection of independent samples can be increased by one of the techniques (3-5) identified

above. Detailed consideration must therefore be given to the potential advantages and engineering feasibility of each alternative so that it may be decided which if any should be implemented. We begin in this subsection with the frequency sweeping technique.

The method of Section 7 for choosing the operating frequencies has assumed that each is monochromatic. Small deviations from these values can be tolerated without destroying the designed insensitivity of the combined signal to unwanted background, temperature and water vapor effects. However, if a sweep of $\sim$ 100 MHz is required then the effects of these atmospheric parameters on the accuracy of the pressure measurement must be re-examined.

The fundamental reason why sweeping over a range of frequencies can provide a number of independent samples is that signals at a pair of different, but close, frequencies will have uncorrelated received echo amplitudes after reflection at the sea surface if the frequency separation is large enough. To increase the sample collection rate over that produced by satellite motion the sweeping must be accomplished within the time taken for the satellite to be displaced by the spatial coherence length, ie within a time $t_d = r/V$ (= 34 μs for System A). The following analysis determines how much the frequency must be changed to produce a statistically independent sample.

11.1.3.1 Frequency Coherence Width

Weissman (1973) derives a correlation function $R(\Delta k)$ for two (voltage) signals reflected from the ocean at normal incidence when the frequency separation of the two radar signals is $\Delta\nu = \frac{c}{2\pi}\Delta k$, (c is the velocity of electromagnetic waves). The correlation function has a magnitude

$$|R(\Delta k)| = \exp\left[-2\sigma^2(\Delta k)^2\right] \frac{1}{\left[1+\left|\frac{(\Delta k)h\theta_3^2}{5.544}\right|^2\right]^{\frac{1}{2}}} \qquad 11.7$$

where σ is the r.m.s. ocean wave height and the other symbols have been previously defined. The two factors which contribute to the correlation function derive independently from the wave height statistics and the antenna pattern function. This analytic expression for $R(\Delta k)$ was obtained by Weissman by

integrations over the wave height distribution and the antenna beamshape. The integrations were facilitated by assuming a Gaussian distribution of waveheights and a Gaussian beamshape.

We require the separation, $w_\nu = \frac{c}{2\pi} w_k$, of two frequencies such that the two received signal powers are statistically independent. This we define as the frequency coherence width and it may be expressed in terms of Weissman's correlation function by

$$w_k = \int_{-\infty}^{\infty} |R(\Delta k)|^2 \, d(\Delta k) \qquad 11.8$$

Approaching the problem in a slightly different way Peckham (1975) calculates w_k for that part of the correlation function due to the beamshape. He uses a Bessel function antenna pattern function and by numerical integration obtains

$$w_k = 0.5672 \frac{\pi k^2 r^2}{h} \qquad 11.9$$

where $k = 2\pi\nu/c$.

Alternatively, w_k may be obtained from the beamshape factor of equation 11.7 thus

$$w_k = \int_{-\infty}^{\infty} \frac{d(\Delta k)}{\left[1 + \left(\frac{(\Delta k) h\theta_3{}^2}{5.544}\right)^2\right]} = 5.544\pi \frac{1}{h\theta_3{}^2} \qquad 11.10$$

Now, the 3db beamwidth, θ_3, for an antenna beam shape given by $G(\theta) = \frac{2J_1(kr\theta)^2}{kr\theta}$ is $3.2326/kr$, so that

$$w_k = .5305 \frac{\pi k^2 r^2}{h} \qquad 11.11$$

and this is in good agreement with equation 11.9 above. It is readily shown by substituting the coherence width, equation 11.10, into equation 11.7 that for a frequency separation of w_k the power correlation coefficient $|R(\Delta k)|^2$ has the value $(1 + \pi^2)^{-1} = 0.092$ when the ocean is smooth ($\sigma << 1$).

11.1.3.2 Surface Effect on Frequency Coherence Width

The effects of sea surface statistics on the frequency coherence width may be determined by repeating the integration, equation 11.8 with both factors of equation 11.6 included in $|R(\Delta k)|^2$. The new coherence width w_k^1 is best expressed in terms of the previous w_k, equation 11.11. With the help of standard integrals we obtain

$$w_k^1 = w_k \left[1 - \Phi\left(\frac{2\sigma w_k}{\pi}\right)\right] \exp\left[\left(\frac{2\sigma w_k}{\pi}\right)^2\right]. \qquad 11.12$$

and the function

$$\Phi\left(\frac{2\sigma w_k}{\pi}\right) = \frac{2}{\sqrt{\pi}} \int_0^{\left(\frac{2\sigma w_k}{\pi}\right)} \rho^{-t^2}\, dt \qquad 11.13$$

can be obtained from tables of the error function. To facilitate interpretation of this result, equations 11.11 and 11.12 may be written explicitly as frequency coherence widths, w_ν and w_ν^1, in terms of the frequency ν:

$$w_\nu = 10.5\ \frac{\nu^2 r^2}{ch} \qquad 11.14$$

and

$$w_\nu^1 = w_\nu \left[1 - \Phi\left(\frac{4\sigma w_\nu}{c}\right)\right] \exp\left[\left(\frac{4\sigma w_\nu}{c}\right)^2\right]. \qquad 11.15$$

Then values of the ratio of frequency coherence width $\frac{w_\nu^1}{w_\nu}$ are tabulated for a range of values of the argument $\left(\frac{4\sigma w_\nu}{c}\right)$ (ie for a range of sea states) in Table 9.

$\frac{4\sigma w_\nu}{c}$	.1	.2	.5	1	2	5	10	20
$\frac{w_\nu^1}{w_\nu}$	.99	.80	.62	.43	.25	.11	.056	.028

Table 9. Effect of Ocean Surface Statistics on the Frequency Coherence Width (see text for explanation).

The table shows that roughness of the sea surface reduces the frequency coherence width, to w_ν^1 is always less than w_ν. A "smooth" sea, where $4\sigma w_\nu/c \ll 1$ is sufficient definition of a smooth sea for present purposes, has little effect on the coherence width. However, when the argument, $4\sigma w_\nu/c$, is large the ratio, w_ν^1/w_ν approaches the value $\left(\frac{c}{4\sigma w_\nu} \cdot \frac{1}{\sqrt{\pi}}\right)$ and the frequency coherence width is determined principally by the sea surface effect rather than the antenna beam shape.

For a given set of experimental parameters the relative importance of surface height statistics and beam shape on the frequency decorrelation can now be determined. For System A above with ν = 50 GHz the frequency coherence width w_ν = 10.9 MHz and if σ = 1 m (a moderately rough sea) $(40\ w_\nu/c) = 0.14$. Thus the beam shape is the dominating factor. The 14 GHz correlation radar used by Weissman and Johnson (1977) to determine wave heights had a 1 m diameter antenna and was operated from an aircraft at 3 km altitude. In this case w_ν = 4.8 GHz but since $(40\ w_\nu/c) = 64$, at σ = 1 m, the frequency coherence width, when the sea surface effect is included, w_ν^1 = 42 MHz. As expected the surface effects dominate. The main reason for these two example systems being at either end of the scale is the difference in altitude between the satellite and aircraft platforms.

In a swept frequency system, suitable for pressure sounding from a satellite and therefore, as presently envisaged, with parameter values not very different from System A, the beam shape will be the important factor and equation 11.14 is a satisfactory approximation for the frequency coherence width.

11.1.3.3 Implementation and Bandwidth

A frequency swept system requires a larger value of bandwidth than the fixed frequency scheme. The range of frequencies being received at any instant is determined by the rate at which the frequency is swept and the time delay between the signals reflected from immediately below the satellite and from the edges of the antenna beam. If the sample collection rate is to be increased by a factor m, and thus the sea surface statistical error reduced by $m^{-\frac{1}{2}}$, then the total sweep

$$\Delta\nu_s = m w_\nu \quad \text{Hz} \qquad 11.16$$

must be completed in a time r/V and the sweep rate is

$$\delta\nu_s = m\ 10.5\ \frac{\nu^2 rV}{ch} \quad \text{Hz s}^{-1} \qquad 11.17$$

A reasonable minimum value of m is 9 to reduce the statistical error by 1/3. This gives for System A

$$\Delta\nu_s = 100 \text{ MHz} \quad \text{and} \quad \delta\nu_s = 3 \text{ MHz } \mu\text{s}^{-1}.$$

These values are rather large and would necessitate development of suitable millimeter wave sources with either current or varactor tuning. In addition the large total sweep means that the frequency selection procedure should be revised to ensure retention of the insensitivities previously specified.

It can be readily shown that the minimum bandwidth required is

$$\Delta f = 4.2\ m\ \frac{V}{r} \qquad 11.18$$

where V/r is just the bandwidth for a fixed frequency scheme. The factor of 4.2 in this equation makes the signal-to-noise for any swept system at least 3db worse than for a fixed frequency system. Specifically, when m = 9 the bandwidth is 1 MHz and the S:N is 8db worse.

These values assume that the frequency swept mode is used to full advantage by having a tracking local oscillator such that the IF band and the received band of frequencies are the same. For these to coincide within 1% of the bandwidth the implied phase sychronization of the local oscillator sweep modulation is equivalent to a knowledge of the satellite altitude within ($c/24\ w_\nu$) meters ($\sim$ 1 m for System A). Continuous operation over the ocean, where the altitude changes only slowly, does not present a severe sychronization problem and can probably be accomplished with appropriate processing of the pressure sounder signals. However, after each land-to-ocean coastal crossing the local oscillator phase will need to be relocked.

The use of a tracking local oscillator with a larger receiver IF than the minimum, 11.18, does not significantly reduce the synchronization problem.

A simpler mode of operation is to use a fixed frequency local oscillator and a receiver bandwidth of $\Delta\nu_s$ but this will reduce S:N even more and is therefore probably not viable.

Besides providing an increased sample collection rate, frequency sweeping also gives a considerable degree of range resolution. However, this does not constitute a valid reason for choosing a swept frequency system since backscatter from aerosols is negligible when cloud attenuation is small enough to allow operation of the pressure sounder.

As alternatives to continuous sweeping of the frequency, step changes equal to the frequency coherence width may be made to obtain the independent samples or nanosecond pulses may be used. These techniques do not appear to offer any additional advantages and are no easier to implement.

11.1.4 Antenna Scanning

An independent sample can be obtained with a fixed frequency radar by swinging the antenna beam through half the angular beamwidth so that more than half the area of sea illuminated is changed. The scanning can be either along the sub-satellite path or transverse to it. The rate of collection of independent samples can be increased by a factor m over the natural rate by sweeping through m/2 beamwidths in a time r/V. Since r/V = 33 μs for System A this implies scanning rates of several kHz. Mechanical scanning of the primary antenna at this rate is not possible and the problem is only slightly reduced if scanning with the feed or a sub-reflector is considered. Because six frequencies are needed, electronic scanning with a phased array is complicated unless several antenna are used and if a multiple antenna system is anticipated then it is probably better used as indicated in Section 11.1.5 below.

Antenna scanning does not appear to be feasible at this stage. Nevertheless it is worthwhile to identify some of the advantages of the technique.

With antenna scanning a larger antenna can be used to advantage. For a swept frequency scheme a larger antenna makes implementation more difficult

by increasing both the total sweep range and the sweep rate to maintain the rate of collection of independent samples. In contrast, with a scanned antenna system, a larger antenna requires to be scanned over the same total angle but at a reduced sweep rate to maintain the collection rate and the techniques becomes more feasible. A larger antenna is desirable because of the improvement in received signal strength and the reduction in noise through a narrower Doppler bandwidth. The consequent improvement in S:N allows more accurate measurements under worse atmospheric conditions.

The scanned antenna system is more complicated than the frequency swept scheme if it is to be used to full advantage because synchronization of the transmit and receive antenna scans must be used in addition to the control of the local oscillator frequency (for along track scanning). When used in this way there is also a degree of height discrimination. The tight tracking constraints can be relaxed with a reduction in the advantages by using antennae of unequal size and widening the receiver bandwidth. This leads to numerous alternative methods for implementing an antenna scanned system each of which has different consequences for the rate of collection of independent samples, the S:N ratio and the height discrimination while each imposes different constraints on the system design in terms of sweep rate, precision required in sychronized tracking and local oscillator frequency control. All of these quantities can be readily determined for a specific design.

11.1.5 Multiple Antennae

The sample collection rate can be increased by a factor m by using m multifrequency antennae, each with its own IF chain and square law detector. Although this has the advantage of redundancy and can be used in combination with any of the previous techniques, size, weight and cost considerations suggest that the concept is only of value when the antennae are small and an increase in the collection rate of less than ten is desired.

11.2 Signal to Noise Errors

The sources of noise which contribute to the error in pressure measurement and must therefore be taken into account are:

1. Receiver noise;
2. Atmospheric and surface emission attenuated by intervening atmospheric layers;
3. Atmospheric aerosol backscatter of the transmitted signal; and
4. Atmospheric and surface backscatter of other sources.

Of these, the first is generally most important, being 8 to 12db higher than the second, while the third source of noise is insignificant whenever atmospheric attenuation is not so high as to prevent measurements from being made. If the satellite orbit allows pressure measurements to be made at or near local noon when the sun is overlead then solar glitter will be a problem. An orbit which avoids the angular conditions for specular reflection of the sun into the receiver aperture is preferred. In these circumstances assessment of S:N errors can be sufficiently well approximated by considering the dominating receiver noise alone.

The effect of noise is reduced by making a direct measurement of it and subtracting this from the signal-plus-noise measurement. The post-detection noise-equivalent-power in each channel is then

$$N_i = 4kT \left(\frac{\Delta f}{tD}\right)^{\frac{1}{2}} F_i \qquad 11.19$$

where F_i is the detector noise figure. The return power at each frequency can be calculated from equation 3.7

$$P_D = 0.25\, P_T \eta_T \eta_R \frac{r^2}{h^2} \left(\tau_o^2\, \tau_w^2\, \tau_A^2\right) \sigma^o \qquad 11.20$$

for known transmissivities corresponding to particular atmospheric and sea states. Using the bandwidths of Section 11.1 for fixed or frequency swept schemes, equations 11.19 and 11.20 give single channel S:N figures which can be combined to determine the total S:N error. In Section 12 this procedure is used to evaluate errors for particular system designs.

11.3 Other System Design Considerations

Measurements of the ratio of the return signal powers are meaningful only if the transmitted power levels are measured or controlled. Active control to achieve the desired accuracy is more suited to a space instrument than precision measurement of power. It is proposed that the inherent accuracy

of null-balancing techniques should be utilized for control purposes. Although a comparison of the received and transmitted powers could be made at each frequency it is probably more satisfactory to control the ratio of transmitted powers at a pair of frequencies, $P_T(\nu_1)/P_T(\nu_2)$, so as to equalize the received echo power in the absence of atmospheric attenuation.

Fluctuations in the gain of the IF amplifier can be overcome by using the same IF chain and detection system to amplify and ratio the received signals of a frequency pair.

Although a 4-frequency, 3-ratio scheme may appear simpler than a 6-frequency instrument, the system architecture detailed above means that the power outputs at all four frequencies must be related and the detector must accept all four return signals. Consequently a 6-frequency scheme with three separate ratiometers is an easier option to implement.

12. Specific System Designs

The analyses of Sections 7 and 11 enable the primary design parameters identified in Section 3 to be assigned optimized values for complete specification of a Microwave Pressure Sounder. The potential performance of the instrument, in terms of the surface resolution and measurement accuracy, can also be evaluated under specific operating conditions (orbit altitude and integration time) and for particular atmospheric and surface conditions. Details are given below of the design and performance of baseline fixed-frequency and swept-frequency systems so that the merits of these two alternative implementation possibilities can be compared.

12.1 Fixed-Frequency Microwave Pressure Sounder

12.1.1 Primary System Design Parameters

The operating frequencies and other design parameters of Section 3 must be supplemented by the system efficiencies, η_T and η_R, the satellite speed, V, and the duty cycle, D, to complete the instrument specification. Table 10 gives the values of these basic parameters for a fixed frequency system operating at two altitudes. Since a rectangular antenna is specified, the radius has been replaced by the overall dimensions.

ν_i	Operating Frequencies (GHz)	29.2555 36.5555	44.80 52.80	67.51 73.01
α, β	Indices	-1.60, 1.00		
P_T	Transmitter power	2W		
η_T, η_R	Feed efficiencies	0.85		
(r)	Antenna dimensions	20 x 150 cm		
t	Integration time	12 s		
D	Duty cycle	0.166		
h	Satellite altitude	500	800	km
V	Satellite speed	7.61	7.45	kms^{-1}
Δf	Receiver bandwidth	76.1	74.5	kHz
2h/c	Pulse length	3.33	5.33	ms

Table 10. Fixed Frequency System Design Parameters

12.1.2 Derived Performance Data

The parameter values of Table 10 enable the instrument performance to be evaluated. Those data which are not dependent on atmospheric surface conditions are given here in Table 11.

Sensitivity of Index S to pressure change	1.	0.74% per mb
Sensitivity of pressure measurement to: a) Background variation of the form $(a + b\nu + c\nu^2)$ b) Surface temperature c) Total water vapor	From Frequencies	negligible $800^{\circ}C$ per mb 8 gm cm^{-2} per mb
R.m.s. atmospheric variability error	From numerical simulation	± 0.4 mb
Signal processing accuracy required in each channel for ± 3mb r.m.s. error	From 1 above	0.73%
Number of independent samples per channel in time t	$N = \frac{VtD}{1.08r}$	1.4×10^5
Accuracy per channel	$N^{\frac{1}{2}}$	0.27%
Total statistical error	Sum over all channels	± 1.1 mb

Beamwidths and Surface Resolution

Channel	Frequency (GHz)	Wavelength (mm)	3db Beamwidths (°)	Ground Resolution (km) h=500 km	Ground Resolution (km) h=800 km
1	29.2555	10.25	1.30 x 0.17	136 x 6.8	162 x 10.9
2	36.5555	8.21	1.04 x 0.14	126 x 5.5	145 x 8.7
3	44.80	6.70	0.85 x 0.11	118 x 4.5	133 x 7.1
4	52.80	5.68	0.72 x 0.096	113 x 3.8	125 x 6.0
5	67.51	4.44	0.56 x 0.075	107 x 3.0	115 x 4.7
6	73.01	4.11	0.52 x 0.070	105 x 2.7	112 x 4.4
Effective along-track ground resolution, all channels				85 km	80 km

Table 11. Fixed Frequency System Performance

The signal processing accuracy indicates that output power and detection stabilities of the order of 0.1% are required from the instrumentation.

The channel dependent ground resolution in this table is the total surface area included within the first zero of the antenna pattern function as smeared by the satellite motion. However more than 80% of the total energy received during the integration time comes from within the subsatellite path length. This is therefore the effective along track ground resolution and is the same for all channels.

12.1.3 Total Error Calculations

The values of two components of the total error, the atmospheric variability error, E_{AV}, and the error due to the sea surface statistics E_{SS}, have been given in Table 11. While these are constants of the system, the third source of error, signal-to-noise, has a wide variation which is dependent on atmospheric and ocean surface conditions. The noise-equivalent-power and the return power at each frequency, equations 11.19 and 11.20, can be used to evaluate this error, E_{SN}, when the detector noise figure, F, the atmospheric transmissivity and the surface reflectivity are specified at each frequency. Table 12 presents the data needed for these calculations for a range of operating conditions. The cloud attenuation data was obtained from equation 9.3 and the variation of sea surface backscatter with frequency is from equation 10.1.

Channel		1	2	3	4	5	6
Receiver noise figure		7.0	7.0	7.5	8.0	8.5	8.5
Atmospheric Transmission	τ_o^2 pg = 1013mb	-0.18	-0.33	-0.88	-9.14	-7.31	-1.68
	τ_w^2 2.6 gm cm^{-2}	-0.47	-0.52	-0.72	-0.99	-1.59	-1.86
	τ_A^2 1 km, Cloud 1 gmm^{-3}	-1.29	-1.99	-2.97	-4.09	-6.60	-7.69
Backscatter Cross-Section	σ^o Very calm sea	15.48	15.28	15.07	14.87	14.51	14.38
	Moderate sea	10.48	10.28	10.07	9.87	9.51	9.38
	Very rough sea	6.48	6.28	6.07	5.87	5.51	5.38
	$\sigma(14^o)$ Very calm sea	-10.52	-10.72	-10.93	-11.13	-11.49	-11.62
	Moderate sea	2.48	2.28	2.07	1.87	1.51	1.38
	Very rough sea	4.48	4.28	4.07	3.87	3.51	3.38

Table 12. Typical Atmospheric and Surface Data (db)

In Table 13 the total measurement error in mb is shown for both 500 km and 800 km orbit altitudes and for various atmospheric and sea surface states. The total is obtained by adding the three components E_{SS}, E_{AV} and E_{SN} as independent random errors. It can be seen that the r.m.s. error with this instrument is 1.2 mb for the most frequently occurring conditions but, as expected, it will not be able to provide sufficiently accurate results in heavy cloud or away from nadir over very calm sea. The 500 km orbit is slightly better than the 800 km orbit but the latter may be preferred because in this case measurements 14° from the nadir are 200 km from the sub satellite path compared with 125 km away for the 500 km orbit. Curvature of the Earth has been neglected, thus 14° from nadir is equated with 14° from vertical - an error of $\sim 1.8°$.

Sea State	Atmospheric Conditions				
	Surface Pressure	1013mb	1013mb	1013mb	990mb
	Water Vapor	2.6 gm cm^{-2}	5.2 gm cm^{-2}	3.5 gm cm^{-2}	3.5 gm cm^{-2}
500 km Orbit	Uniform Cloud	None	0.5 km 0.5 gm m^{-3}	1 km 1 gm m^{-3}	2 km 1.5 gm m^{-3}
Very calm	Nadir	1.17	1.17	1.17	1.19
	14°	2.06	3.23	>5	>25
Moderate	Nadir	1.17	1.17	1.17	1.39
	14°	1.17	1.18	1.21	>5
Very rough	Nadir	1.17	1.17	1.18	2.22
	14°	1.17	1.17	1.18	3.6
800 km Orbit					
Very calm	Nadir	1.17	1.17	1.17	1.32
	14°	4.45	>5	>10	>25
Moderate	Nadir	1.17	1.17	1.18	2.23
	14°	1.19	1.23	1.42	>10
Very rough	Nadir	1.17	1.18	1.20	4.92
	14°	1.18	1.19	1.28	>5

Table 13. Total r.m.s. Errors (mb) With Fixed Frequency MPS

12.1.4 Hardware Implementation

The system specifications of 12.1.1 have been used to define an outline hardware implementation of the Microwave Pressure Sounder. The instrument comprises three ratiometers which are of similar designs but differ in their operating frequencies. The block diagram of a two-frequency ratiometer is shown in Figure 30. Each ratiometer has the following subsystems: power supply and frequency control; transmitter; RF output power equalization; receiver and ratioing electronics. A single multifrequency dual-antenna subsystem serves all three ratiometers while common electronics include timing and modulation control, signal processing and satellite power and data interfaces. A pointing subsystem is also required.

The instrumentation is based, with one exception, on existing technology. The Gunn effect or Impatt sources used as the first stage oscillators of the transmitter subsystem have their frequencies crystal controlled. These are used to drive the injection-locked millimeter wave power oscillators. The devices at present available for this second stage do not provide sufficient RF power. However, suitable multi-diode Impatt devices with a gain of up to 10db and an output power of 2W cw are currently being developed commercially.

The two frequencies are transmitted alternately and this enables the output power equalization loop to utilize phase sensitive detector control of a ferrite modulator. The loop must provide equal output energies at the two frequencies over the integration period or any sub-division of this for which the ratio is computed. Set level attenuators are used to accommodate asymmetries between the two branches and differential RF detector response. Experiments have shown that such a loop provides more than adequate equalization of the output powers.

The most suitable antenna has a multi-frequency feed, similar perhaps to that used for the SMMR on SEASAT A. The corrugated horn feed on this instrument has a high efficiency over a 6 to 1 frequency range. Separate transmit and receive antennae are preferred over a single antenna with 6 circulators because of the smaller loss.

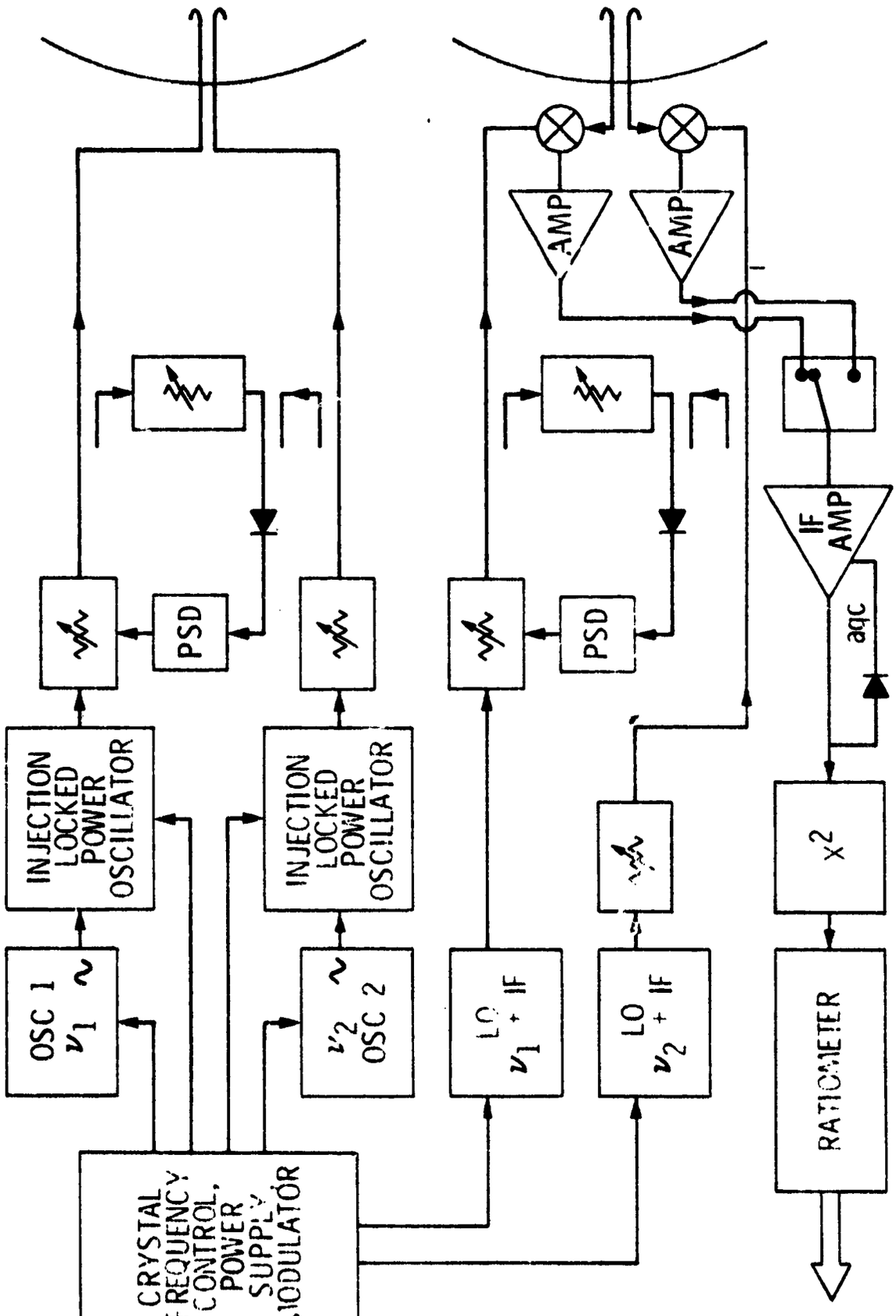

Figure 30. Two Frequency Ratiometer Schematic

It is possible to use a single mixer in the receiver but the large difference between a frequency pair means that its response to each frequency will be different. However, it is easier to match the response of separate mixer-preamplifiers than to do this with a single device. Consequently this arrangement is chosen for the front-end while the main IF amplifier chain and the detector are common. Automatic gain control with a long time constant is used to reduce the dynamic range required from the square law detector and the final ratioing is accomplished digitally. It has been demonstrated that the stability and accuracy specifications of the detection and ratiometer electronics can be met.

The modulation sequence for each of the separate ratiometers must allow for measurements to be made of the signal and noise at each frequency when the instrument is not transmitting. Operation of the transmitters is then in an intermittent c.w. mode with pulse lengths equivalent to the time taken for a signal to be reflected at the surface and returned to the receiver, ie 2h/c seconds. A full cycle of operations takes six of these periods, two for transmission and 4 for detection. The large differences between the six frequencies will allow the three ratiometers to be operated simultaneously with synchronized transmit and receive sequences. Figure 31 shows the proposed oscillator and detector modulation sequence. Dynamic control of the repetition rate can be used to accommodate variations in the orbit height. It may be possible that, with sufficient filtering, noise measurement could be made at one frequency of a pair while the other was being transmitted. This would improve the duty cycle and reduce the surface statistical error by a factor of 0.82.

Further specification of component performance, stability and tolerances is required. Although the hardware design is based on available technology the RF power stability requirements for this instrument are not generally needed in radar systems and have therefore not previously been demonstrated. However, the use of phase sensitive detector control of the output powers and matched mixer-detectors should enable the specifications to be met. Some parts of the system have been investigated but further testing, particularly of the receiver subsystem, is needed. Careful preflight calibration and stability tests of the completed instrument will also be essential.

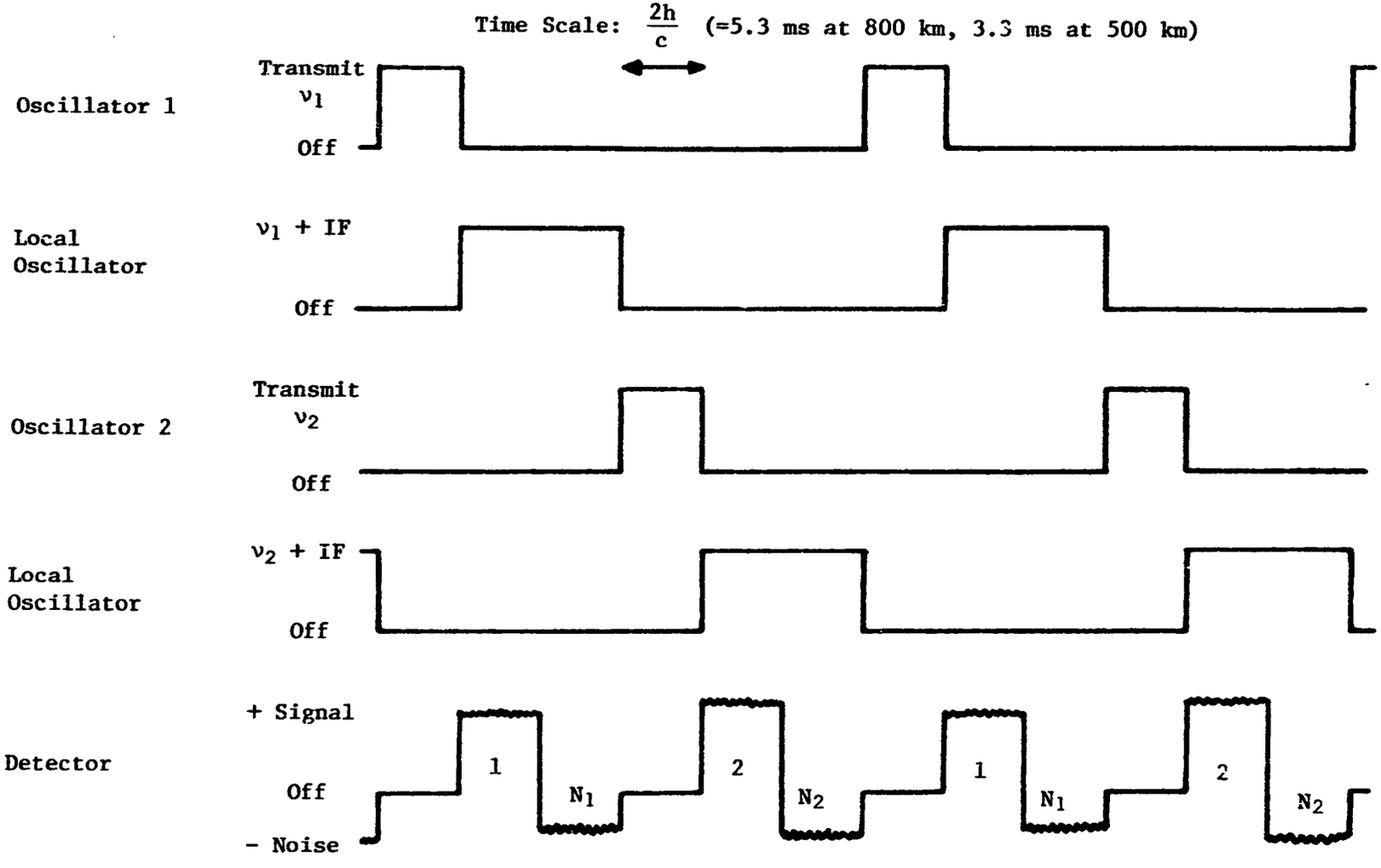

Figure 31. Modulation sequence of the two-frequency ratiometer.

12.2 Swept Frequency Microwave Pressure Sounder

12.2.1 Primary System Design Parameters

The example of a swept frequency system used here for comparison has the majority of its design parameters the same as for the fixed frequency example above. To these parameters we must add the factor, m, by which frequency sweeping increases the sample collection rate. This then defines the total sweep and the sweep rate, which are height and frequency dependent, and the minimum receiver bandwidth. We choose a larger antenna to partially compensate for the worsening of signal-to-noise by an increased bandwidth. However, if the total sweep is to be kept within reasonable bounds (< 100 MHz) the increase in antenna size must be limited. The complete system specification is given in Table 14.

ν_i	Operating Frequencies (GHz)	29.2555	44.80	67.51
		36.5555	52.80	73.01
α, β	Indices	-1.60, 1.00		
P_T	Transmitter power	2W		
η_T, η_R	Feed efficiencies	0.85		
(r)	Antenna dimensions	28 x 150 cm		
t	Integration time	12s		
D	Duty cycle	0.166		
m	Factor	12		
h	Satellite altitude	500		800 km
V	Satellite speed	7.61		7.45 kms^{-1}
Δf	Receiver bandwidth	76.1		74.5 kHz
2h/c	Pulse length	3.33		5.33 ms
	Sweep repetition time	18.4		18.8 μs

Total Sweep (MHz) and Sweep Rate (MHz μs^{-1}) for A500 km, B800 km

Channel	1	2	3	4	5	6
A. Total Sweep	14.1	22.0	33.0	45.9	75.0	87.8
Sweep Rate	.766	1.20	1.80	2.49	4.08	4.77
B. Total Sweep	8.81	13.7	20.6	28.7	46.9	54.8
Sweep Rate	.469	.732	1.10	1.53	2.50	2.92

Table 14. Swept Frequency System Design Parameters

12.2.2 Derived Performance Data

The main difference in the performance of this system when compared with the details of Table 11 for the fixed frequency system is the improved rate of collection of independent samples provided by the frequency sweeping. The factor m and the antenna size both affect this and make the instrumental error attributable to the sea surface statistics ± 0.38 mb for this implementation.

Detailed calculations have not been performed to find the sensitivity of the measurement to changes in the various atmospheric factors. However it is reasonable to expect that this or a similar set of operating frequencies will result in a r.m.s. atmospheric variability error close to ± 0.4 mb as found for the fixed frequency scheme.

The effective along-track ground resolution, being the product of satellite ground speed and integration time, is not changed by the increase in antenna size although this increase is along the direction of satellite motion. However, the reductions in beamwidths and smeared spot sizes mean that a greater proportion of the integrated energy comes from within the effective resolution cell area.

An abbreviated list of performance data is given in Table 15.

Rms atmospheric variability error	± 0.4 mb	
Rms statistical error	± 0.38 mb	
Effective along-track ground resolution; for satellite altitude:	85 km 500 km	80 km 800 km

Table 15. Abbreviated Swept Frequency System Performance

12.2.3 Total Error Calculations

The use of frequency sweeping allows the reduction in sea-surface statistical error, due to the sweeping to be traded for an increase in the signal-to-noise error, due to the wider receiver bandwidth needed. The following results show the effects of this trade-off for the example system specified above. It has been assumed that fullest advantages is taken of the swept frequency system by using the minimum receiver bandwidth.

The data of Table 12 has been used to calculate the signal-to-noise error, E_{SN}, for the set of atmosperic and surface conditions in Table 13. E_{SN} is then combined with E_{AV} and E_{SS} to produce the total r.m.s. errors in measured pressure. The results presented in Table 16 are directly comparable with the values for the fixed frequency scheme in Table 13.

Sea State	Atmospheric Conditions				
	Surface Pressure	1013mb	1013mb	1013mb	990mb
	Water Vapor	2.6 gm cm^{-2}	5.2 gm cm^{-2}	3.5 gm cm^{-2}	3.5 gm cm^{-2}
500 km Orbit	Uniform Cloud	None	0.5 km 0.5 gm m^{-3}	1 km 1 gm m^{-3}	2 km 1.5 gm m^{-3}
Very calm	Nadir	0.55	0.55	0.55	0.56
	14°	>5	>10	>25	>25
Moderate	Nadir	0.55	0.56	0.59	3.84
	14°	0.70	0.94	1.71	>25
Very rough	Nadir	0.57	0.61	0.78	>5
	14°	0.61	0.73	1.16	>10
800 km Orbit					
Very calm	Nadir	0.55	0.56	0.58	3.09
	14°	>10	>25	>25	>25
Moderate	Nadir	0.57	0.61	0.76	>5
	14°	1.22	2.01	4.14	>25
Very rough	Nadir	0.67	0.87	1.46	>10
	14°	0.88	1.34	2.65	>25

Table 16. Total r.m.s. Errors (mb) With Frequency Swept MPS

Under favorable conditions the error has been halved to ± 0.6 mb but for some frequently occurring cloud and sea states the error is larger and the range of conditions for which the frequency swept system operates with sufficient accuracy is more restricted. It should also be noted that the limitations are more severe for the preferred 800 km orbit. The improved accuracy has been bought at the expense of reduced coverage and increased system complexity.

12.2.4 Hardware Implementation

The frequency swept system will consist of three ratiometers each of which has the same subsystems as described in Section 12.1.4 for the fixed frequency scheme. The block diagram of one of these ratiometers, Figure 30, is also applicable although some of the components are used differently.

Sweeping of the transmitter frequency must be accomplished with either current or varactor control. Extensive development will be necessary to produce sources with sufficient power and the required sweep characteristics. The local oscillator is to be swept over the same frequency range and accurate synchronization of its cycle must be provided by altimeter type measurements which can be obtained from the pressure sounder signals. The modulation sequence is as in Figure 31 but each transmission period includes many sweeps through the range of frequencies.

Successful operation of this frequency swept instrument will depend upon careful design and calibration for the 20 to 100 MHz bandwidth used at each frequency.

12.3 Payload Physical Characteristics

The additional data (approximate values) in Table 17 of size, weight etc. complete the payload specifications for either of the implementation alternatives described above.

Overall size	1.5 x 0.6 x 0.5 m
Weight	< 100 kg
Field of view	5° x 0.5°
Pointing angle	Nadir; ± 14° (cross-track)
Pointing accuracy	± 0.2°
Power	<100 W
Data Rate	1 kbps

Table 17. M.P.S. Physical Characteristics

12.4 Platform Requirements

The most suitable orbit for use of the Microwave Pressure Sounder as part of an operational meteorological data collection network is a near-polar, sun synchronous orbit at about 800 km. Potential missions on which to demonstrate the long-term capability of the instrument, prior to its operational application, are Oceansat, Climsat or the proposed Microwave Observatory. Shuttle/Spacelab sortie missions could be used for proof-of-concept flights with essentially the same instrumentation.

Aircraft testing of the technique is possible only for a fixed frequency system. The difference in altitude between an aircraft and a satellite means that the frequency coherence width is too large to allow sweeping to be used to increase the sample collection rate with the lower platform. Even with the fixed frequency system extensive modifications to the integration time, bandwidth and modulation timing are required for aircraft operation. In addition, because the instrument is designed to measure the integrated effect of the total atmosphere, accurate measurements of pressure at the aircraft altitude would be necessary and a different set of operating frequencies might be required. Careful consideration would also need to be

given to the stability requirements of the aircraft platform for meaningful measurements. Nevertheless, development of an aircraft instrument may be of value for its potential application to severe storm monitoring on flight paths through a storm.

13. Coverage and Resolution

The Microwave Pressure Sounder instrument specifications of Section 12 can be used to define the coverage and resolution which can be achieved with particular orbit characteristics. In Section 13.1 below the capabilities of the fixed frequency instrument in an 800 km orbit are used as a point of reference for discussion of the possibilities with other operational alternatives. This is followed by a consideration in Section 13.2 of how coverage will be reduced by atmospheric or surface effects.

13.1 Global-Ocean Coverage and Resolution

The fixed frequency MPS of Section 12.1 is designed to measure atmospheric pressure at the ocean surface directly below the satellite and on either side of the sub-satellite path at an angle of $\sim 14^{o}$ from the nadir. Although the off-track scan is limited it is an important capability since it allows the horizontal pressure gradient to be determined over the instrumental swath width. To illustrate the coverage and resolution obtainable with this instrument we have chosen an orbit of 796 km altitude at an inclination of 108^{o} (the Seasat A orbit).

Figure 32 shows the surface cell size and the positions of sequential measurement cells near the equator for part of an orbit. The separation between adjacent measurements is 200 or 240 km which is compatible with the 1.2 mb measurement accuracy and typical pressure gradients. By comparison, the resolution now being demanded from temperature and water vapor sounders is an order of magnitude smaller. However, these variables show significant changes over the smaller scale while pressure gradients are generally smooth and between 0 and 2mb per 100 km, reaching 3 mb/100 km in the vicinity of major storms. Consequently 200 km resolution is felt to be adequate for the pressure sounder.

Figure 33 shows the potential daily global coverage with an effective swath width of 600 km (3 measurements each separated by 200 km). The existing stations reporting surface pressure and typical shipping reports as in Figure 1 are also indicated on this diagram. The instrumental integration time of 12 sec enables some 5000 measurements of surface pressure to be made over the oceans in 24 hours. Since these measurements are divided

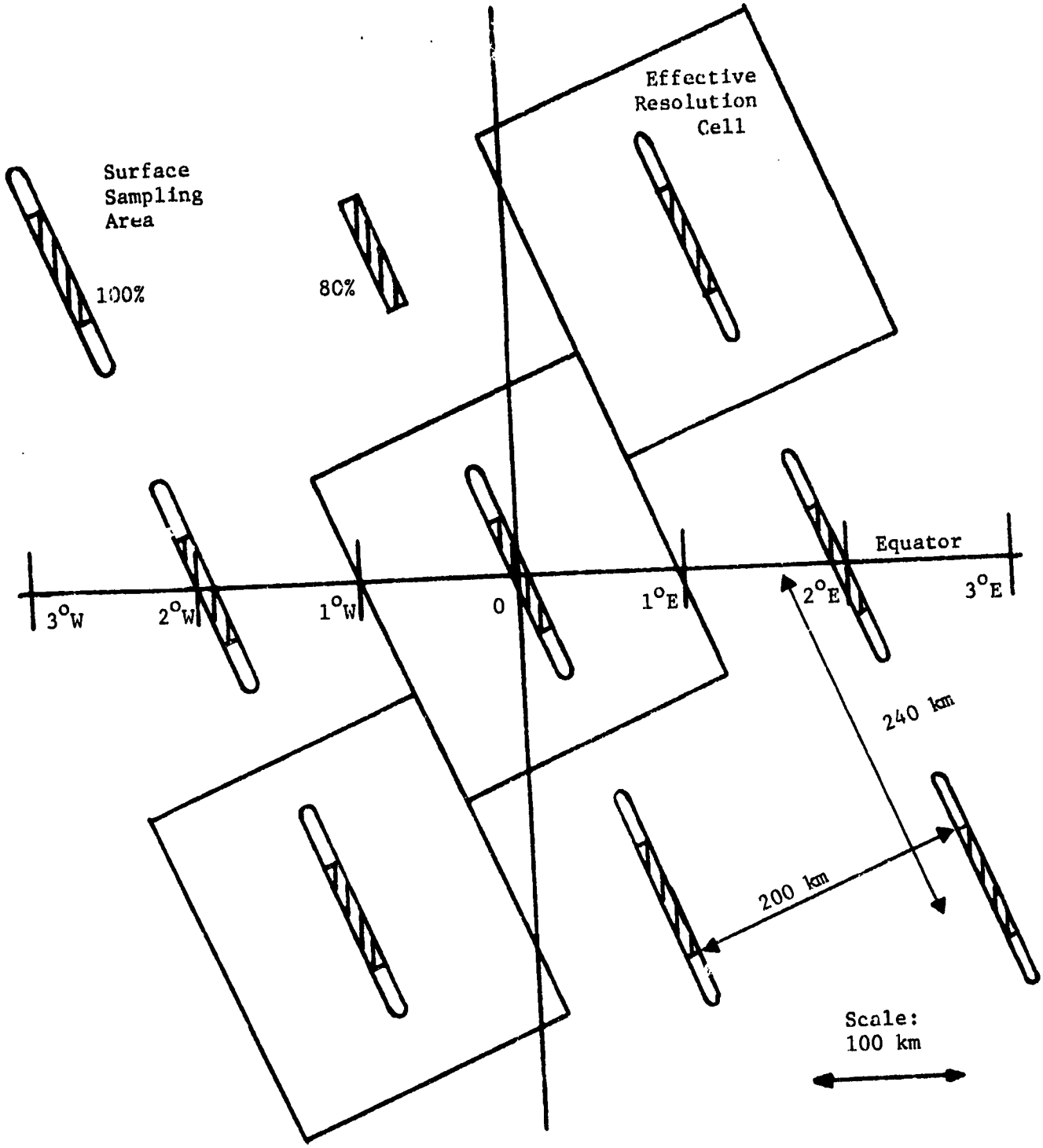

Figure 32. Surface cell size at the equator

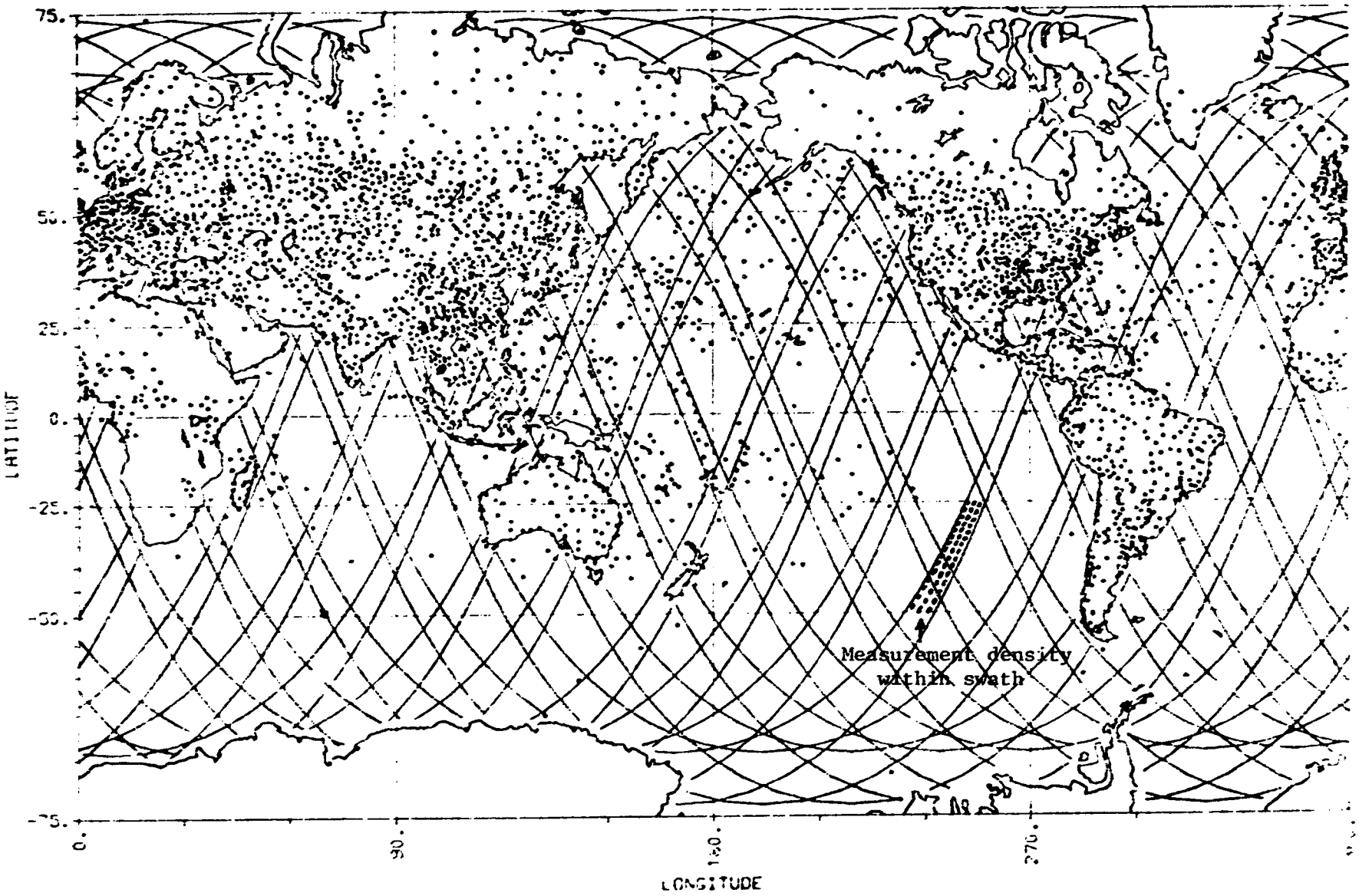

Figure 33. Potential daily coverage of surface pressure measurement with MPS in a SEASAT orbit compared with present coverage.

between daytime and nighttime there are effectively 2500 new surface pressure data points, roughly doubling the present network.

Current plans for an advanced operational meteorological satellite network call for 2 or 3 near polar orbiters. Such a multisatellite system could be used to increase the density of surface pressure measurements. Figure 34 shows the separation of data points at various latitudes for three satellites with mutually displaced orbits of altitude and inclination as above. With these three satellites there are gaps in the coverage in the tropics but it is probably adequate in view of the fairly stable atmosphere which prevails in this geographical belt. Coverage is more-or-less continuous in the important and very variable mid-latitude while the overlapping which occurs at high latitude could, if it were desirable, be removed and the resolution improved by reducing the angular scan for these parts of the orbit.

It should be noted that the measurement density represented by Figure 34 is for a 12 hour period. The non-coincident nature of these measurements is characteristic of all meteorological observations from satellites and should not detract seriously from their potential value for numerical weather forecasting.

With the standard of coverage set for one particular implementation of the fixed frequency instrument we can now examine briefly the implications of various alternatives. Coverage and resolution with the swept frequency MPS in an 800 km orbit is essentially the same. Either instrument in the lower, 500 km orbit improves the cross-track resolution to 125 km but leaves gaps in the coverage at mid-latitudes as well as increasing those gaps in the tropics. More satellites could be used to improve the coverage and the resolution or tropical coverage could be selectively increased with a high inclination ($\sim 150^{\circ}$) orbit. A decrease in the integration time can be used to improve the along-track separation of measurement points but this must be at the expense of reduced accuracy. For example, a 5 sec integration makes the along track resolution 100 km and the r.m.s. error 1.8mb with the fixed frequency scheme or 1.0mb with the swept frequency scheme.

Meteorological requirements will ultimately dictate which balance between accuracy, resolution, coverage and cost is most appropriate for operational application.

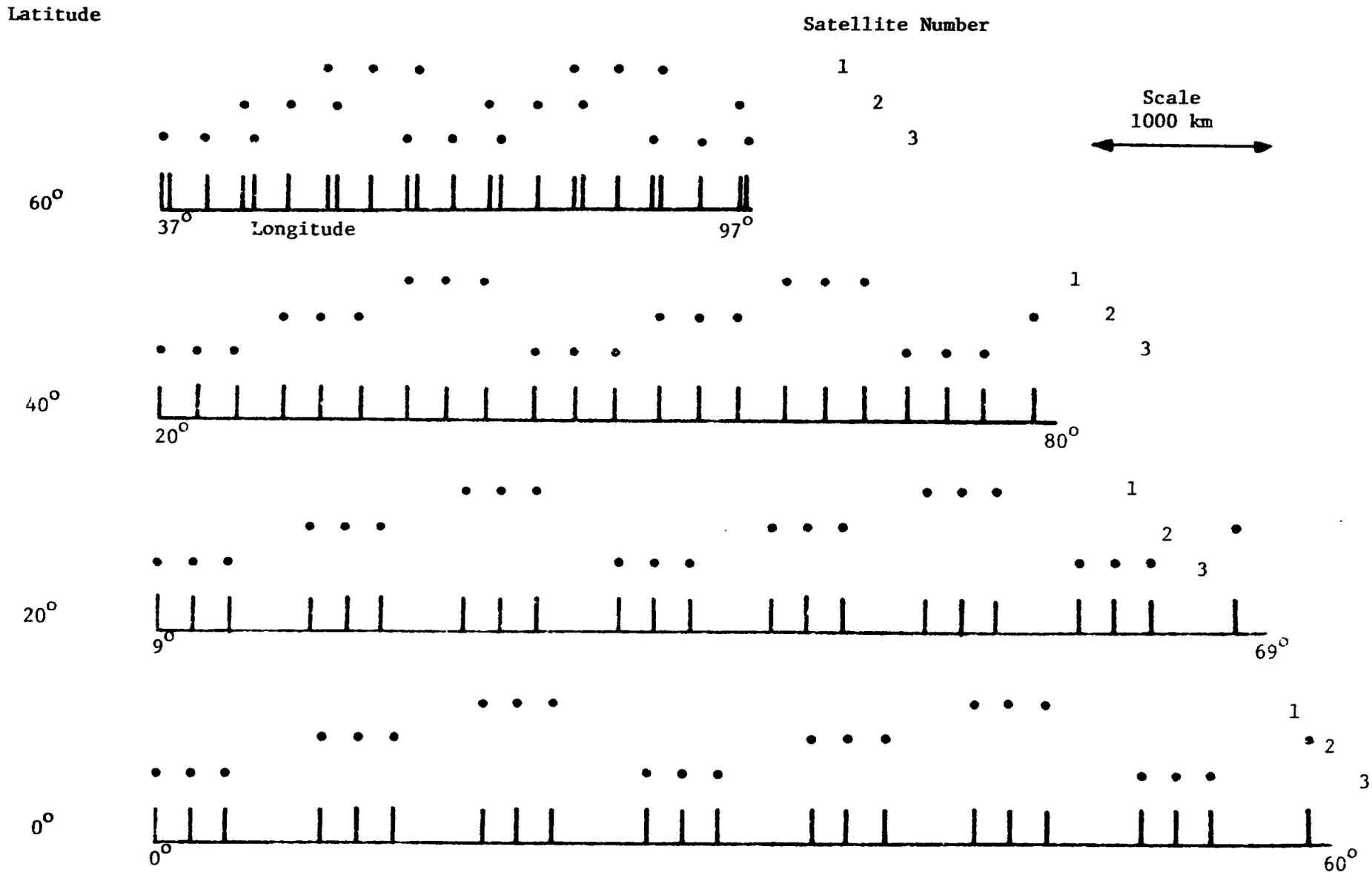

Figure 24. Separation of data points at various latitudes with a 3 satellite network.

13.2 Coverage Reduction by Atmospheric and Surface Effects

The Microwave Pressure Sounder has been designed for operation over the open ocean. During much of the winter and spring large areas of the Arctic and Antarctic Oceans become covered with ice as illustrated by the seasonal variation in polar ice cover shown in Figures 35 and 36. The ice thickness grows to 2 or 3 meters so that, provided its reflectivity is high enough, measurements will not be prevented by an inadequate knowledge of the reflecting surface height. Measurements by Gloersen et al (1973) indicate an emissivity for new ice of $\sim$.9 and for old ice of $\sim$0.8. These data are consistent with backscatter measurements at 13.3 GHz (AMWR, 1975, p. 216) and at 35 GHz (Sackinger and Byrd, 1972) which give normalized backscatter cross-sections in the range (3 to -5db) at normal incidence and (3 to -10db) at $\sim 14^{\circ}$. While these results suggest a reflectivity sufficiently large to enable measurements to be made in many conditions there is inadequate data available on frequency variations. The technique which has been adopted of combining ratio measurements to account for second order variations has great flexibility and will probably cover this situation with tolerable accuracy. Occasional inadequate compliance with the design conditions or reduced reflectivity can be anticipated and these would lead to some reduction in coverage which it is not possible to quantify at this time. Experimental measurements with a concept proving flight are needed to assure the validity of MPS measured surface pressure values in ice cover situations.

The total error calculations, Tables 13 and 16, show that measurements will become interrupted when cloud cover is greater than 1 km of density 1 gm m^{-3} equivalent to 0.1 gm cm^{-2} integrated liquid water. Although global cloud cover is typically near 50%, measurements by Staelin et al (1976) with NEMS show that the liquid water content of the atmosphere over the oceans exceeds .1 gm cm^{-2} for only a small fraction of the time, Figure 37. Some care must be taken in applying these results to estimate MPS coverage since the large angular beam width of the instrument means that these are averages over 200 x 300 km ground resolution cells. Somewhat more frequent occurrence of such high cloud density can be expected for the 10 x 100 km cell size of the MPS. Rain cannot be expected to reduce the coverage much further since it will usually be accompanied by cloud which is denser than the above limit.

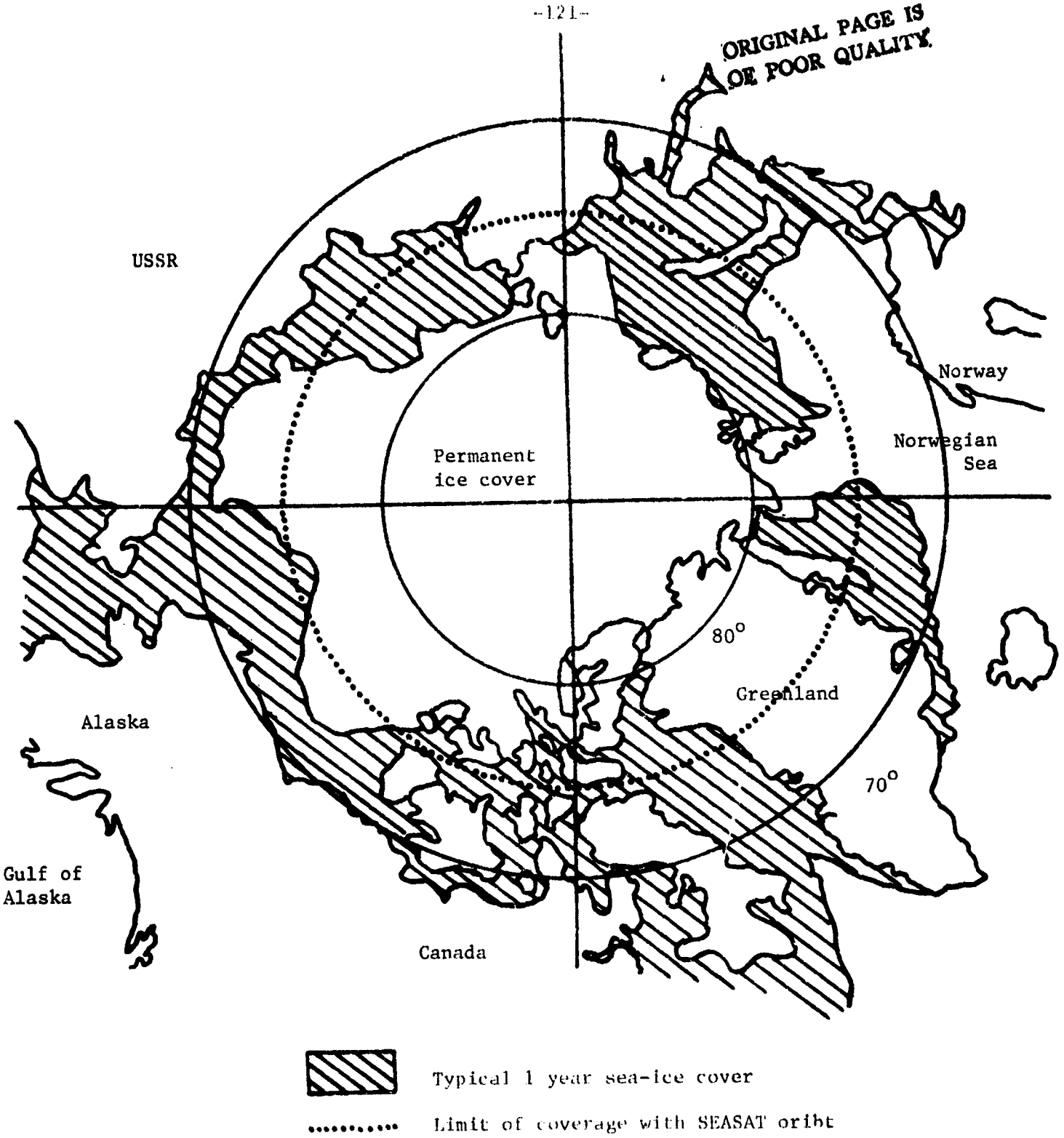

Figure 35. Extent of polar ice-cover, Northern Hemisphere

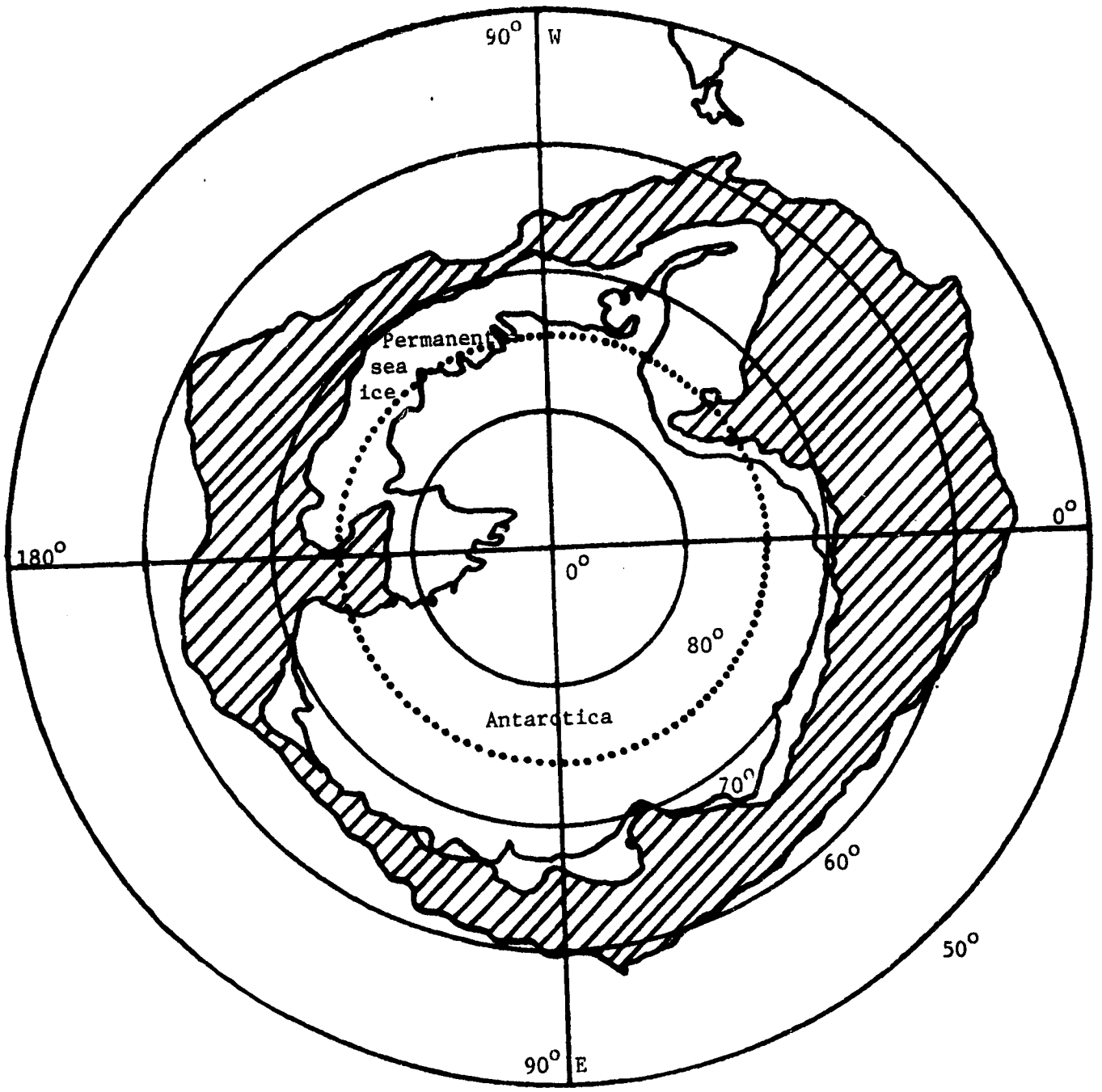

Figure 36. Extent of polar ice cover, Southern Hemisphere.

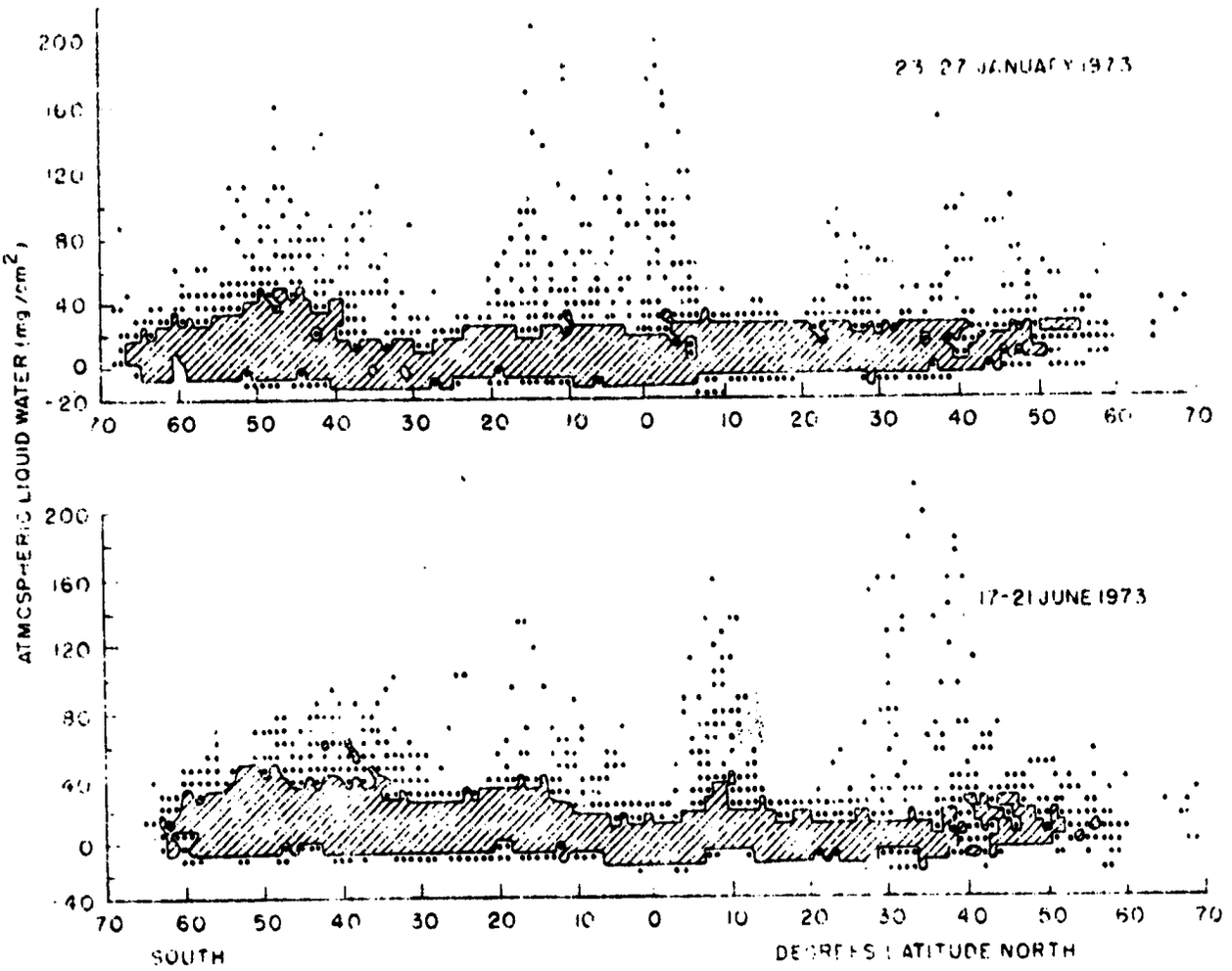

Figure 37. Observations of liquid water content of the atmosphere over the oceans. Dots: one or two occurrences; cross-hatching: more than two (From Staelin et al, 1976).

As noted in Section 12 some sea states will also prevent measurements being made but these adverse conditions occur infrequently. Also, those orbits for which solar radiation might also be reflected into the receiver aperture should also be avoided for, although this noise source is one which will be removed by the direct measurement, it will reduce the accuracy of pressure measurement.

In contrast to these factors which reduce coverage, it may be that some measurements over land will be possible if the surface height is reasonably uniform and its reflection characteristics are appropriate. However, insufficient data on surface reflectivity exists to specify these areas and indeed it is not a worthwhile exercise to try to do so at this time since the locations can more easily be identified with confidence by operational experience.

It is difficult to quantify the total reduction in coverage which can be expected from the effects of the atmospheric and surface factors. However it is probably not unreasonable to anticipate for the 800 km orbit a 10% loss of data with the fixed frequency instrument and a 20% loss for the swept frequency instrument. For the lower, 500 km orbit these losses would perhaps be nearly halved. The most unfortunate aspect of this problem of reduced coverage is that the data would be lost from the most interesting meteorological features viz cyclones, with their associated obscuring heavy cloud and where surface pressure measurements could provide valuable information on the depth of the depression. Nevertheless, if technology continues to advance at the present pace, increases in millimeter wavelength source powers should, within the foreseeable future, make it possible to measure surface pressure under these adverse conditions.

Microwave Pressure Sounders with the design specified in Section 12 on a three satellite network would provide some 7000 globally distributed surface pressure values twice daily with an accuracy of 1 to 2 mb and contribute significantly to the bank of meteorological data available for numerical weather forecasting.

14. Conclusions

Atmospheric pressure at the Earth's surface is arguably the most important meteorological parameter since it is the driving force for atmospheric circulation and has historically served as the primary basis for synoptic weather forecasting. The Microwave Pressure Sounder proposed here would provide consistent measurements over the at present inadequately monitored oceans to supplement the data available from ground based stations and approach the requirements of the GARP program for a comprehensive meteorological data set. As well as contributing to the initial conditions for large scale numerical forecasting, the data would be of considerable value for atmospheric dynamic studies with General Circulation Models. Because a surface resolution of 100 to 200 km can be achieved, its use would extend to localized forecasting and to oceanography by assisting with the interpretation of sea state, surface wind and sea surface topography observations from other satellite-borne sensors. Recent publication of a Climate Plan (ICAS, 1977) has stimulated vigorous activity in climate research. A significant addition to the data resources available for this program would be the consistent set of global pressure fields provided daily over a long period of time by operationally deployed Microwave Pressure Sounders.

Absorption by a vertical atmospheric column at a frequency in the wing of the oxygen band centered on 60 GHz is a measure of the total amount of oxygen in the column. The surface pressure can be deduced from this measurement which must be made with an active instrument. The selection of optimum operating frequencies is based upon accepted models of surface reflection, oxygen, water vapor and cloud absorption. By combining the ratios of transmission at three pairs of frequencies the measurement of surface pressure is made essentially independent of variations in the atmospheric temperature and humidity profiles, cloud cover and sea state. This means that the final output of the instrument is a direct measurement of surface pressure and therefore no sophisticated inversion procedure is required. A numerical simulation experiment using real profiles defined by radiosonde observations has shown that the error due to atmospheric profile variability is less than 0.5mb.

The set of operating frequencies used in the specific designs to show the potential capabilities of the MPS are not necessarily those which should be used in a flight experiment. Current investigations show that the sensitivity to pressure can be maintained or slightly improved with sets which have less susceptibility to errors from broken cloud states. While the effects of changes in the antenna size and integration time are readily discernable from the illustrative systems, the consequences of changing the operating frequencies cannot in general be simply defined but instead need a detailed analysis. For example, if the channel at 52.8 GHz were changed to 53.3 GHz the other operating frequencies must be altered to retain temperature, water vapor and background insensitivities, the accuracy of the fixed frequency system would be improved by ∿20% and a slight loss of data would result. A better definition of accuracy, resolution and coverage requirements, within the limitations presented in this report, will assist in determining the best set of operating frequencies.

The choices available for hardware implementation have been illustrated by system definitions based on fixed and swept frequency alternatives. Full analyses of the errors define the balance between accuracy and resolution which are available with each of these designs. Coverage and cost are introduced as further factors by a consideration of operational application alternatives. The fixed frequency instrument in an 800 km near-polar orbit can provide surface pressure with an r.m.s. error of 1.2mb and a surface resolution of 10 x 100 km. With these measurements separated by ∿ 200 km both across and along the sub-satellite path a three instrument network would provide satisfactory global-ocean coverage at 12 hour intervals. Resolution and coverage with a swept frequency instrument would be similar but its accuracy is somewhat better at ±0.6mb. This improvement in performance is however at the expense of increased susceptibility to data loss through adverse sea state or cloud conditions and increased component development costs. Meteorological or other user requirements will ultimately dictate the most appropriate system design and operational application mode.

While some of the proposed techniques are relatively untested, the designs have been based, with the exception of the transmitter subsystem, on existing technology. The state-of-the-art for power output from milli-

meter wave sources is anticipated to be 2W within the next year and this will satisfy the requirements of the fixed frequency design. In contrast, the swept-frequency system will require rather more development of suitable sources. Sources more powerful than 2W would extend the range of atmospheric conditions in which the pressure sounder would operate with sufficient accuracy to be useful.

Although it is recognized that these active multifrequency measurements include information on parameters other than surface pressure, no consideration has as yet been given to the extraction of data on water vapor and liquid water content of the atmosphere, sea state or surface level which are potentially available.

A continuing program of experiment definition studies, instrumentation evaluation and ground based atmospheric transmission measurements is being pursued at the Jet Propulsion Laboratory in cooperation with Heriot-Watt University and the Appleton Laboratory in the U.K. This work is directed toward a proof-of-concept Shuttle/Spacelab flight in the early 1980's in preparation for operational application by the late 1980's.

ACKNOWLEDGMENTS

This report presents the results of research carried out at Heriot-Watt University, Edinburgh, Scotland and at the Jet Propulsion Laboratory of the California Institute of Technology, Pasadena, California. Financial support was provided by the U.K. Science Research Council under grants SGD 00314 and SG/S/0607 and by NASA under contract NAS 7-100 sponsored by the Weather and Climate Program Office of the Office of Applications, National Aeronautics and Space Administration.

Scientific and technical contributions to this work by R. Sandwell, C. Wykes, H. W. Lightfoot, C. Gatley and J. Powell are gratefully acknowledged as are the many useful discussions with J. W. Waters and R. K. Kakar. Gratitude is also expressed to Heriot-Watt University for granting leave of absence to D. A. Flower and to the Physics Department of Heriot-Watt University, the Jet Propulsion Laboratory and the SRC Appleton Laboratory for their continuing support of the project.

LIST OF SYMBOLS

partial list identifies the most important symbols and those which used in more than one section. The section or subsection in which first used is also given. Other symbols have been introduced and n the text but their use is generally confined to one section only. ve convention the same symbol has occasionally been used with two meanings but this should not cause confusion since the correct clear from the context.

A	3.2	Antenna area
a, b, c	3.3	Coefficients of polynomial
D	11.1	Duty Cycle
Δf	3.2	Bandwidth
F	3.2	Receiver noise figure
F_A	7.4	Fractional accuracy
h	3.2	Height of satellite
N	3.2	Noise power
N_i	7.4	Noise power in channel i
P_T, P_R, P_D	3.2	Transmitted, received, detected power
p	4.2	Pressure
p_g	3.3	Surface pressure
r	3.2	Antenna radius
s	7.1	Index of surface pressure
S_I, S_A, S_B	7.1	Instrumental, atmospheric, background factors of S
T	3.2	Temperature
t	3.2	Integration time
v	11.1	Satellite velocity
α, β	7.2	Indices
β	4.3	Water vapor mass mixing ratio
γ	4.1	Absorption coefficient (db km^{-1})
$\Gamma_o, \Gamma_w, \Gamma_A$	3.3	Integrated absorption coefficient for oxygen, water vapor, and other constituents

η_T, η_R	3.2	Transmit, receive antenna feed efficiency
θ_3, ϕ_3	3.2	3db beam width
λ	3.2	Wavelength
ν	3.3	Frequency
ν_1	7.1	Operating frequency
σ°	3.2	Normalized backscatter cross-section at nadir
τ	3.2	Atmospheric transmissivity
τ_o, τ_w, τ_A	3.3	Transmissivity of the atmosphere due to oxygen, water vapor, and other constituents